Automatic Road Sign Detection and Recognition

By

Usman Zakir

A Doctoral Thesis for the degree of Doctor of Philosophy

Department of Computer Science

Loughborough University

August 2011

Supervisor:

Dr. Eran A. Edirisinghe

Loughborough University

Thesis Access Form

Copy No……..……**Location**……..…

Author……..……..…….

Title……..

Status of access OPEN / RESTRICTED / CONFIDENTIAL

Moratorium Period:……years, ending……../……200…….

Conditions of access approved by (CAPITALS):……

Supervisor (Signature)……...……...

School of……...……

Author's Declaration: *I agree the following conditions:*

Open access work shall be made available (in the University and externally) and reproduced as necessary at the discretion of the University Librarian or Dean of School. It may also be digitised by the British Library and made freely available on the Internet to registered users of the EThOS service subject to the EThOS supply agreements.

*The statement itself shall apply to **ALL** copies including electronic copies:*

This copy has been supplied on the understanding that it is copyright material and that no quotation from the thesis may be published without proper acknowledgement.

Restricted/confidential work: All access and any photocopying shall be strictly subject to written permission from the University Dean of School and any external sponsor, if any.

Author's signature…….Date……...……...……...

Users declaration: for signature during any Moratorium period (Not Open work): ***I undertake to uphold the above conditions:***			
Date	Name (CAPITALS)	Signature	Address

4.1e

Loughborough University

CERTIFICATE OF ORIGINALITY

This is to certify that I am responsible for the work submitted in this thesis, that the original work is my own except as specified in acknowledgments or in footnotes, and that neither the thesis nor the original work contained therein has been submitted to this or any other institution for a degree.

……

Usman Zakir

25th August 2011

To my beloved Parents

(*Muhammad Zakir Nasim & Waheeda Zakir*)

&

My whole family

Acknowledgements

The chain of my appreciation begins with the name of Almighty Allah (S.W.T.) the Most Gracious, and the Most Merciful who has blessed me always in every situation. He (S.W.T.) is the one who has provided me the knowledge and courage to accomplish my research.

I shall like to express my deep and sincere gratitude to my supervisor Dr. Eran A. Edirisinghe for taking me under his supervision. Like for every other member of DIRG (Digital Imaging Research Group), I have also received his kindness, invaluable assistance, critical advice and guidance from the very beginning, until the end of my research. He has also helped me in developing my professional career by involving me in various industrial projects. His deep knowledge in digital imaging and logical way of solving problems has always been a great asset for my research. His constructive comments, technical and editorial advices helped me in the completion of this thesis.

I shall also like to thank my DIRG colleagues for providing a friendly and helpful atmosphere for my study. I shall like to thank to Dr. Dhammike Wickramanayake, Dr. Iffat Zafar, Dr. Fatima Al-Abri, Dr. Rizwan Faiz, Dr Min Jiang, Dr. Muhammad Athar Ali, Mr. M. Akramshah Ismail, Ms. Sara Saravi, Ms. Nesreen Otoum and Mr. Andrew Leonce for their association with me as professionals and friends. I would also like to thank Professor Serpil Acar, Dr. Qinggang Meng, Mr. Gurbinder Singh Samra and Ms. Christine Bagley for their invaluable support and encouragement.

I shall also like to express my deep and sincere gratitude to my AVRC (Applied Vision Research Centre) colleagues for their patience and support during the writing-up of this thesis. I would also like to add a special thank you to my line manager Professor Alastair G. Gale for his kindness and helpful advices that supported me enormously in the completion of my thesis.

Finally but not least I would like to pay my gratitude to my family. My parents deserve special mention for their unconditional, inseparable support, prayers and endless love. My Father,

Mohammad Zakir Nasim, my role model; who helped in the development of foundations for my learning character. I will always be indebted to him for the kindness and care he has shown to me since my birth and his endless support in every aspect of my life which has no replacement. My Mother, Waheeda Zakir is the one who has sincerely raised me with her caring and gentle love and prayed for my success day and night. My special gratitude to my beloved wife Asima Usman, to my brothers: Rizwan Zakir, Irfan Zakir, Tayyab Zakir, Farhan Zakir, Haseeb Zakir, Ahmed Zakir and Safi Zakir, to my sisters: Misbah Zakir and Atifa Adnan, to my brothers and sisters in law, my nieces and nephews. Thank you all for being supportive, loving and caring during my entire educational career. I could not have reached this far without your support and encouragement.

Usman Zakir

August 2011

Abstract

Road Sign Detection and Recognition (RSDR) systems provide an additional level of driver assistance, leading to improved safety for passengers, road users and vehicles. As part of Advanced Driving Assistance Systems (ADAS), *RSDR* can be used to benefit drivers (specially with driving disabilities) by alerting them about the presence of road signs to reduce risks in situations of driving distraction, fatigue ,poor sight and weather conditions. Although a number of *RSDR* systems have been proposed in literature; the design of a robust algorithm still remains an open research problem. This thesis aims to resolve some of the outstanding research challenges in *RSDR,* while considering variations in colour illumination, scale, rotation, translation, occlusion, computational complexity and functional limitations. *RSDR* pipeline is divided into three parts namely; Colour Segmentation, Shape Classification and Content Recognition. This thesis presents each part as a separate chapter, except for Colour Segmentation that introduces two distinct approaches for Road Sign region of interest (*ROI*) selection. The first approach in Colour Segmentation presents a detailed investigation of computer based colour spaces i.e. *YCbCr, YIQ, RGB, CIElab, CYMK and HSV,* whereas second approach presents the development and utilisation of an illumination invariant *Combined Colour Model (CCM)* on Gamma Corrected images containing road signs considering varying illumination conditions. Shape Classification of the road sign acts as second part of *RSDR* pipeline consisting on shape feature extraction and shape feature classification stages. Shape features of road signs are extracted by introducing *Contourlet Transforms* at the decomposition level-3 with '*haar'* filters for generating the *Laplacian Pyramid (LP)* and *Directional Filter Bank (DFB)*. The third part of the *RSDR* system presented in this thesis is the Content Recognition, which is carried out by extracting the *LESH (Local Energy based Shape Histogram)* features of the normalized road sign contents. Extracted shape and content features are utilised to train a *Support Vector Machine (SVM) polynomial kernel* which are later classified with the input candidate road sign shapes and contents respectively. The thesis further highlights possible extensions and improvements to the proposed approaches for *RSDR*.

Usman Zakir

August 2011

Table of Contents

Chapter 3:

Research Background.....28-41

Chapter 4:

Road Sign Segmentation Based on Colour Spaces: A Comparative Study.....42-64

List of Figures and Tables

Figures

Tables

Abbreviations and Notations

Abbreviations

RSDR	Road sign detection and recognition
HSI	Hue, Saturation, Intensity
RGB	Red, Green, Blue
HSV	Hue, Saturation, Value
CYMK	Cyan, Yellow, Magenta, Karbon(Black)
CIElab	Commission Internationale de l'Eclairage,lab
HSL	Hue, Saturation, Luminance
DtB	Distance to Border
SVM	Support Vector Machine
FRS	Fast Radial symmetry
FFT	Fast Fourier Transform
2D	2-Dimentional
ROI	Region of Interest
RANSAC	RANdom Sampling and Consensus
MLP	Multi Layer Perceptrons
SIFT	Scale Invariant Feature Transform
ART1	Adaptive Resonance Theory 1
RBF	Radial Basis Function
LESH	Local Energy based Shape Histogram
ADAS	Advanced Driver Assistance Systems
YIQ	Y(Luminance), In-phase, Quadrature
NTSC	National Television System Committee
CCM	Combined Colour Model
WEKA	Waikato Environment for Knowledge Analysis
PCA	Principal Component Analysis

ROC	Receiver Operating Characteristic
CBH	Colour Barycenters Haxagon
LoG	Laplacian of Gaussian
RP	Resilient Backpropagation
MLP	Multilayer Perceptrons
LUT	Lookup Table
ANN	Artificial Neural Networks
DCT	Discrete Cosine Transform
GA	Genetic Algorithm
SVF	Support Vector Filter
SCG	Scaled Conjugate Gradient
PAL	Phase Alternating Line
MAP	maximum a posteriori
SA	Simulated Annealing
kNN	k-nearest-neighbor
ART2	Adaptive Resonance Theory 2
HDTV	High Definition Television
SECAM	Séquentiel couleur à mémoire
ARFF	Attribute-Relation File Format
CLI	Command Line Interface
LP	Laplacian Pyramid
DFB	Directional Filter Bank
POI	Pixels of Interest
TP	True Positives
TN	True Negatives
FP	False Positives
FN	False Negatives

Notations

$\boldsymbol{\alpha - \beta - \gamma}$	Alpha-Beta-Gamma
$\boldsymbol{\gamma - value}$	Gamma Value
$\boldsymbol{cd}$	Cohen and Daubechies
$\boldsymbol{5\text{-}3}$	MacClellan transformed
$\boldsymbol{H_{r1}}$	Hue of Red colour at 0.00
$\boldsymbol{H_{r2}}$	Hue of Red colour at 1.00
$\boldsymbol{H_g}$	Hue of Green colour
$\boldsymbol{H_b}$	Hue of Blue colour
$\boldsymbol{min(R,G,B)}$	Minimum value of red,green,blue
$\boldsymbol{max\ (R,G,B)}$	Maximum value of red, green, blue
$\boldsymbol{2\pi}$	Radian angle where $\pi = 3.142$
$\boldsymbol{2\pi r}$	Circumference
$\boldsymbol{\pi r^2}$	Area of a circle
$\boldsymbol{r}$	Radius of a circle
$\boldsymbol{\frac{1}{2}ah}$	Area of a triangle
$\boldsymbol{h}$	Altitude of a triangle equivalent to 'a sin 60^o'
$\boldsymbol{R_{Area}}$	Area of a rectangle
$\cup$	Union of two sets
$\boldsymbol{2^n}$	n , levels of decomposition
$\boldsymbol{Map_d}$	directional map
$\boldsymbol{C_{l,d}}$	contourlet sub band image
$\boldsymbol{dataset_i}$	Union of features and related class labels
$\boldsymbol{CT}$	Contourlet Transform
$\boldsymbol{w}$	Feature mapping
$\boldsymbol{p_r(r_j)}$	probability of occurrence of intensity level , r_j
$\boldsymbol{T(r_k)}$	histogram equalization
$\boldsymbol{I_{binary}}$	Binary Image

$\boldsymbol{X_k}$	Connected binary components
$\boldsymbol{W(x)}$	weighting of the frequency spread
$\boldsymbol{A_n(x)}$	Amplitude
$\boldsymbol{\phi_n(x)}$	phase angle
$\boldsymbol{T}$	noise cancellation factor
$\boldsymbol{\varepsilon}$	Constant to avoid division by zero value
$*$	convolution operator
$\boldsymbol{G_{u,v}(z)}$	Gabor kernel where $\mathrm{z} = (\mathrm{x}, \mathrm{y})$ represents image postion
$\boldsymbol{u}$	Orientation
$\boldsymbol{v}$	Scale
$\boldsymbol{\Psi_{u,v}(z)}$	Gabor Wavelet Kernel
$\boldsymbol{e}$	Gaussian envelope
$\boldsymbol{\sigma}$	Angle equivalent to 2π
$\boldsymbol{h_{r,b}}$	Local histogram
$\boldsymbol{\delta_{Lb}}$	Kronecker's delta
$\boldsymbol{E}$	Local Energy
$\boldsymbol{L}$	Orientation label map
$\boldsymbol{b}$	Current bin
$\boldsymbol{w_r}$	Gaussian weighting function of region r

Chapter 1

An Overview

1.0 Introduction

Road sign detection and recognition (RSDR) has drawn considerable research attention in recent years due to its challenging nature as a computer vision problem. Road signs have a direct impact on ones daily life as possible life threats can easily be formed due to a lack of concentration or ignorance. In recent years a number of *Driver Assistance Systems* have been proposed and implemented including vision based algorithms claiming to be efficient towards *RSDR*. In addition, due to increased amount of possible threats on the roadside the impact of road signs on road users has considerably increased during the last decades. Many new road signs have been introduced according to the necessity and due to increase usage of the roads. Vehicle drivers specially need to learn to identify all road signs for road safety. For example drivers require having the knowledge of cyclist signs, pedestrian signs, obligatory signs and advisory signs etc. and ignorance of any sign can cause possible accident hazards.

In conjunction to other *Advanced Driver Assistance Systems* (ADAS) such as *lane departure warning systems*, *in-car navigation systems*, *adaptive cruise control system*, *automatic parking* etc.; *RSDR* systems help in detecting and translating the road signs for the attention and understanding of drivers. Specifically, drivers with visual impairments can benefit from this important computer based visual aid. In more sophisticated systems, *RSDR* systems can utilise other features of *ADAS* such as *adaptive cruise control system* to automatically drive the vehicle according to varying road speeds.

Highway agencies and road maintenance engineers have the responsibilities to maintain the roads and the state of signposting which are vital for the safety of road users. *RSDR* can be used for road sign inventory and inspection purposes. Damaged, occluded, tilted, rotated, colour faded road signs can be recognised and used to reduce possible risks.

With *RSDR*, the inventory and inspection process can be made semi-automatic where video footage of the road with signage information is recorded prior to locating and investigating a particular damage.

1.1 Properties of Road Signs & Challenges in their Automatic Computer based Detection & Recognition

Generally road signs consist of three properties. Firstly they are represented by colours such as Red, Green, Blue, and Brown etc. Secondly they consist of particular shapes such as Circular, Triangular, Octagonal, Square patterns etc. The inner contents of road signs represent the third property, which vary depending on the application of the road sign. For example road signs used on motorway roads have different appearance than road signs used in town and city areas. In this thesis we have highlighted the importance of using these properties separately in road sign detection and recognition by considering each of them as a different problem: in the presence of varying lighting conditions, scaling, angular rotation and occlusion.

The perceptual colour of a road sign appears to be different due to varying outdoor lighting and weather conditions. This makes it difficult to extract the accurate colour information of road sign. The weather defined by rain, fog, snow etc., and time of the day defined by day, dusk, night etc., play an important role in creating the above mentioned variations of illumination.

The size of a road sign as appearing in a scene has an impact on its detection and identification accuracies. Road signs that appear small will not be detected as the recognition of the colour or shape of small objects is still a challenging issue for even the best computer vision algorithms. Therefore it is important to include a system functionality, which keeps track of a candidate sign from the point it first becomes visible in the scene until a recognizable size.

Furthermore, the detection and recognition of a road sign in the presence of likely angular rotation is also a further challenging computer vision problem which needs to be

addressed and resolved. The detection and recognition of a road sign can also be affected by occlusion, i.e., due to the presence of objects in the field of view. In the proposed approaches the verification of the road sign is completed at multiple stages. This helps to overcome partial occlusion at a high success rate.

To accommodate the recognition ability of all categories of road signs it is important to distinguish road signs not only by their contents but also by their colour and shape information. Table 1.1 shows different categorical divisions of road signs according to their colour and shape information.

Triangle	Red Circle	Hexagon	Blue Circle	Square
				

Table 1.1: Different road signs categorized according to colour and shape information

1.2 Research Motivations

Generally, the *RSDR* literature can be divided into two groups, namely those that concentrate on 1: Road Sign Detection and 2: Road Sign Recognition. Road sign detection consists of extracting the candidate road sign from an outdoor scene. Majority of the work in road sign detection is initiated using colour information of the road signs called colour segmentation. The colour segmentation of the candidate sign from the scene is more frequently carried out by employing a colour space. The most popular colour spaces used for this purpose are *HSI, RGB, CIElab, YCbCr, CYMK* and *HSV*. In colour based segmentation approaches images are first converted to a designated colour space and then a segmentation algorithm e.g. thresholding, is applied [68]. In [4], [23], [34], colour based segmentation of road signs has been achieved by first transforming the

original image to the *HSI* colour space and subsequently marking the desired colour pixels (such as Red, Green, Blue etc.) by a white pixel. Pixels that are outside the threshold ranges are treated as background or noise. Thus a binary image is formed in which white pixels represent the desired coloured area and black pixels represent noise or background. In [19], [25], segmentation has been achieved using *RGB* colour space and the desired pixels are extracted by using threshold values for each colour. These threshold values are obtained on the basis of changing illumination conditions during different times of the day [17]. In [68], [28], [48], segmentation is performed by transforming the images to *HSV* colour space to obtain thresholds using *Otsu's algorithm* [24]. In [41], though the segmentation is performed in the *HSV* colour space, the pixels of interest are obtained by employing a set of fuzzy rules. In [2], the *CIElab* colour space is employed with a Gaussian model to target the colour information and in [98] chromatic channels are transformed to binary images using *Otsu's algorithm*. *YCbCr* colour space is employed in [32] and an adaptive thresholding has been performed to obtain the pixels of interest. In [8] *CIECAM97* colour space is employed to segment out the road signs and colour segmentation results are compared with *HSI, RGB* and *CIELUV* colour spaces.

Recently a number of attempts have been made to employ combined colour spaces and models in road sign colour detection. In [47] a joint colour space segmentation approach has been adopted. The Hue of the *HSV* colour space and image chrominance (*U, V*) values from *YUV* colour space have been jointly used. The results of the two colour spaces are combined by a logical *AND* operation. *256 RGB* and *HSL* transforms are used in [33] to construct colour distinctions of the image by following simple thresholding. *RGB* and *HSI* colour spaces are jointly used to threshold the image in [24]. *HSI* threshold values for Blue and Red colours were also tabulated. A joint colour space has been employed [20] in which the *HSI* is used to extract the chromatic information and *RGB* is employed to extract the achromatic information. An adaptive chrominance and luminance thresholding has been achieved in [22] by employing joint colour space i.e. *CIElab* and *HSI*. In [99] a four colour space based colour classifier has been introduced to segment road signs which were captured under various weather and lighting conditions.

In conjunction with colour based approaches, shape based approaches are seldom used in road sign detection. In this case the colour information is either used as a pre-processing step or never used at all. Two shape measures are used for circular and triangular road signs by using a *fuzzy shape recognizer* in [5]. *DtB* vectors are obtained of the segmented road sign from four different views and the shape is classified by using a linear *SVM* [6]. For shape determination *Hough Transform* [24] and a *median filter* are applied to detect the triangular and circular road sign shapes [17]. The circular shapes are identified through a *Fast Radial symmetry detection* method (FRS) and the triangular and square shapes are identified by using the *Harris corner detection* algorithm [18]. Difference of candidate *background histogram* and *template histogram* are used to obtain the shape information of the candidate sign [19]. *Fast Fourier Transform (FFT)* is employed to retrieve shape signatures by comparing it with the shape reference methods in [22] and [52]. The *2D correlation coefficients* are derived to represent the shape similarity by correlating the candidate *ROI* with *2D* binary template in [25]. A *coarse-to-fine scheme* is proposed for candidate shape verification in [27]. *Hopfield neural networks* are used to determine triangular and rectangular shapes by obtaining information related to angle, gradient and distance between edges [29]. The *RANdom Sampling and Consensus (RANSAC)* algorithm is used to examine and determine the circular shapes in [32]. The shape context and its invariance to rotation and scale distortions are determined by employing *corners as salient points* in [35]. Geometric properties of different road sign shapes are computed by using the *Affine Moment Invariants* in [41].

Both the recognition and classification of road signs have been carried out by employing a series of approaches which include *Multi-Layer Perceptrons (MLP), Neural Networks* [34] with feed forward topology as described in [28]. To recognize road signs a *template matching* technique was proposed in [5]. Different types of *Neural Networks* are employed in the recognition and classification of road signs such as *LWN++* in [6], *3-layered* [7], *Hopfield* [29], *back propagation* [46] and *ART1* [44]. *Scale Invariant Feature Transform (SIFT)* is used in the recognition of road signs in [13] where the similarity measures among the features are obtained through objective functions [47]. *SVM Gaussian kernel* is used for content recognition in [26]. A two class *SVM* classifier is

used in [100], one versus all *SVM* classifier in conjunction with *RBF* kernel is proposed in [49] and *SVM polynomial kernel* is used with regards to *AdaBoost naive Bayes* in [31]. The classification of road signs has been performed by *Normalized Correlations* in [16] while *Normalized Cross Correlation* method is introduced in [11]. Other recognition methods such as, *Fuzzy Shape recognizers* [41], *Adaptive Hausdorff distance* based on similarity weights [23] and *Gabour Wavelets* [24] filters have also been used.

The shortcomings of the existing approaches to *RSDR* motivated the research work presented in this thesis. One main focus is to investigate the limitations of the existing end-to-end *RSDR* systems and propose robust detection and recognition approaches. Literature in *RSDR* (see chapter 2) revealed that the colour segmentation is carried out by employing various colour spaces and the selection of the colour space on the basis of its performance and application under various illumination conditions leaves significant amount of research gap to be bridged. This provides motivation to study the behaviour of various colour spaces in different illumination conditions and to evaluate their performances. Further to that, the illumination correction of captured images is also adopted by employing gamma correction which is neither considered nor discussed in the literature. A Combined Colour Model is also proposed in connection with the colour based segmentation of road signs, that is invariant to light variations and provides high detection rates. The shape of the road sign is also an important factor in the vision based system considering that road signs can appear as translated, rotated, scaled and occluded. The literature (see chapter 2) has also revealed that not all forms of road sign geometrical shapes are considered leaving with a significant amount of research gap. In chapter 6 the above research gap is convincingly addressed and covered by introducing a novel shape extractor based on the Contourlet Transform [53]. The content recognition is carried out using a LESH [107] feature extractor, which is facilitated for noise removal by colour segmentation and shape detection stages. This helps the overall *RSDR* system to operate, efficiently under different illuminations, scales, rotations and occlusion distortions. Figure 1.1 illustrates the detailed block diagram of the proposed *RSDR* framework which aims to bridge the research gap highlighted above.

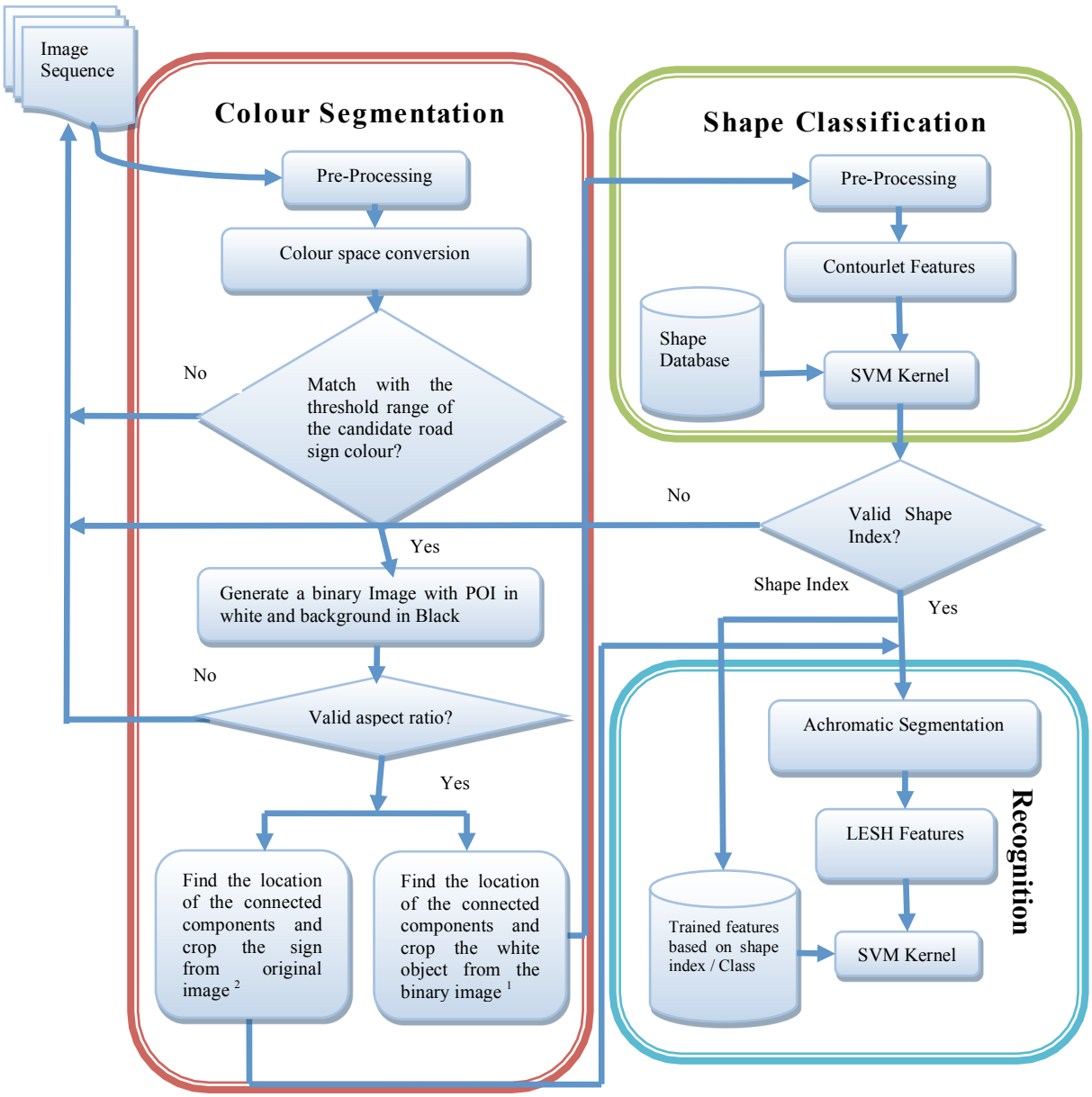

Figure 1.1: Road Sign Detection and Recognition framework

1. Objects used for shape classification (see chapter 6)

2. Objects used for content recognition (see chapter 7)

1.3 Aim and Objectives

Aim: To design and develop robust detection and classification algorithms for road traffic signs, giving rise to systems that will be able to enhance the fool proof nature of *ADAS*.

The specific objectives of this research are listed as follows:

- To investigate the effectiveness of *YCbCr, YIQ, RGB, CIElab, CYMK* and *HSV* colour spaces during varying lighting conditions such as *Brighter/Day, Rain/Wet, Evening and Night* times.
- To propose optimal threshold parameters for *HSV* colour space based on its effectiveness and high rate of experimental accuracy amongst all other computer based colour spaces.
- To propose Gamma Correction to correct the luminance level of the captured image/video on the basis of the output device and other video systems such as *NTSC.*
- To propose an illumination invariant *Combined Colour Model (CCM)* for colour image segmentation by combining *HSV, RGB, CIElab* and *CYMK* colour spaces.
- To propose a robust geometric shape detector invariant to scale, rotation and partial occlusion.
- To propose a robust local feature extractor to represent a road sign accurately and in cost effective way.
- To assess and identify the performances of the proposed algorithms and outlining the future research directions.

1.4 Organization of Thesis

This thesis is organized into eight chapters as summarized below.

Chapter 1 provides an overview of the *RSDR* domain providing a summary of problems and proposed solutions.

Chapter 2 reviews the existing literature on *RSDR*. For the understanding of the reader, the taxonomy in *RSDR* domain is presented in section 2.1 which tabulates the approaches that researchers have adopted over the years. The literature review is carried out for those key approaches which are specifically utilized in the Detection and Recognition of the road sign.

Chapter 3 briefly summarizes the background theories upon which the novel *RSDR* algorithms have been proposed. The chapter discusses the colour spaces and their usage in section 3.1. The *WEKA* [84] data mining tool is also briefly explained with its working environment in section 3.2. *Contourlet Transform* [53] used for shape recognition in this thesis is briefly explained in section 3.3.

Chapters 4 presents a detailed investigation of computer based colour spaces i.e. *YCbCr, YIQ, RGB, CIElab, CYMK and HSV* on Gamma Corrected images to segment the colour of the road sign under varying outdoor lighting conditions. This investigation helps in finding the optimum colour space i.e. *HSV*, which is proved to be effective in colour segmentation during *Bright/Day, Wet/Rain, Evening and Night* time lighting conditions.

Chapters 5 presents the development of an illumination invariant *Combined Colour Model (CCM)* and its usability in adverse weather conditions. The purpose of introducing *CCM* is to combine properties of four computer based colour spaces which

individually produce better colour segmentations according to varying outdoor lighting conditions.

Chapter 6 contributes towards the development of the geometric shape descriptor for detection and classification of the road sign shapes. The shape features of the road signs are extracted by introducing *Contourlet Transforms* at level 3 directional decomposition and 'H*aar'* filters are utilized for generating the *Laplacian Pyramid (LP)* and *Directional Filter Bank (DFB)*.

Chapter 7 presents the last contribution of this thesis towards *RSDR* systems. The content recognition stage of the road sign is carried out in this chapter by extracting the *Local Energy based Shape Histogram (LESH)* features of the normalized road sign content.

Chapter 8 concludes the research presented in this thesis with an insight into the future directions and enhancements.

Chapter 2

Literature Review

2.0. Introduction

This chapter introduces existing literature in the application domain of *RSDR*. The study of these approaches will conceptually allow the performance of the proposed approaches to be compared with state-of-the-art approaches. Such a comparison is particularly valuable since no standard dataset is available for researchers to carry out performance analysis tests, therefore allowing a fair comparison.

Figure 2.1 illustrates the general framework used in the majority of the road sign detection and recognition approaches proposed in literature. These approaches largely differ due to the differences in the algorithms used within each of the three functional blocks of Figure 2.1. All existing *RSDR* algorithms are detailed in section 2.2.

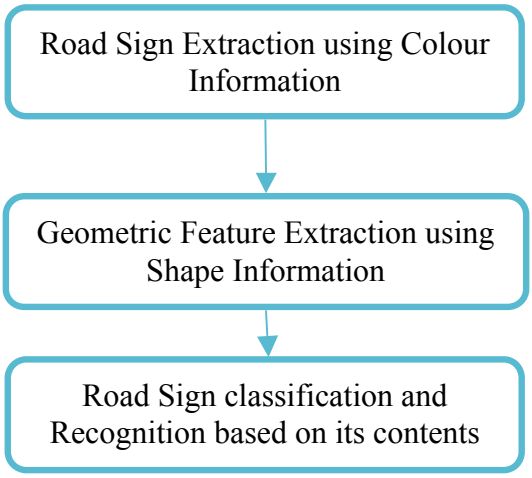

Figure 2.1: General framework of Road Sign Detection and Recognition

For the clarity of presentation this chapter is divided into three sections. Section 2.1 discusses the approaches used to detect and recognise road signs from image or image sequences. It also includes the taxonomy of road sign detection and recognition algorithms for ease of comparison. Section 2.2 provides a detailed literature review of the state-of-the-art algorithms in *RSDR* domain. Finally section 2.3 provides a summary and draws conclusions.

2.1 A Taxonomy of *RSDR* Approaches

Road sign detection from an image or image sequence is the first key step of *RSDR*. An extensive investigation of existing literature has been made as part of the research presented in this thesis which reflects that the detection step is carried out by using the properties of colour, shape or joint information. Secondly road sign recognition is performed on the contents of the candidate road signs detected and is mostly dependent on an extensive shape analysis and classification. In addition road sign tracking is adopted by some researchers to enhance the accuracy of the detection and recognition stages and to reduce the computational cost of having to repeat the above processes on every frame of a given video sequence. Table 2.1 provides the taxonomy of road sign detection whereas Table 2.2 provides the taxonomy for RSDR recognition and tracking algorithms.

Reference No.	Colour Segmentation	Shape Recognition	Stream Type
[4]	HSI Colour Space	DtB Vectors	Video Stream
[5]	HSV Colour Space	Fuzzy Shape Descriptor	Images
[6]	RGB colour space	Pattern Matching	Images
[7]	Colour NN	Shape NN	Images
[11]	CIELab with Otsu Thresholding	Cross -correlation based template matching	Video Stream

[12]	HSI Colour Space	DtB Vectors	Video Stream
[16]	HSI Colour Space with LUTs	Gradient Energy with Simulated Annealing and Canny edge detection	Images
[17]	HSI Colour Space	Hough Transform with Soble Operator	Images
[18]	HSV(Otsu's Thresholding)	Circular Shapes with FRS	Images
[19]	RGB colour space	Background Shape Histogram	Images
[24]	HSI and RGB Colour Spaces	Hough Transform	Video Stream
[26]	HSI Colour Space	DtB Vectors	Video Stream
[29]	RGB Colour Space	Shape features with Hopfield neural Network	Video Stream
[30]	HSI Colour Space	FFT with 2-D homography	Video Stream
[32]	YCbCr Colour Space	RANSAC	Video Stream
[33]	HSL Colour Space	Horizontal and Vertical Histogram	Images
[35]	HSV with SVM	Canny Edge Detector	Images
[40]	HSI Colour Space	DtB Vectors with Linear SVM	Video Stream
[41]	HSV Colour Space	Fuzzy Shape Recognizer	Images
[49]	HSI Colour Space	DtB Vectors	Video Stream
[52]	HSI Colour Space	Fast Fourier Transform	Images

[54]	RGB Colour Space	Haar Wavelet features and AdaBoost	Video Stream
[56]	RGB Colour space	Hough Transform and Directional Gradient Information	Video Stream
[58]	RGB with a Quad Tree based region of interest locating algorithm	Hough Transform with Confidence-Weighted Means Shift Algorithm	Video Stream
[60]	HSV Colour Space	Canny-Deriche edge Detector with RANSAC	Images
[61]	HSV Colour Space	Area and ratio of width and Height	Images

Table 2.1: A Taxonomy of Road Sign Detection Algorithms

Notes: Complete bibliographic references are given in the References (Pages: 138-151).

Reference No.	**Content Recognition**	**Tracking**	**Stream Type**
[4]	SVM with a Gaussian kernel	No	Video Stream
[11]	Normalised Cross Correlation based rules	Centre of the symmetrical shape to determine the area of sign in the next frame	Video Stream
[12]	SVM with Gaussian kernel	Kalman Filter	Video Stream
[17]	RBF with K-d Trees	No	Images
[26]	SVM with Gaussian kernel	Kalman Filter	Video Stream

[28]	MLP Network	Predicting the position of the object with reference to previous frame	Video Stream
[32]	feed forward MLP neural network	No	Video Stream
[35]	corners and statistical shape contexts	No	Images
[45]	DCT and SVD with ANN, k-NN, and Naive Bayes models	No	Images
[54]	Bayesian Generative Modelling	Simple Motion Model with Temporal Information Propagation	Video Stream
[56]	Template Matching	Kalman Filter	Video Stream
[58]	SimBoost	Random Affine Transformation With Normalised Cross-correlation	Video Stream

Table 2.2: A Taxonomy of Road Sign Recognition and Tracking Algorithms

Notes: Complete bibliographic references are given in the References (Pages: 138-151).

Taxonomy provided in Table 2.1 and 2.2 shows the varying range and combinations of algorithms utilised by *RSDR* systems in the literature within the three key stages (see Figure 2.1). Colour based segmentation is achieved by using different colour models, Shape is also considered as an important feature of the road sign representation and Contents are recognised by utilizing various feature extraction techniques and classifiers. The next section briefly summarises the *RSDR* literature providing conceptual details of the utilised algorithms.

2.2. *RSDR* Literature

Although a complete review of *RSDR* literature is beyond the scope of this thesis; a significant proportion of key approaches used in road sign detection, recognition and tracking are detailed below:

2.2.1 Road Sign Detection

Road sign detection is carried out by using colour and shape information of the road sign. This section provides summary of the approaches adapted to achieve this task.

M. Bénallal and J. Meunier [3]

The RGB values are extracted by studying the changing behaviour of the road sign colour at different timings of the day. The segmentation of the road sign is achieved by using the algorithm detailed in Figure 2.2. The RGB colour space is the primary colour space used in computers to display colour images. In subsequent research work the RGB colour space has experimentally [68] been found to be non-robust in segmenting objects from outdoor environments with changing lighting conditions. Especially when varying lighting conditions generate different shades of colour on a road sign and RGB colour space has been found to be sensitive to reflections and shades.

$$For\ all\ pixels\ i\ in\ image$$
$$\{If\ R_i > G_i \& R_i - G_i \geq \Delta_{RG}; R_i - B_i \geq \Delta_{RB}$$
$$Then\ pixel\ i\ is\ RED$$
$$Else\ If\ G_i > R_i \& G_i - R_i \geq \Delta_{GR}; G_i - B_i \geq \Delta_{GB}$$
$$Then\ pixel\ i\ is\ GREEN$$
$$Else\ If\ B_i > G_i \& B_i - G_i \geq \Delta_{BG}; B_i - R_i \geq \Delta_{BR}$$
$$Then\ pixel\ i\ is\ BLUE$$
$$Else\ pixel\ i\ is\ white(or\ black)$$
$$Endif\}\ EndFor$$

Figure 2.2: Road Sign Colour Segmentation Algorithm for red, green and blue signs [3]

A. Broggi, P. Cerri, P. Medici, P. P. Porta and G. Ghisio [6]

In this paper the road sign detection is carried out by using the *RGB* colour space along with Pattern matching and edge detection used for shape evaluation. The colour based segmentation is carried after a pre processing stage which consists of light source identification and chromatic correction of the image. The light source identification is achieved by analyzing the colour of the road surface. Subsequently a chromatic equalization constituting of a linear gamma correction stage is applied to reduce the computational time. A merge and split method is introduced on all signs if the height of the segmented image is double in size as compared to the width. The shape evaluation consists of two stages; at first stage a simple *pattern matching* is applied on the resample images. The second stage consists of *remarks about edge* of the segmented image which starts from the centre of the image and expanding towards its borders at several directions.

X. Gao, K. Hong, P. Passmore, L. Podladchikova and D. Shaposhnikov [8]

In this paper colour segmentation is proposed by using *CIECAM* while considering sunny, cloudy and rainy outdoor conditions. The viewing conditions are determined by using the texture of the road surface and saturation of the sky colour. The comparison of *HSI* and *CIELUV* colour spaces is also presented. The accuracy figures for sunny, cloudy and rainy conditions are recorded as 94%, 90% and 85% respectively.

M. Shneier [9]

In this paper a road sign detection and recognition system is presented and applied on video streams. The road sign detection is carried out in the *RGB* colour space by constructing a binary image where 1's represent the pixels belonging to the candidate sign. The candidate road signs are further processed for the subsequent recognition stage with the help of erosion, dilation and aspect ratio of the blobs in the binary image. The

recognition of the candidate signs is achieved by template matching. Recognition accuracy of 78% has been recorded overall.

V. Andrey and K. H. Jo [19]

The paper proposes an algorithm for road sign detection and recognition while considering informative, advisory and obligatory road signs. The sign detection is based on colour segmentation which is achieved by using the *RGB* colour space. The candidate shape analysis is carried out using a background shape histogram as shown in the Figure 2.3. Shape of each candidate sign was resized to the shape of the template sign and the difference between them was used to predict the actual road sign shape. The inner area of the road sign is obtained by creating a binary mask and the recognition is achieved by applying template matching.

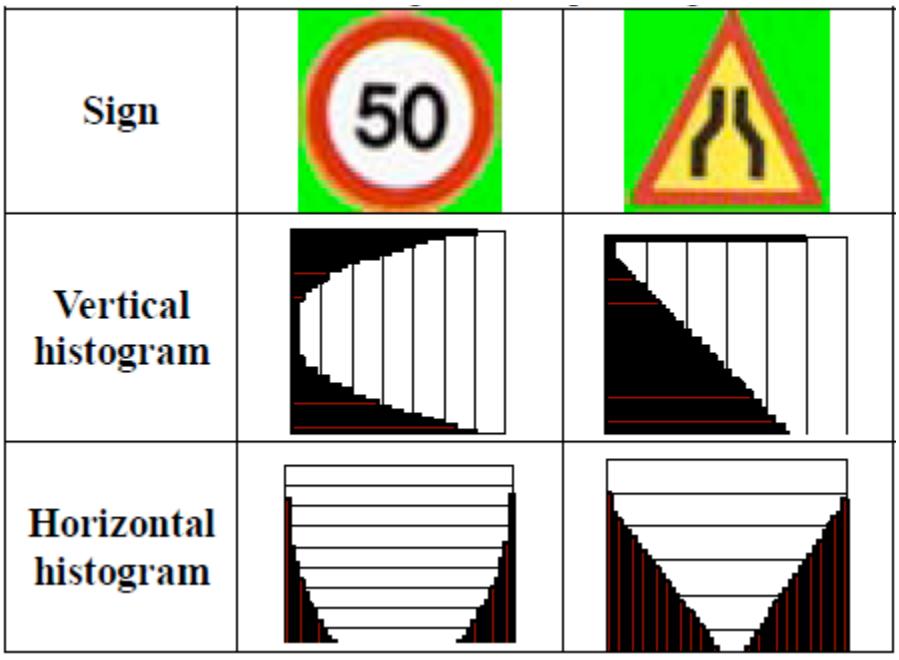

Figure 2.3: Background Shape Histogram[19]

H. Huang, C. Chen, Y. Jia, and S. Tang [24]

A two-stage automatic detection and recognition algorithm for circular road signs found in china was presented in this paper. The first stage consists of detection of road signs by using its colour and shape properties. The colour of the road sign is extracted by using both *HSI* and *RGB* colour spaces. The shape determination of the road sign is carried out on the extracted binary regions where circular shapes are studied by employing Hough Transform. The second stage named as road sign recognition consists of pre-processing and recognition steps. Pre-processing is further divided into Pictograph segmentation and edge map detection. Pictograph segmentation is basically an extraction of content area which is carried out by employing *Otsu's threshold and Niblack algorithms*. Edge map detection is carried out on the segmented pictographs and the output is normalised in the square sized image for final recognition stage. The recognition step is carried out on the outputs of the pre-processing stage by using *Adaptive Hausdorff Distance based on Similarity Weights*.

G. H. Kim, H. G. Sohn and Y. S. Song [29]

A vehicle-based mobile mapping system to maintain and updated transportation database system is presented in this paper. Colour regions of the road signs are extracted by using adaptive threshold parameters of *RGB* colour space. Edges that belong to road signs are detected and located by employing Hopfield neural networks. The triangular and rectangular road sign models are represented as two intersection edges. The five measuring features defining these models are shown in the Figure 2.4.
The contents of the road signs are identified by applying seven invariant moments which were found independent to scale and rotation of the road sign. The geometric characteristics of the road signs are added to the system to increase the classification accuracy which was recorded to be 99%.

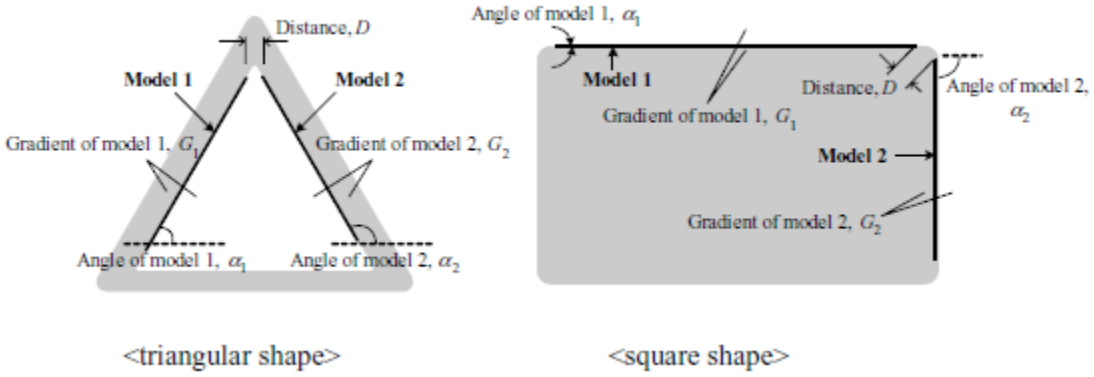

Figure 2.4: Model of triangular and square shaped road signs using Hopfield neural network [29]

S. M. Bascon, S. L. Arroyo, P. Siegmann, H. G. Moreno and F.J. A. Rodrıguez [30]

A traffic sign detection and recognition system for inventory purposes is presented in this paper. The colour segmentation is carried out by employing the *HSI* colour space due to its robustness to outdoor light variations. A *Support Vector Machine (SVM)* based method is used to classify the pixels of an image that helps in the extraction of the colour information. The shape of the road sign object and its location in the image are the performed tasks in the detection block of the system. Normalised *Fast Fourier Transform (FFT)* is used to determine the shape where as *2-D homography* is utilized to identify the location. The recognition stage consists of a *SVM* with a *Gaussian kernel* where the inputs are normalized gray level images of square size.

H. Fleyeh [41]

A novel fuzzy approach for traffic sign detection and recognition is presented in this paper. A colour based segmentation algorithm was carried with the conversion of *RGB* images to *HSV* colour space due to its invariant nature to the change in lighting conditions. Seven fuzzy rules were applied to detect and segment a particular colour from the image while using Hue and Saturation components of *HSV* colour space as shown in

the Figure 2.5. These images are normalised into square sized images for the development of fuzzy shape recognizer.

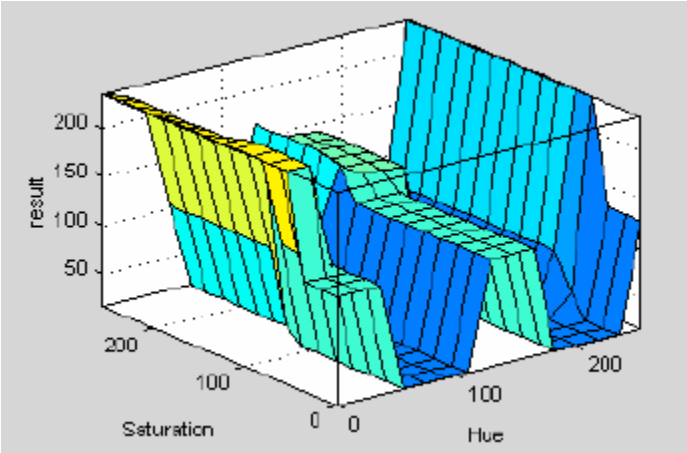

Figure 2.5 The Fuzzy System Surface [41]

Four shape measures are used for circular, triangular, rectangular and octagonal shapes by employing affine moment invariants. A fuzzy shape recognizer is used for the classification of the road sign contents which consists of five fuzzy input variables and one output variable. The best performance is noted as 95% for the images collected in the sunny conditions and/or well lit up road conditions.

2.2.2 Road Sign Recognition and Tracking

This section provides summary of the approaches adapted to achieve content recognition and tracking of the road signs.

S. M. Bascón, S. L. Arroyo, P. G. Jiménez, H. G. Moreno and F. L. Ferreras [4]

The paper presents a road sign detection and recognition system that addresses challenging outdoor environmental conditions such as occlusion, different scales and varying illumination conditions. The detection of the road sign is initiated by converting the acquired images from *RGB* colour space to *HSI* colour space. The images are captured in different lighting conditions and various camera sources have been used to

acquire them. The segmentation of the road signs using colour information is achieved by using fixed threshold values. These threshold values are obtained by generating histograms of all three components of *HSI* image. Colour based segmentation (Chromatic Segmentation) and achromatic segmentation (White & Black colours) are independently dealt within the system. The approach adapted to segment road signs during night time is based on the *HSI* colour space. The selection criteria of the segmented road signs is derived according to size and aspect ratio of the object. The objects not meeting these selection criteria are ignored as false positives or noise. The selected potential objects of interest are passed through a shape classifier which uses *DtB* with linear SVM classifier. The shape classifier reduces the false detections of the segmentation process and reduces the computational cost of the road sign recognition stage. The *DtB* vectors shown in Figure 2.6 are claimed to be invariant to translation, scale and rotation. The scheme acquires images from various camera sources which use different image/video capturing systems such as *NTSC*, PAL etc. These systems use various Gamma values which therefore need to be adjusted before applying the colour segmentation algorithms. It was reported in the paper that the *DtB* vectors occasionally fail to detect the octagonal shapes which contains obligatory STOP signs. The recognition stage consists of a SVM with a *Gaussian kernel* where the inputs are normalized, square, gray level images. In [49] the recognition of the road signs has been achieved by employing a one-versus-all SVM classifier with a Radial basis function (*RBF*) kernel. In [12] tracking of road signs is introduced which is shown to be a non-trivial task due to presence of relative motion between camera, static road signs and the background environment itself. Kalman filter and Alpha-Beta-Gamma ($\alpha - \beta - \gamma$) filter are the fundamental tools used to achieve the tracking of object in successive frames. A predictive filter that consists of fundamental steps i.e. initialisation, prediction and correction, is used. Initialisation step locates the initial position of an object in the image. The prediction step estimates the position of an object at time $t + 1$. The correction step corrects the previously predicted position of the candidate sign with its real position measured by utilising detection and recognition systems.

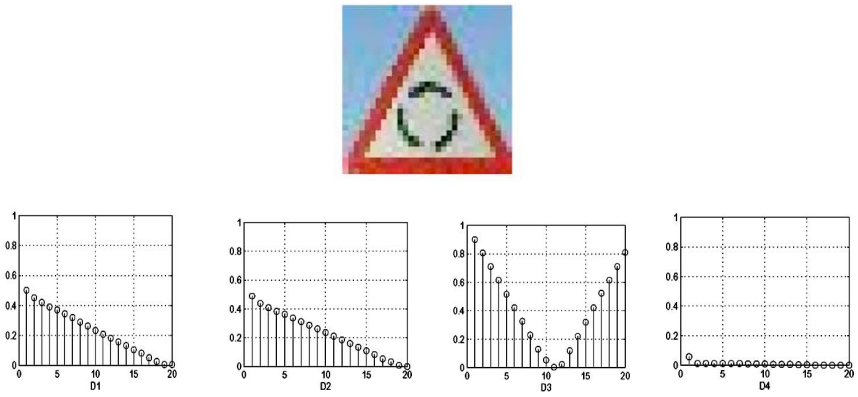

Figure 2.6: DtB vectors for the triangular sign [4]

R. Malik, J. Khurshid and S. N. Ahmad [5]

The paper described road sign detection technique which uses HSV colour space and Fuzzy shape descriptor. The system is initiated with the transformation of the RGB image to HSV colour space and threshold range is used to extract only red colour road signs. The binary image is produced where white regions reflect the candidate sign and black regions representing the background. The 8-connected white regions are labelled as same class considering them to be a candidate sign. Area filtration is introduced to filter out those white regions which satisfy a certain threshold size range. The shape measures of the filtered region are calculated by employing Fuzzy Shape Descriptor which uses the area and centre of the mass properties of the input region. Only two shape measures are considered for the experiments consisting of Triangular and Circular shapes. Total of 100 images are tested from which 96% and 94% accuracy figures were calculated for colour segmentation and shape detection respectively. The paper presents an effective approach towards road sign detection system but has ignored some of the key factors which can be used to enhance this effectiveness. The *red* colour which is the only colour considered during the research has found most varying colour during the day time. In HSV colour space as the H (Hue) component representing *red* colour at very start or at the end of its circular colour gamut. Due to change in the lighting conditions the threshold values needs to be adjusted in an adaptive way so that the colour can be extracted more effectively.

G. K. Siogkas and E. S. Dermatas [11]

The paper described a complete automatic imaging system for road sign detection, tracking and classification. The detection module initiates with colour based

segmentation which is achieved by transforming *RGB* images to *L*a*b* colour space and using Otsu's thresholding algorithm. The fast radial symmetry detection method is employed on four chromatic coefficients for the scanning of symmetric road sign shapes. The determination of shape is carried out by localising the centre of symmetric shapes and performing cross correlation based template matching. Circular shapes of the road signs were the only considered shapes in this research work. The rest of the symmetric shapes were determined and separated by adjusting the radial strictness factor α. The tracking of the road signs is designed to utilize the centre coordinates of symmetrical shapes to determine the area of the road sign in the next frame of the video stream. The classification module uses normalised cross correlation rules on the successfully detected symmetrical shapes as candidate road signs. The detection and classification accuracies of the road signs are recorded as 95.3% and 81.2% respectively.

W. J. Kuo and C. C. Lin [17]

This paper presents a road sign detection and recognition method that uses a two-stage classification strategy. The road sign detection is achieved by using road sign colour and shape information. The colour information of the road sign is extracted with the help of the *HSI* colour space and an anisotropic diffusion method is adopted to reduce the noise in the image. The circular and triangular road sign shapes are considered for geometric analysis, which is initiated by obtaining an edge map using Soble operators. For triangular signs Hough lines are obtained and its intersection with the edge map is used to estimate the candidate region. Circular Hough transform is used for circular shapes by estimating the centre of the object. The median filtration and dilation processes are used to remove noise and to obtain the extended candidate region. The candidate regions are normalised to 100×100 pixel images by using bi-cubic interpolation for the recognition stage. The recognition is achieved in two-stages; First a Radial Basis Function (*RBF*) neural network is utilised to classify the group of the road signs to reduce the error rate and actual recognition is achieved subsequently by using *K-d* trees. The recognition accuracy recorded was 92.45% and 97.78% for triangular and circular road signs respectively.

M. L. Eichner and T. P. Breckon [32]

A speed limit sign detection and recognition system from a real-time video sequences is presented in this paper. The proposed system is a two stage process; robust detection and then classification of the speed limit signs. The colour and shape information are used to detect the road sign from the video frames. The colour segmentation is carried out by employing adaptive threshold of *YCbCr* colour space that helps to segment the red circles of the speed signs from the scene. *RANdom Sampling And Consensus (RANSAC)* is adopted for the geometric shape detection (i.e. Circle). The recognition stage consists of two steps: candidate normalization and the use of a Neural Network. *Candidate normalization* step uses gray level image and transforms them into their binary representation. A *feed forward multi-layer perceptron neural network* consists of 400 neurons in the input layer is used to classify the speed limit signs.

H. M. Yang, C. L. Liu, K. H. Liu, and S. M. Huang [45]

The paper proposed a traffic sign detection and recognition system in images captured from unfavourable environmental conditions. The red colour road signs are considered in this research where the colour segmentation is carried out by using *RGB* colour space. A Laplacian of Gaussian (*LoG*) edge detector is applied to group the red pixels and subsequently the 8-connected neighbourhood principle is used to determine which pixels belong to the connected object(s). Similarly the objects with inappropriate height/width ratios are removed by considering them as noisy objects. The traffic sign recognition is followed after normalizing the images where Discrete Cosine Transform (*DCT*) and the Singular Value Decomposition (*SVD*) procedures are used for extracting the features of the ideographs. The pattern recognition task is carried out by investigating the effectiveness of artificial neural networks, *k*-nearest-neighbor (kNN) and naive bayes models.

N. Kehtarnavaz and A. Ahmad [46]

Traffic sign recognition in noisy outdoor scenes is presented in this paper by using both colour and shape attributes. *RGB* images are transformed to *YIQ* colour space to segment the desired colour components which are later fed into an Adaptive Resonance Theory 2 (*ART2*) neural network. The rotation and scale variances of segmented binary image are analysed by using a log-polar-exponential grid and Fourier Transformations. A back propagation neural network is trained and tested to distinguish the signatures of different traffic signs.

A. Ruta,Y. Li and X. Liu [56]

In this paper a comprehensive approach to traffic sign detection, tracking and recognition from video inputs was presented. The detection stage uses the *RGB* colour space to generate a colour-enhanced image that is subsequently utilised for '*Haar'* wavelet feature extraction. A generalised Hough Transform is introduced to detect the shape of the obtained sign where as equiangular polygons shapes are detected by using directional gradient information. A three stage tracker uses colour and shape information for *Kalman filter* to localise the search region of the candidate sign. The recognition is achieved according to the maximum likelihood approach by using template matching. The recognition rate is recorded of being 93% of accuracy with a processing speed of 20-25 frames per second.

2.3. Summary and Conclusion

In this chapter, existing algorithms in the *RSDR* domain have been briefly introduced and analysed. Section 2.1 provided taxonomy of the state-of-the-art approaches used in road sign detection and recognition; it is obvious that *RSDR* is a relatively unexplored research area that can benefit from further research. The image segmentation can be improved by introducing pre processing stages for colour correction and image enhancement. Further to that a selection of optimum colour spaces or a combination of

colour spaces can improve the colour segmentation task. A feature extraction technique to represent geometrical features and contours of all possible shapes of the road sign can enhance the accuracy in the detection stage. The recognition stage can be improved in terms of accuracy and computational cost by introducing *LESH* with *SVM* which are having capability to identify similar feature within maximum likelihood areas.

Considering the above shortcomings of the existing algorithms, a number of novel approaches to *RSDR* have been proposed in chapters 4 to 7. Chapter 3 introduces the reader to some fundamental concepts of the techniques used within the contributory chapters (*see chapters 4 to 7*).

Chapter 3

Research Background

3.0. Introduction

Road sign detection and recognition algorithms proposed in this thesis attempt to overcome the limitations of the existing approaches and provide practical solutions. This chapter introduces the reader to the fundamental concepts, theories and techniques on which the proposed algorithms are defined.

For the clarity of the presentation this chapter is divided into several sections. Section 3.1 introduces the foundations of the six colour spaces analysed and used in chapter 4 and 5 for colour based road sign region of interest segmentation. It also introduces the popular standard video systems by which our images/videos are captured. Section 3.2 introduces the data mining tool WEKA [84], its working environment and relevant functionality upon which our Combined Colour Model is constructed. Section 3.3 introduces the theory of Contourlet Transform [53] on which the shape detection algorithm proposed in Chapter 6 is based. Finally section 3.4 summarises providing a brief conclusion.

3.1. Colour Spaces

This section introduces computer based colour spaces used within this thesis to represent colour pixel values and their inter-colour space conversion in particular to commonly used RGB representation. The following sub sections introduce six popular colour spaces, their conversion from RGB colour space and their usability in various practical application domains. The section also presents three different video representation formats used in digital media and printing industry.

3.1.1. The RGB Colour Space

RGB (Red, Green, and Blue) colour space is the basic colour space widely used in the digital representation of colour picture elements, i.e. pixels. It is represented in the form of a cube in the Cartesian coordinate system in which the x, y and z axes are respectively represented by R, G and B colour components [69]. For a given digital colour image C, RGB vectors are used to represent each pixel (x, y) as defined in equation 3.1.

$$C(x, y) = (R(x, y), G(x, y), B(x, y))^T = (R, G, B)^T \quad (3.1)$$

$(R, G, B)^T$ is an explicit combination the three vector values representing one particular colour in the RGB colour space.

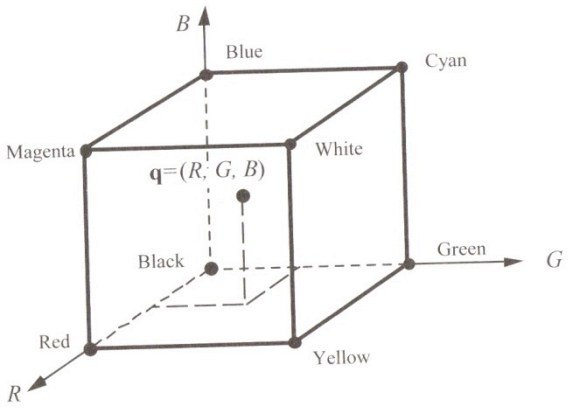

Figure 3.1: RGB colour cube, $q = (R, G, B)$ vector represents a unique colour value [71].

Figure 3.1 shows RGB colour cube in which R, G and B channels are forming the three dimensional vector space. In a 8-bit / byte word the minimum value of any RGB channel is represented by 0 and maximum by 255. The RGB colour space is also considered an additive colour space due to its ability to form various shades of colours by combining different intensities of the three primary colours i.e. R, G and B. In particular in the RGB colour space an all-zero vector represents a pixel of black colour and a all-one vector represent a pixel of colour-white. For further details on the RGB colour space and their use in digital and print media, readers are referred to [71] and [83].

3.1.2. The HSV Colour Space

HSV (Hue, Saturation and Value) colour space belongs to the group of perception based colour spaces and is fundamentally based on the human perception of colours. HSV colour space is mostly utilised in the fields of computer vision and computer graphics. Figure 3.2 illustrates the standard representation of the HSV colour space, where figure 3.2(a) represents the HSV colour gamut in which the H (Hue) component defines the fundamental colour of a pixel and its shades. Different shades and colours are defined and represented when moving anti clock wise from 0 degrees to 360 degrees. S (Saturation) defines and represents the number of pixels available to represent a given colour. S increases towards the edge of a circular cross section of the cone and decreases towards the centre. 1 and 0 represents the highest and lowest saturation of a colour, respectively. V (Value) contains the information related to the brightness or darkness of a pixel. V increases when moving towards pixels with higher intensity values and vice versa. 1 and 0 represents the highest and lowest intensity values of a colour, respectively.

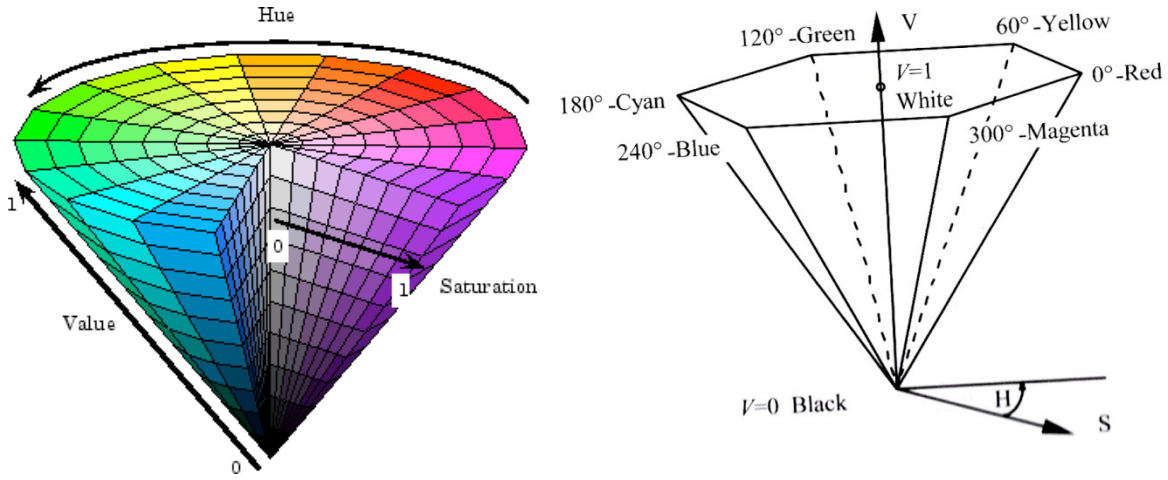

(a) **(b)**

Figure 3. 2: HSV colour space, (a) HSV colour gamut [80] (b) HSV colour gamut representing angular values of different colours [71]

Figure 3.2 (b) illustrates how the H component, using angular values, define all colours that the HSV colour gamut can represent. Its circular gamut starts and ends at the same colour, which is Red colour found at 0^o and 360^o. Moving anti clock wise in the HSV

gamut the colours, Yellow, Green, Cyan, Blue, Magenta are represented at 60^o, 120^o, 180^o, 240^o and 300^o respectively.

An image represented in the RGB colour space can be converted to an image represented in the HSV colour space using the equations 3.2, 3.3 and 3.4 below [65].

$$H = cos^{-1}\left(\frac{0.5\,(R-G)+(R-B)}{\sqrt{(R-G)^2+(R-B)(G-B)}}\right) \tag{3.2}$$

$$S = 1 - \left(\frac{3}{R+G+B}\right) min(R,G,B) \tag{3.3}$$

$$V = max\,(R,G,B) \tag{3.4}$$

There are inherent dependencies between the three HSV components. H component will have no significance when S or V are representing by the lowest value i.e. 0. The colour will be shown black if V component is represented by the lowest value. Pure white colour is obtained when the V component is represented by the highest value, i.e. 1 and S component is represented by the lowest value, i.e. 0. For further useful reading on the HSV colour space readers are referred to [71] and [83].

3.1.3. The CIElab Colour Space

CIE (Commission Internationale de l'Eclairage) $\boldsymbol{lab}$ is a uniform colour space [71] used mostly to describe the body colours (non luminance materials) of components. The$'$ $\boldsymbol{lab}'$ represents one luminance component $\boldsymbol{l}$, and two chrominance components $\boldsymbol{a}$, and $\boldsymbol{b}$. The $\boldsymbol{a}$, component represents two colours; $green$ and red respectively at negative $(-a)$ and positive $(+a)$ ends. The $\boldsymbol{b}$, component also represents two colours; $blue$ and $yellow$ respectively at negative $(-b)$ and positive $(+b)$ ends. The above is illustrated in figure 3.3.

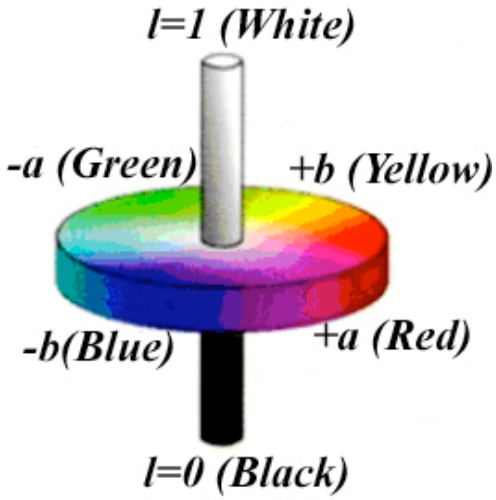

Figure 3.3: $CIElab$ colour space

The conversion from RGB to $CIElab$ colour space is a two-fold process. Firstly the RGB colour space is converted to an intermediate XYZ colour space. The intermediate components are subsequently used to convert to the CIE lab colour space. Equations 3.6 and 3.7 represent the relevant mathematical formulae used.

$$\begin{pmatrix} X \\ Y \\ Z \end{pmatrix} = (M) \begin{pmatrix} R \\ G \\ B \end{pmatrix} \tag{3.5}$$

Where,

$$(M) = \begin{pmatrix} S_r X_r & S_g X_g & S_b X_b \\ S_r Y_r & S_g Y_g & S_b Y_b \\ S_r Z_r & S_g Z_g & S_b Z_b \end{pmatrix} \tag{3.6}$$

$$\begin{aligned} l &= 116.Y^* - 16, \\ a &= 500.(X^* - Y^*), \\ b &= 200.(Y^* - Z^*) \end{aligned} \tag{3.7}$$

For further details on the $CIElab$ colour space, the readers are referred to [71] and [74].

3.1.4. The YIQ Colour Space

The ***YIQ*** (Luminace, In-phase, Quadrature) colour space is popularly used in television systems utilising the $NTSC$ video format. The colour information is represented by using I and Q components of the YIQ colour space (see figure 3.4). Note that I and Q values are normalised between -1 and 1.

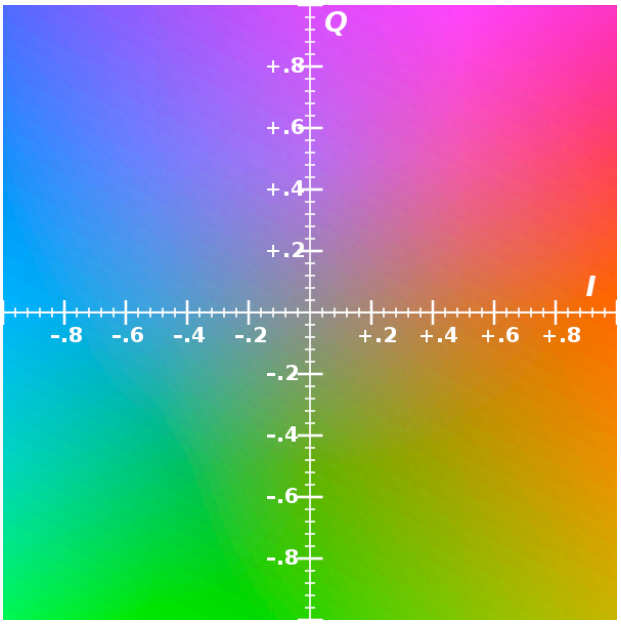

Figure 3.4: YIQ Color space in the IQ plane, where Y = 0.5 [72]

I (In-phase) represent cyan colour at the negative horizontal edge and yellow colour at the positive horizontal edge. Q (Quadrature) on the other hand presents green colour at the negative vertical edge and magenta colour at the positive vertical edge. Colour shades can be extracted by adjusting In-phase and Quadrature values while moving along horizontal and vertical directions. White colour can only be extracted at the intersection point of I and Q components and by adjusting the Luminance (Y) component to its maximum value, i.e. 1. Black colour can be obtained in a same way by adjusting the Y component to its minimum value, i.e. 0. For further reading of the YIQ colour space's usage in NTSC television systems readers are referred to [71], [72] and [83].

An image represented in the RGB colour space can be converted into the YIQ colour space by using the equation 3.8.

$$\begin{pmatrix} Y \\ I \\ Q \end{pmatrix} = \begin{pmatrix} 0.299 & 0.587 & 0.114 \\ 0.596 & -0.274 & -0.322 \\ 0.211 & -0.523 & 0.312 \end{pmatrix} . \begin{pmatrix} R \\ G \\ B \end{pmatrix} \tag{3.8}$$

3.1.5. The YC_bC_r Colour Space

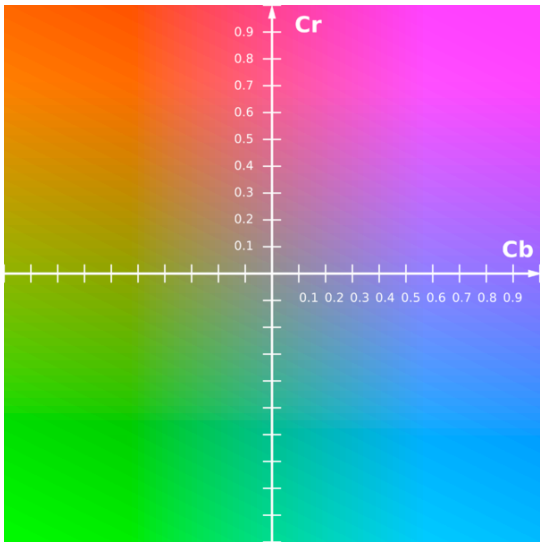

Figure 3.5: YC_bC_r colour space in C_bC_r plane where $Y = 0.5$ [73]

$\boldsymbol{YC_bC_r}$ colour space is increasingly gaining importance in the area of digital video representation, transmission and processing. It was originally developed for the pixel colour representation related to the newer television formats but does not support HDTV (High Definition Television) format. It is similar to YIQ and YUV colour spaces, which were also developed to work with digital television representation formats. The Y component represents Luminance while C_b and C_r components represent the chrominance of a pixel.

The conversion of a pixel represented in the RGB colour space to the YC_bC_r colour space is defined by equation 3.9.

$$\begin{pmatrix} Y \\ C_b \\ C_r \end{pmatrix} = \begin{pmatrix} 16 \\ 128 \\ 128 \end{pmatrix} + \frac{1}{256} \begin{pmatrix} 65.738 & 129.057 & 25.064 \\ -37.945 & -74.494 & 112.439 \\ 112.439 & -94.154 & -18.285 \end{pmatrix} . \begin{pmatrix} R_N \\ G_N \\ B_N \end{pmatrix} \quad (3.9)$$

YC_bC_r colour space in C_bC_r plane is presented in figure 3.5 where C_b and C_r are plotted along the x-axis and y-axis respectively, with values ranging in between -1 and 1. It is assumed that the RGB image is Gamma Corrected before the transformation to YC_bC_r colour space is carried out. Readers interested in further details of the YC_bC_r colour are referred to [71] and [73].

3.1.6. The CYMK Colour Space

CYMK colour space is commonly used in colour printers for printing purposes. It is a subtractive colour space in which primary colours are Cyan, Magenta, Yellow and Black (Karbon). Figure 3.6 represents a CYMK colour cube where as transformation from RGB colour space to CMYK colour space is presented in equation 3.10.

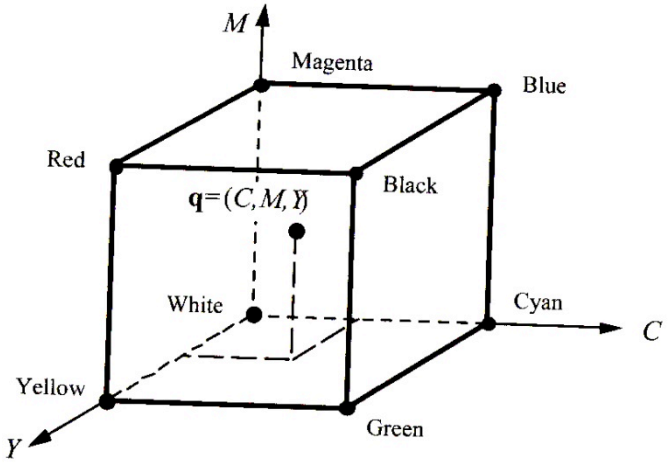

Figure 3.6: CMY(K) colour cube [71]

$$\begin{pmatrix} C \\ M \\ Y \end{pmatrix} = \begin{pmatrix} G_{max} \\ G_{max} \\ G_{max} \end{pmatrix} - \begin{pmatrix} R \\ G \\ B \end{pmatrix} \tag{3.10}$$

Although Black colour, represented by the component K can be produced by overlapping Cyan, Magenta and Yellow; however a separate K component is used in the CMYK colour space for three essential reasons. Firstly the black ink is less expensive to manufacture than Cyan, Magenta and Yellow. Secondly if the overlapping process is used to produce black colour then three times more ink fluid is required and the drying time increases considerably as compared to using a separate black ink. The third reason is due to differences in mechanical tolerances as all three colours i.e. Cyan, Magenta and Yellow, do not print at the same place to produce the black colour. This difference is more visible in ink-jet and bubble jet printers where colour edges can be seen along black borders. For further reading on CYMK colour space readers are referred to [71] and [83].

3.1.7. The Digital Video Representation Systems

Video cameras capture and transmit/store videos by utilizing the standardized video representation systems such as NTSC, PAL or SECAM. NTSC (National Television System Committee) was developed in 1941 and is widely used in North America and Japan. The NTSC colour encoding provides 29.97 interlaced frames of video per second when used with a system M television signal [75]. PAL unveiled in 1963 is an acronym for Phase Alternating Line and is an analogue television encoding system developed in Germany. PAL television system is the standard television format used by the majority of the countries in the world and uses 625 lines and 25 frames per second [76]. SECAM is an acronym for *Séquentiel couleur à mémoire,* and it is an analogue colour television system introduced in France in the late fifties [77].

	PAL	**NTSC**	**SECAM**
$\boldsymbol{\gamma - value}$	2.8	2.2	2.8

Table 3.1: Gamma Values for television systems [71]

The videos and images used for the experiments presented in this thesis have used *Canon IXUS80IS* digital camera having a resolution of 2592×1944. This digital camera supports two video representation systems i.e. NTSC and PAL. The camera contains no features to disable the gamma correction, which means that images/videos captured are gamma encoded. Thus the captured images/videos are required to be gamma decoded according to display device and the video system selected for acquisition. Typical Gamma values of monitors ranges from 2.0 and 3.0. Table 3.1 shows gamma values used in different television representation systems. For further reading on different video representation systems and their possible effect on the display intensity, readers are referred to [71], [75], [76], [77], [81] and [109].

3.2. WEKA Data Mining Tool

WEKA [84] is a data mining tool which is a collection of data pre processing tools and state of the art machine learning algorithms. The WEKA [84] software package has been designed to provide the flexibility in fully analysing a dataset using a collection of implementations of a large set of most popular data processing and machine learning algorithms. WEKA [84] supports algorithms for preparation of input data, selection and evaluation of learning schemes statistically and at the end visualisation of the results with regards to data inputs.

WEKA [84] was introduced and developed at the University of Waikato based in New Zealand. It is an acronym for *Waikato Environment for Knowledge Analysis* and supports a diverse range of platforms including Windows, Macintosh and Linux. It supports to analyse data mining problems such as Regression, Classification, Attribute Selection and Clustering. Data is represented as single relational table in the 'ARFF format' which is accepted by all algorithms of the WEKA [84] tool as an input. ARFF is an acronym of *Attribute-Relation File Format*. An example is illustrated in table 3.2.

The ARFF file contains @RELATION, @ATTRIBUTE and @DATA mandatory fields where as comments can be included followed by % sign. @RELATION defines the

relationship of attributes and data in entire ARFF file. @ATTRIBUTE defines the type of data and actual order of their appearance in @DATA section. @DATA is actual data as defined in the @ATTRIBUTE section and each data field is separated with comma.

```
@RELATION Colour_Classification

@ATTRIBUTE C  NUMERIC
@ATTRIBUTE C  NUMERIC
@ATTRIBUTE M  NUMERIC
% @ATTRIBUTE A  NUMERIC

@ATTRIBUTE class {1,2,3}

@DATA

-0.336917,1.29002,-1.21949,1
-0.434601,1.183829,-1.26679,1
-0.555368,1.03141,-1.262202,1
-0.674794,0.864902,-1.226107,1
0.968457,0.224578,-0.254463,1
-0.044558,-0.431208,-0.38478,2
-0.168069,-0.27983,-0.428716,2
-0.303298,-0.081341,-0.466087,2
-0.416189,0.156447,-0.520429,2
0.320031,0.371116,-0.167772,3
0.13246,0.270437,-0.070438,3
-0.070251,0.162637,0.037398,3
-0.330352,0.078844,0.138324,3
```

Table 3.2: ARFF file for colour classification

There are four interfaces to interact with the WEKA [84] data mining tool, including three graphical user interfaces and one command line interface. The easiest way to interact with WEKA [84] is by using *Explorer* that provides a valuable graphical user interface. The interface provides data input/selection via drop down menus, selection buttons, radio buttons, check boxes and more over provides important and helpful tool tips for the usage of particular property. *Explorer* can be used for a small data set as it utilises main memory to load and process the data which is one of the fundamental disadvantage of its usage. The *Knowledge Flow Interface* is another graphical user interface that provides the facilities in terms of drag and drop boxes which includes data sources, pre processing tools, learning algorithms, evaluation methods and visualisation modules. Third graphical user interface is *Experimenter* which is a collection of regression and classification techniques. The *Experimenter* provides two modes, *simple* for less complex problems and *Advanced* for large scale statistical experiments. *Simple-CLI* (Command Line Interface) is a textual command based interface categorised as fourth interface of WEKA Applications. Further reading material related to WEKA Package can be found in [84] and [97].

3.3. Contourlet Transform

The Contourlet Transform [53] was originally introduced as an improvement over several inefficiencies of wavelet transform. Specifically it overcomes the lack of directionality of wavelet transforms and captures the geometrical smoothness of the contours in an image. Though the Contourlet Transform uses multi scale and time-frequency-localization properties of wavelets, in addition it offers image representation at multi- resolution, high degree of directionality and anisotropy. Figure 3.7 illustrates wavelet square support to capture the point discontinuities and Contourlets elongated support to capture linear segments of contours [53]. It shows that Countourlets approximate the contours more accurately.

The application of Contourlet Transform [53] consists of two filtering stages named as Pyramidal Filtering and Directional Filtering. The Pyramidal Filter is constructed based

on a Laplacian Pyramid (*LP*) [78, 95], which helps to obtain the multi scale decomposition of the image. The Directional Filter consists of a Directional Filter Bank (*DFB*) [79], which helps in obtaining the wedge-shaped frequency decomposition.

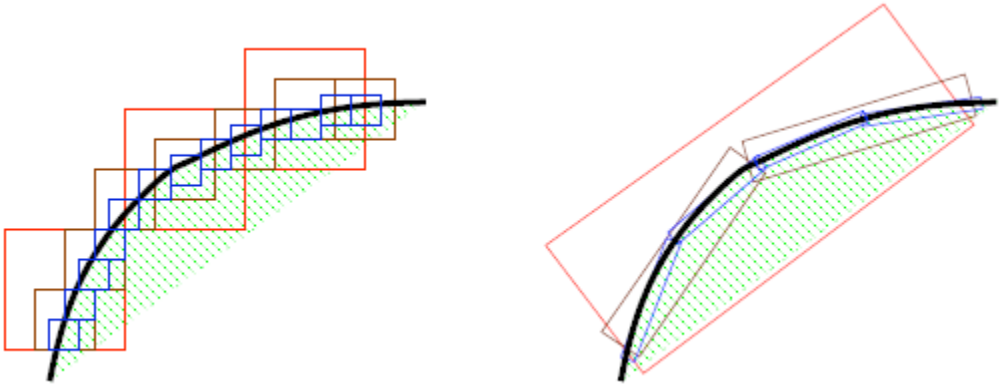

Wavelet Transform representation

Contourlet Transform representation

Figure 3.7: Illustration of wavelet square support to capture the point discontinuities and Contourlets elongated support to capture linear segments of contours [53]

The *DFB* utilises a two-channel quincunx filter bank [96] with a fan filter to obtain the horizontal and vertical directional frequency information. Secondly it uses a shearing operator to obtain the angular information. Pyramidal and directional filters utilise the commonly used filters such as *haar*, *5-3* (MacClellan transformed), *cd* and *9-7* (Cohen and Daubechies), *pkva* and *Burt* filters. The decomposition pyramid can create 2^n sub-bands, where n represents the number of levels. For example $n = 3$ produces eight band pass images by utilising the selected filter. In the construction of band pass images the *DFB* fan filter can adoptively be utilised to extract any particular directional information such as horizontal, vertical or both sides. Figure 3.8 illustrates the evolution of support sizes of a Contourlet function that satisfies the parabolic scaling [53].

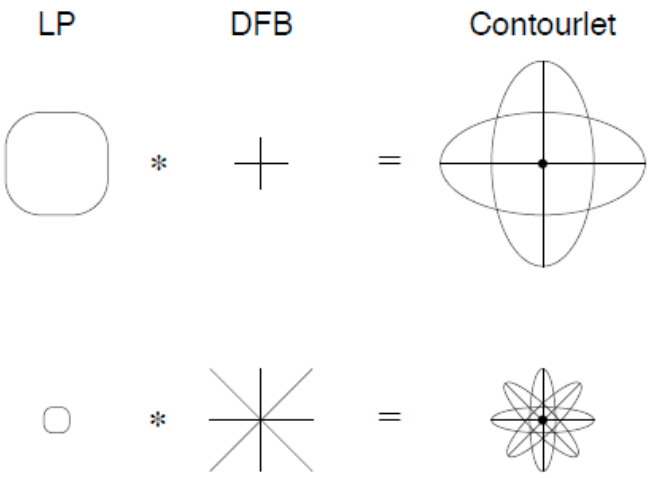

Figure 3.8: Illustrating the evolution of support sizes of Contourlet functions that satisfy the parabolic scaling [53]

3.4. Summary and Conclusion

This chapter has presented the fundamental theories, the adopted algorithms and the tools utilised in building the novel approaches to road sign detection and recognition presented in chapters 4 to 7. Section 3.1 presented the theoretical background of the colour spaces used for initial road sign Region of Interest (ROI) extraction within the research presented in this thesis. The conversion formulas and designated usage of the colour space is also presented. Section 3.2 provides a brief summary of the WEKA data mining tool and its interfacing environment. The WEKA package is utilised in the design and implementation of the Combined Colour Model (see chapter 5) and an example of data file in ARFF file format is also presented. Section 3.3 presents a summary of Contourlet Transform and its fundamental application structure and methodology. In this thesis the Contourlet Transform is utilised for the extraction of geometrical shape features (see chapter 6). The chapter also provides a number of references to the original research work that resulted in the development of the theory and practices used as background of the proposed work.

Chapter 4

Road Sign Segmentation Based on Colour Spaces: A Comparative Study

4.0. Preface

Significant amount of research has already been carried out towards providing practical solutions to automatic road sign detection. Due to the prominence played by colour, an obvious first step of an automatic road sign detection algorithm is colour based segmentation of regions of interest suspected to be road signs. A number of colour spaces have been utilized for this purpose. However due to the variations of colour as a result of illumination changes, bad weather conditions and fading due to exposure to sun-light, makes the threshold selection problem in any colour space a significant challenge. Chapter 2 (*Literature Review*) revealed that no previous work has been carried out to extensively investigate the robustness of threshold selection, when using different colour spaces in road sign detection. Rather the threshold values have been merely stated and used. In this chapter we have investigated the use of six colour spaces, specifically by recommending the threshold ranges that can be used to robustly segment road signs under different lighting and weather conditions.

For the clarity of presentation this chapter has been organised as follows: Apart from this section in which the research problem is defined and its practical relevance is highlighted, Section 4.1 introduces automatic road sign detection. Section 4.2 provides the methodology we have adopted in colour detection of the road signs. Section 4.3 presents the experimental setup and results obtained. A summary and conclusion is presented in Section 4.4.

4.1. Introduction

Road signs give important information to the road users, especially to 'drivers' and 'cyclists'. The meanings of these signs are very much dependant on their colour and contents included within. In this chapter we are only considering the colour information of the road signs. Primarily road signs are of colours, Red, Blue, Green, Brown, Yellow, Black or White, which signifies and categorises their importance (see Table 4.1), e.g. *red* for obligatory signs and *blue* for advisory signs. Therefore colour plays an important initial role in a typical road sign detection task. Due to varying lighting and weather conditions, the segmentation of road signs using colour information; especially in outdoor images is a significantly challenging task. Nevertheless a correct segmentation of these signs helps to recognise the contents and shape of the sign in the later stages. A detailed literature review carried out (see chapter 2) on automatic road sign detection and recognition revealed that even though a significant amount of research has been carried

Colour	**Location**	**Meanings**
Blue	City/Town Roads/Motorway	Advisory Signs/Information
Red	City/Town Roads	Prohibition/Danger
Yellow	Road Works (Towns/Motorways)	Construction/Road Woks
Brown	City/Town Roads/Motorway	Tourist Attraction/Viewable Places
Green	City/Town Roads	Directions

Table 4.1: Significance of Colour as a Notation

out in the general area of road sign recognition none of the published work has either considered the use of all available colour representation schemes in colour based segmentation nor attempted to provide a detailed comparison as to how different colour spaces perform under changes of illumination and weather conditions. Further the identification of various parameters and the segmentation thresholds that can be used in optimising the performance of various colour spaces has not been investigated. This chapter is an attempt to bridge this research gap with the ultimate aim of recommending

the best colour space to be used in automatic road sign detection, under varying conditions. The research results will also contribute generally to the area of object segmentation.

4.2. Methodology

Detailed investigations were carried out within six of the computer colour spaces (i.e., YCbCr, YIQ, RGB, CIElab, CYMK and HSV) detailed in chapter 3. The methodology presented in this section explains the procedure that has been followed to segment colour information of a road sign from a roadside scene. As illustrated in the block diagram of Figure 4.1 the raw images captured by the camera are initially pre processed which is presented in the section 4.2.1. The transformation of RGB images to HSV [65] colour space is carried out subsequently and it is explained in the section 4.2.2. Further analysis on the segmented objects is carried out after pixels of interest selection and it is presented in the section 4.2.3.

4.2.1. Pre Processing

RGB images captured by a digital camera are not always appropriate to perform the desired image processing tasks. Different video systems such as NTSC [75], PAL [76], and SECAM [77] that are used to capture the images significantly affect the original (i.e. raw) pixel intensity values by Gamma Encoding [81]. The Gamma is represented with the Greek letter γ , has encoding and decoding standard values according to the above mentioned video systems which are tabulated in the section 3.1.7 (see chapter 3). The videos/Images captured for experimental purposes within this thesis have adopted the NTSC [75] video system, which encodes gamma at the rate $\gamma = 1/2.2$. This non linearity in the videos/images is required to be decoded in order that the gamma corrected retains the original luminance of the image. Equation 4.1 is utilised for the purpose of gamma correction on to the source image supplied by the capturing device. The gamma corrected image is given by,

$$I_c = I_s^{\gamma} \qquad (4.1)$$

Where I_c *and* I_s, are representing gamma corrected and source images respectively and gamma correction γ is achieved on NTSC [75] video systems at $\gamma = 2.2$.

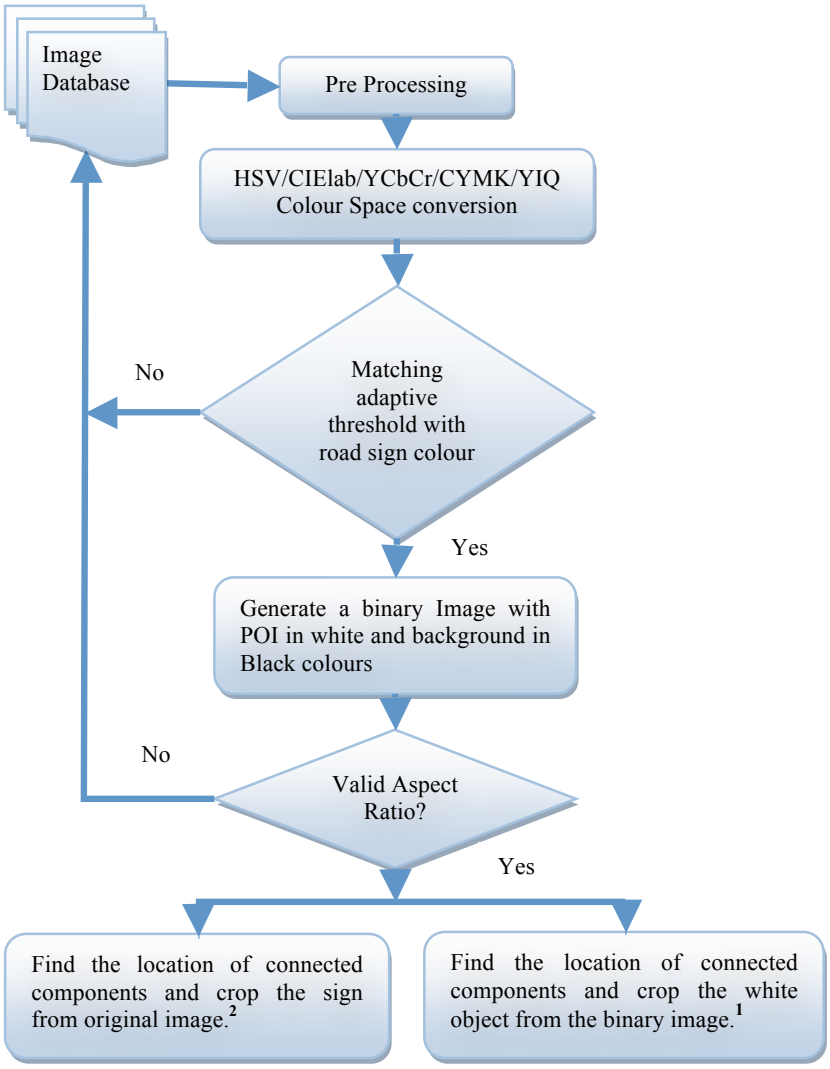

Figure 4.1: Road Sign Segmentation Procedure,

1. Objects used for shape classification (see chapter 6)

2. Objects used for content recognition (see chapter 7)

In Figure 4.2 the dotted line curve represents gamma encoding to the original image acquired by the image sensors. Gamma decoding procedure is presented with a smooth line curve. For the reader's understanding towards the effects of Gamma Correction on raw image considering various platforms can be viewed in [109].

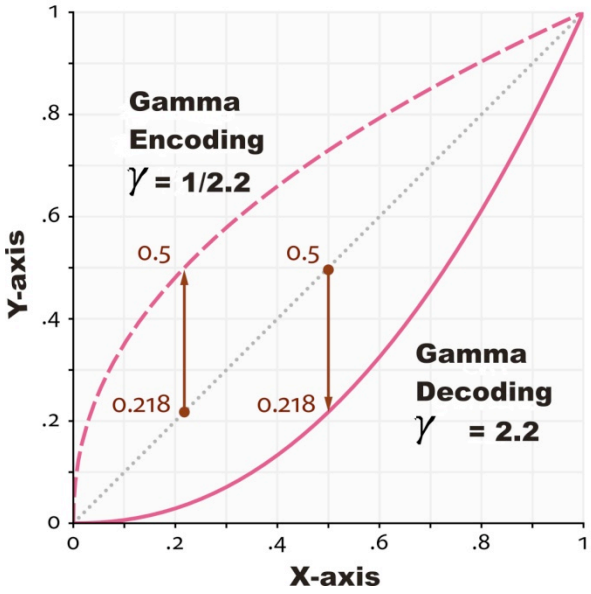

Figure 4.2: Gamma Correction

4.2.2. Pixels of Interest (POI) Selection

POI selection is carried out in the literature review (see chapter 2) by employing computer based colour spaces. The transformation from RGB colour space to other computer colour spaces is presented in section 3.1 (see chapter 3). In this section POI selection is carried out after transforming RGB image to HSV colour space image using the equations presented in [65].

$$H = \cos^{-1}\left(\frac{0.5\,(R-G)+(R-B)}{\sqrt{(R-G)^2+(R-B)(G-B)}}\right) \tag{4.2}$$

$$S = 1 - \left(\frac{3}{R+G+B}\right) min(R,G,B) \tag{4.3}$$

$$V = \max(R,G,B) \tag{4.4}$$

POI selection is carried out by using all three of the above components i.e. $H, S\ and\ V$. The H component contains the colour information and every colour represented by this component has an angular value in HSV colour gamut as presented in section 3.1.2 (see chapter 3). If $S\ and\ V$ components remain constant i.e. $S = 100\%\ and\ V = 100\%$ then Red colour pixels can be found at $0^o\ and\ 360^o$ as shown in Figure 4.3. Green

colour pixels can be seen at 120^o and Blue colour pixels at 240^o as shown in Figure 4.4 and Figure 4.5 respectively.

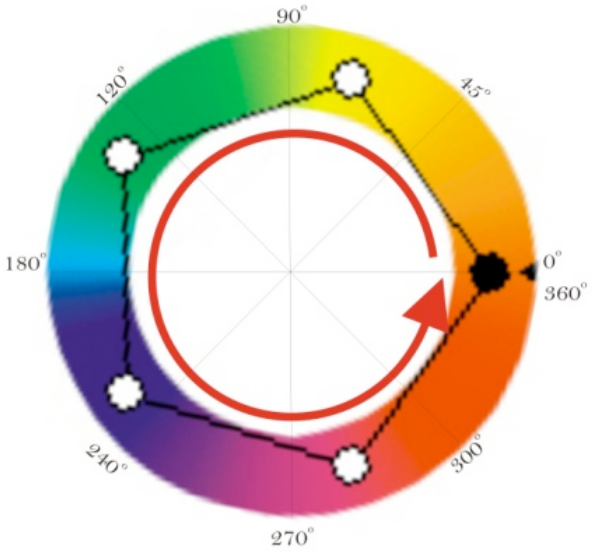

Figure 4.3: Hue of Red colour at 0^o and 360^o

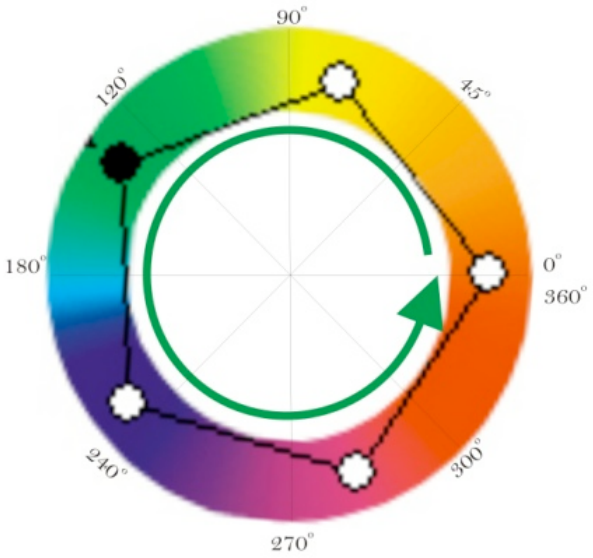

Figure 4.4: Hue of Green colour at 120^o

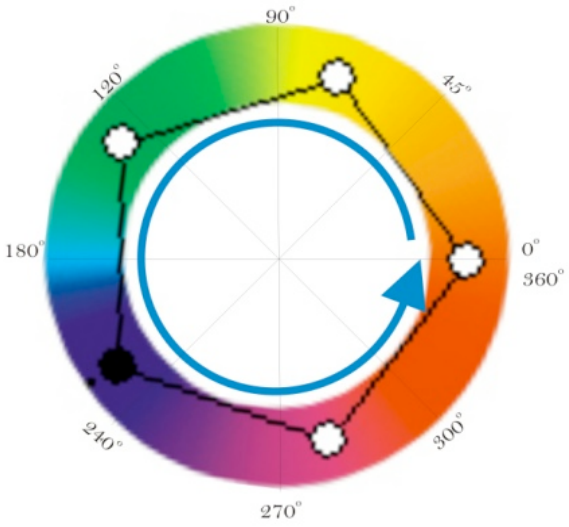

Figure 4.5: Hue of Blue colour at 240^o

Different shades of colour pixels can be obtained by changing the H component either clockwise or anti clockwise. For our experimental purposes we have assumed that each component of HSV, colour space has value ranging in between $0\ and\ 1$. To obtain the thresholds of H, colours in such a limited range we have numbered the basic colours $Red\ = 0\ and\ 3, Green\ =\ 1\ and\ Blue\ = 2$ as shown in the Figure 4.6. The next step to follow is to divide these assigned values by 3 to achieve H colours thresholds normalised in the range $0\ to\ 1$. Equations 4.5 and 4.6 represent the $H,$ range of red colour which can be viewed in the histogram shown in Figure 4.7.

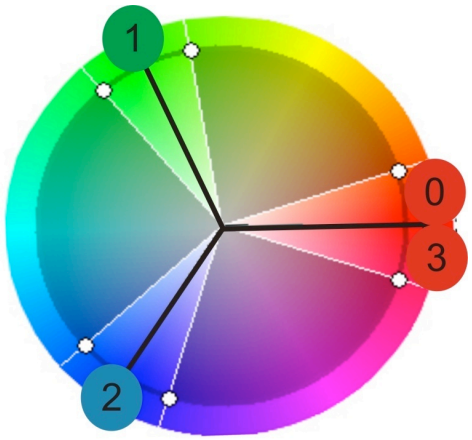

Figure 4.6: Red, Green, Blue distributions in HSV gamut

$$H_{r1} = {}^{0}/_{3} = 0.00, \quad (4.5)$$

$$H_{r2} = {}^{3}/_{3} = 1.00, \quad (4.6)$$

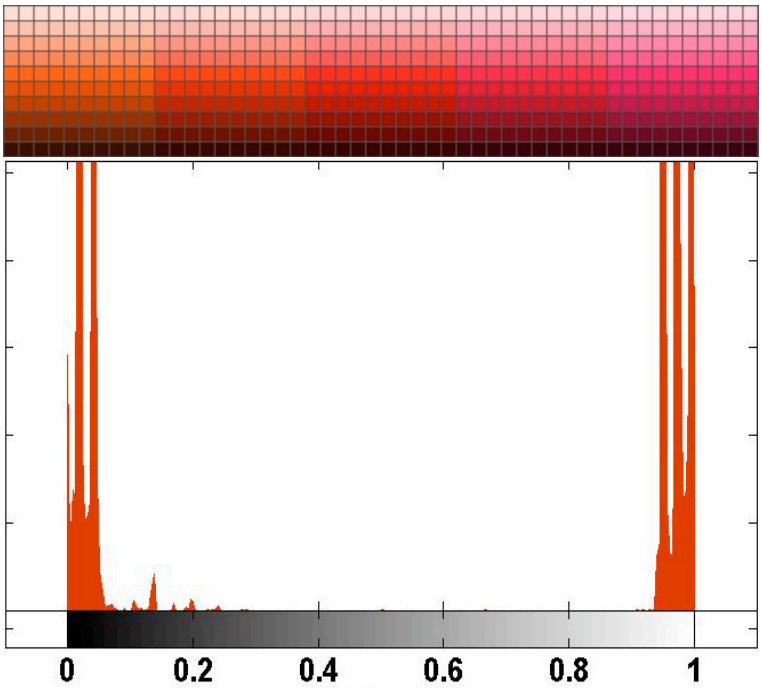

Figure 4.7: Hue histogram of red colour palette

$H_{g,}$ in equation 4.7 is the representation of green colour in HSV colour space. The histogram representation of green colour palette is shown in Figure 4.8. It has to be noted that this representation of green colour is made by varying the $S\ and\ V$ components as can be seen in the green colour palette.

$$H_g = {}^{1}/_{3} = 0.33, \quad (4.7)$$

$H_{b,}$ in equation 4.8 is the representation of blue colour. The histogram of blue colour palette with varying $S\ and\ V$ components is shown in Figure 4.9.

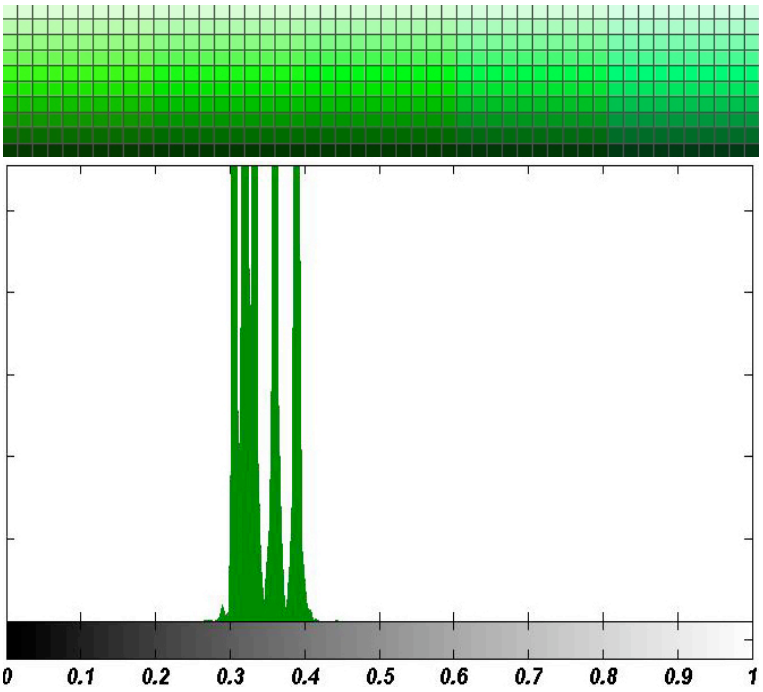

Figure 4.8: Hue histogram of green colour palette

$$H_b = {}^{2}/_{3} = 0.66, \tag{4.8}$$

The other two components of HSV, colour space i.e. $S\ and\ V$ have high impact on the H, component. S, generates different shades of a particular colour and V, indicates the brightness or darkness of a colour. For experimental purposes it is assumed that $0\ and\ 1$ are $low\ and\ high$ threshold values for both $S\ and\ V$ components respectively. The chromatic information (resides in H) cannot be viewed if one of the components i.e. $S\ and\ V$, has a low value. The HSV, colour space model in section 3.1.2 (see chapter 3) explains each of its components and their dependencies on each other.

Road signs colours behave differently due to illumination changes. For example H thresholds for red coloured road signs viewed in the day time will be different than the H thresholds values obtained during the night time. The outdoor light sources such as car headlamps and street lights affect the red colour which perceptually appears as orange during the night time.

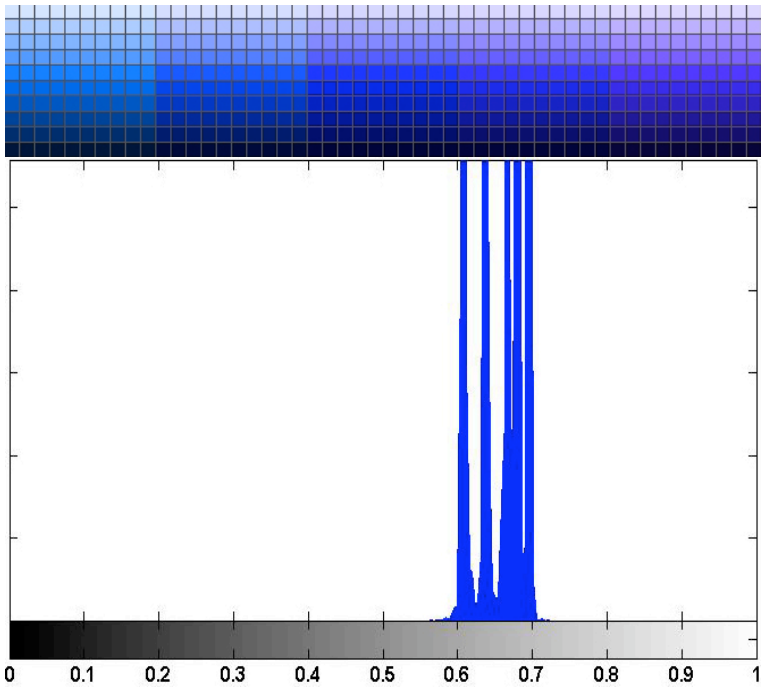

Figure 4.9: Hue histogram of blue colour palette

Figure 4.10 shows red colour variations where (a) represents the road sign image taken during daylight conditions and (b) represents the road sign image captured during night time (with reflections). To resolve this problem and in order to obtain different shades of colours according to $S\ and\ V$ threshold changes, we have used tolerance values for each component of HSV. POI can be selected by using optimum values of these tolerances found experimentally by analysing histograms. Note that segmentation of selected POI results in to a binary image where any pixel area within range of road sign colour threshold value will be represented by white. The pixels outside the threshold range are ignored and in the binary image they are represented as black colour. This has been shown in the section 4.3 as our experimental setup and results. Further post processing stage such as median filtering [88] is utilised that helps to remove noise and smooth the edges which improve the object analysis.

The following section presents segmented object analysis which helps in the selection of candidate road sign areas and to remove false alarms.

(a) (b)

Figure 4.10: The red colour of road sign during (a) Day light (b) Night

4.2.3. Object Analysis

In this section a criteria is presented in which the object areas are selected as potential road sign candidates or discarded as noise depending on the aspect ratios of their bounding boxes [4]. The colour priority is embedded with the bounding box analysis of the candidate road sign to help in the selection and the rejection process. Table 4.2 shows the colour of the road sign, its priority and its possible shape appearance with in the bounding box.

Colour	Priority	Shape
Red	1	Triangle, Circle, Hexagon,
Blue	2	Rectangle, Circle
Green	3	Rectangle

Table 4.2: Road Sign Colours with their priority and shape characteristics

Red colour road signs which have highest priority of seeking human attention can appear to be as Circular, Hexagonal or Triangular in shape in the scene. Similarly Blue colour signs can appear as only Circular or Rectangular shapes, whereas, Green colour signs can only appear as rectangular shapes. The bounding boxes of each object in the binary image are subsequently analysed according to colour priority presented in Table 4.2. The aspect ratio of the corresponding bounding box of each segmented object is determined using width and height characteristics of an object. The bounding box is further analysed for road sign criteria on the basis of 4×4 block size points obtain from the centre and corners of an object as illustrated in the Figure 4.11. The bounding box regions qualifying

the valid aspect ratio and road sign criteria are kept as candidate road sign and vice versa. Figures 4.12(a) and 4.13(a) represents the red and blue colour sign images respectively. The POI based image thresholding is presented in figure 4.12(b) and 4.13(b) which also contains noisy objects. Figure 4.12(c) and 4.13(c) illustrate the ultimate binary images resulting from the removal of objects with unsuitable aspect ratios and road sign criteria.

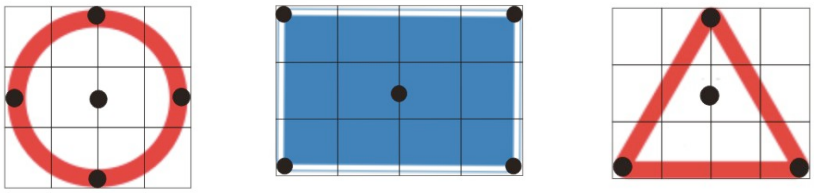

(a) **(b)** **(c)**

Figure 4.11: The Bounding Box and Key Points determination of (a) Circle (b) Square (c) Triangle shaped objects

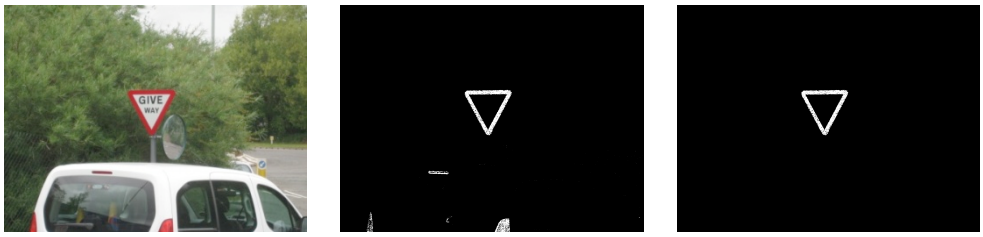

(a) **(b)** **(c)**

Figure 4.12: Red Colour Road Sign Segmentation (a) Original Image (b) POI based thresholding with noise (c) Candidate road signs without noise

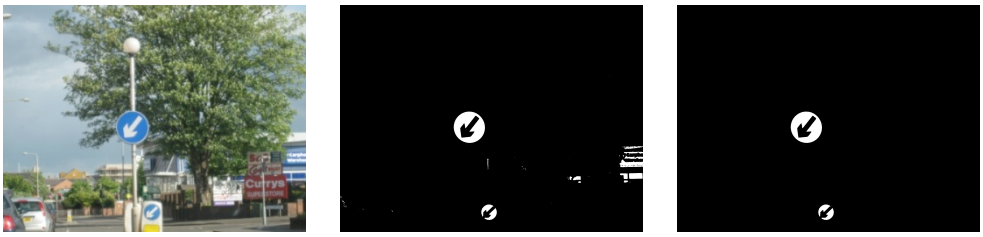

(a) **(b)** **(c)**

Figure 4.13: Blue Colour Road Sign Segmentation (a) Original Image (b) POI based thresholding with noise (c) Candidate road signs without noise

4.3. Experimental Setup and Results

Using a standard photographic camera, mounted on a car, 1200 (*650 of day light, 225 of evening/night time and 300 of road signs represents rainy and foggy conditions*) images of different road signs were captured for the experiments. These signs were captured during various ambient and lit-up levels of illumination and weather conditions. The road signs collected were limited to the basic colours i.e. Red, Green and Blue (see Figure 4.14). All test images were gamma corrected to map them into a perceptually uniform domain. Figure 4.14 illustrates some samples of original images captured with the help of $Canon\ IXUS80IS$ digital camera at a resolution of 2592×1944. In our experiments segmentation results and threshold values from six colour spaces i.e. $YCbCr, YIQ, RGB, CIElab, CYMK\ and\ HSV$ are compared.

Figure 4.14: Original images of red, blue and green colour road signs captured under different environmental conditions

Experiments are carried out to determine the best threshold ranges of an individual colour space when used in conjunction with segmenting red, green and blue road signs under varying illumination and environmental conditions. Initial estimates for the boundary values of threshold ranges were determined by first manually segmenting a known but separate set of road signs and plotting histograms of component values pertaining to red, green and blue road signs separately. Subsequently the ranges of component values were determined by identifying the histogram peaks and selecting the ranges so as to enclose

these peaks. The procedure adopted for the segmentation of Red, Blue and Green colour road signs is detailed in the following sections.

4.3.1. Segmentation of Red Colour Road Signs

Figure 4.15 illustrates the results of red colour road sign segmentation under different lighting or environmental conditions. The images have been captured in four different lighting conditions i.e. $Bright/Day, Wet/Rain, Evening\ and\ Night$. After pre processing and transforming the captured image to the desired colour space, it is then thresholded according to the parameter constraints listed in Table 4.3. Note that the aim of all experiments presented in this section is to segment the red road signs. It was observed that in the $CIElab$, colour space; the a, component remains constant whereas l, and b, components are sensitive to changes in the lighting conditions. In the RGB colour space R, and B, components are sensitive to illumination variations and G, component remains constant in most cases. In the segmentation of red colour using $YCbCr$, colour space, each component only varies by a small amount, under illumination changes. The $CYMK$, colour space although $C, Y\ and\ K$ components were largely non-sensitive to illumination changes, where as the M, component demonstrated a significant change.

In the YIQ, colour space Y component remains constant in all conditions whereas I, component varies marginally in the night scenes. However the Q, component is sensitive to all lighting variations. In the HSV, colour space all components remain constant except in the night scenes where H, component significantly changes, depending of available ambient light sources in the surrounding area.

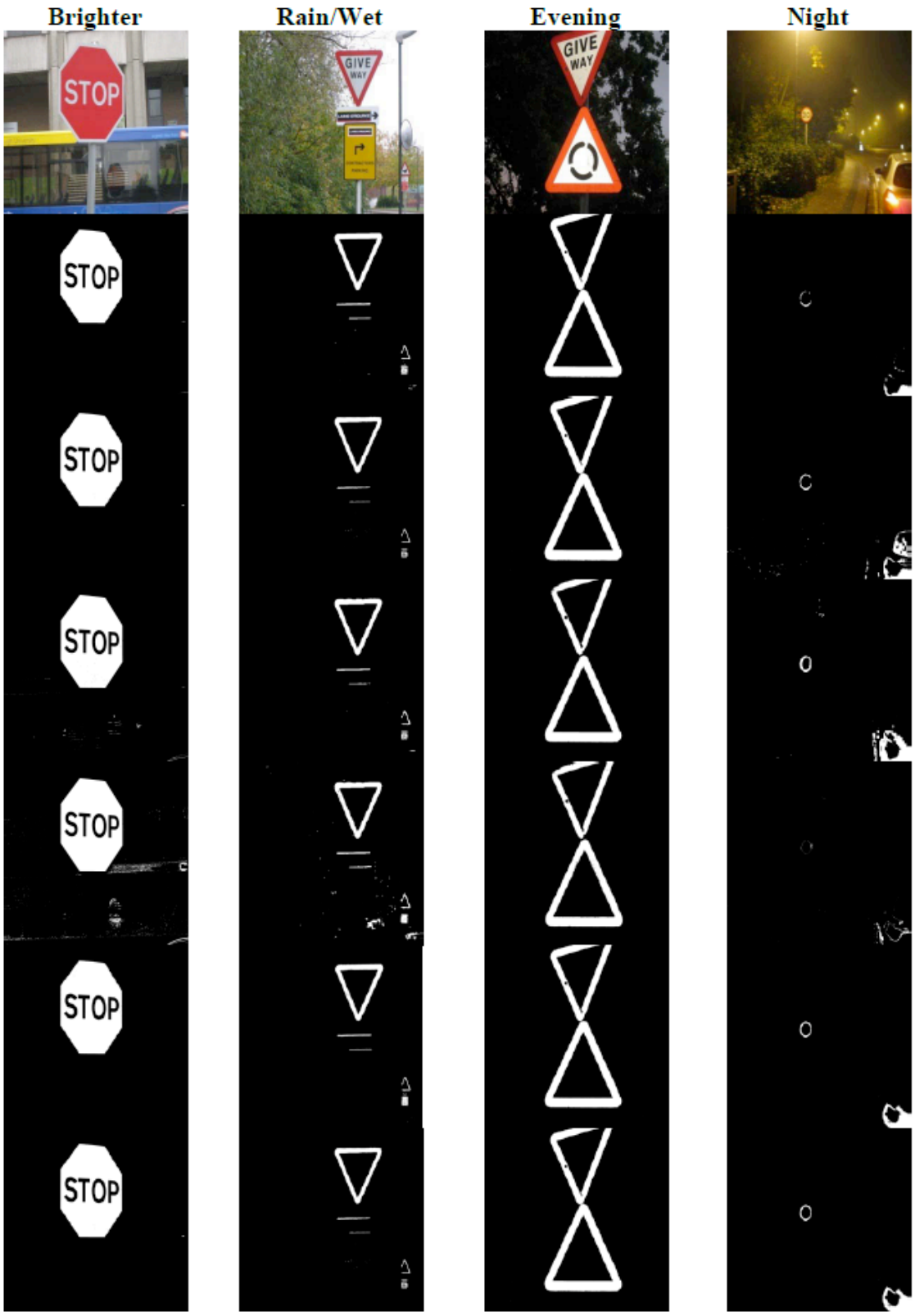

Figure 4.15: Segmentation results; top-to-bottom rows: 1: Original Image, 2: CIElab, 3: RGB, 4: YCbCr, 5: CYMK, 6: YIQ, 7: HSV

	Brighter/Day	Rain/Wet	Evening	Night
CIElab	*30<l<100* *15<a<81* *0 <b<40*	*15<l<100* *15<a<81* *0 <b<70*	*15<l<100* *15<a<81* *0 <b<40*	*15<l<100* *15<a<81* *0 <b<60*
RGB	*129<R<255* *0<G<71* *0<B<96*	*129<R<255* *0<G<71* *0<B<96*	*156<R<255* *0<G<98* *0<B<44*	*100<R<255* *0<G<98* *0<B<20*
YCbCr	*40<Y<120* *100<Cb<128* *140<Cr<200*	*30<Y<120* *100<Cb<128* *150<Cr<200*	*60<Y<170* *77<Cb<115* *170<Cr<206*	*27<Y<180* *70<Cb<120* *156<Cr<207*
CYMK	*0<C<40* *65<Y<215* *130<M<234* *0<K<117*	*5<C<80* *50<Y<206* *100<M<249* *5<K<185*	*0<C<40* *184<Y<239* *188<M<252* *1<K<124*	*0<C<41* *65<Y<244* *130<M<252* *1<K<124*
YIQ	*0<Y<255* *0<I<255* *23<Q<175*	*0<Y<255* *0<I<255* *32<Q<175*	*0<Y<255* *0<I<255* *36<Q<175*	*0<Y<255* *75<I<255* *60<Q<175*
HSV	*0.97<H<1* *0.7<S<1* *0.5<V<1*	*0.97<H<1* *0.7<S<1* *0.5<V<1*	*0.97<H<1* *0.7<S<1* *0.5<V<1*	*0<H<0.06* *0.7<S<1* *0.5<V<1*

Table 4.3: Threshold values used to segment red colour

4.3.2. Segmentation of Blue Colour Road Signs

In this experiment blue colour signs or advisory road signs are segmented and the results are analysed. Figure 4.16 illustrates the segmentation results for blue coloured road signs under varying illumination levels and environmental conditions. Table 4.4 tabulates the threshold ranges that can be recommended for segmenting blue colour road signs captured during Bright/Day, Wet/Rain, Evening and Night conditions. It has been observed that; $CIElab$, can use the same threshold ranges for segmenting blue colour under different outdoor conditions. In $RGB, YCbCr\ and\ CYMK$ all components are

sensitive to change in the lighting conditions. In YIQ, colour space Y, and Q, components remain constant where as I, component demonstrates marginal changes due to change in the illumination.

	Brighter/Day	**Rain/Wet**	**Evening**	**Night**
CIElab	*15<l<100* *0<a<15* *-112<b<-12*	*15<l<100* *0<a<15* *-112<b<-12*	*15<l<100* *0<a<15* *-112<b<-12*	*15<l<100* *0<a<15* *-112<b<-12*
RGB	*0<R<85* *0<G<137* *77<B<200*	*0<R<52* *0<G<58* *80<B<156*	*0<R<77* *0<G<96* *49<B<156*	*0<R<36* *0<G<148* *107<B<158*
YCbCr	*0<Y<105* *0<Cb<179* *0<Cr<102*	*30<Y<200* *150<Cb<255* *25<Cr<120*	*50<Y<200* *50<Cb<255* *25<Cr<120*	*65<Y<117* *50<Cb<198* *55<Cr<107*
CYMK	*159<C<212* *0<Y<13* *76<M<149* *0<K<33*	*128<C<255* *0<Y<190* *51<M<240* *0<K<150*	*128<C<255* *0<Y<190* *51<M<240* *0<K<150*	*180<C<240* *0<Y<7* *95<M<194* *0<K<10*
YIQ	*0<Y<255* *22<I<75* *0<Q<255*	*0<Y<255* *22<I<89* *0<Q<255*	*0<Y<255* *22<I<94* *0<Q<255*	*0<Y<255* *22<I<80* *0<Q<255*
HSV	*0.66<H<0.75* *0.7<S<1* *0.5<V<1*	*0.66<H<0.75* *0.7<S<1* *0.5<V<1*	*0.66<H<0.75* *0.7<S<1* *0.5<V<1*	*0.66<H<0.75* *0.7<S<1* *0.5<V<1*

Table 4.4: Threshold values used to segment blue colour

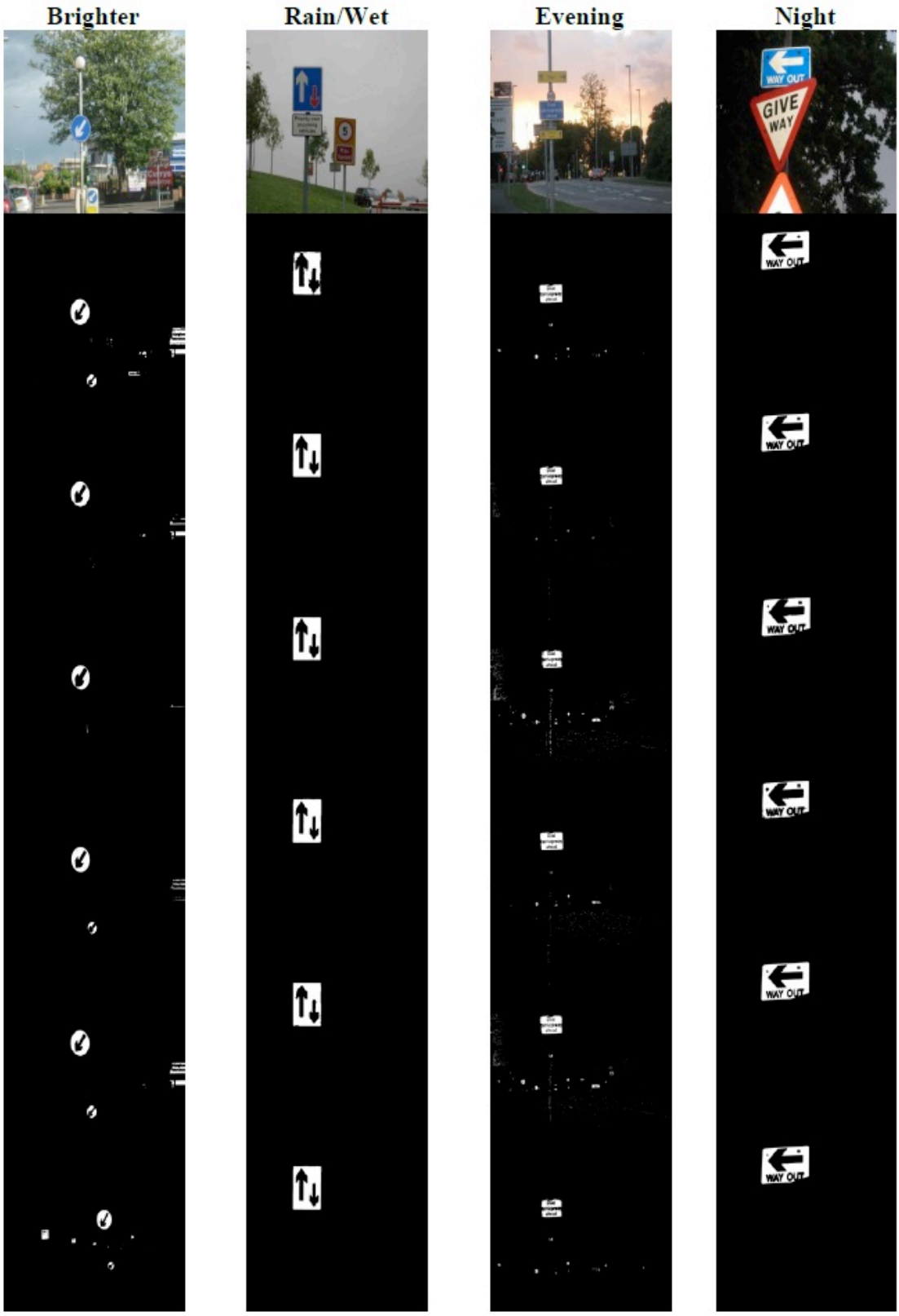

Figure 4.16: Segmentation results - top-to-bottom rows: 1: Original Image, 2: CIElab, 3: RGB, 4: YCbCr, 5: CYMK, 6: YIQ, 7: HSV

In HSV, colour space the H, component remains marginally the same, within the range 0.66 to 0.75. This colour covers all the shades of blue. Here S and V components vary significantly in very poor lighting/weather conditions.

4.3.3. Segmentation of Green Colour Road Signs

In this experiment green colour road signs are segmented and the actual sensitivity of different components of the colour spaces to variations in illumination and environmental conditions is investigated. Figure 4.17 illustrates the segmentation results for green coloured road signs under varying illumination levels and environmental conditions. Table 4.5 tabulates the threshold ranges that can be recommended for segmenting green colour in captured images.

	Brighter/Day		**Rain/Wet**	**Evening**
CIElab	*14<l<100* *-79<a<-14* *0<b<40*	*14<l<100* *-79<a<-14* *0<b<40*	*14<l<100* *-79<a<-12* *0<b<40*	*14<l<100* *-79<a<-12* *0<b<40*
RGB	*0<R<44* *173<G<255* *0<B<137*	*0<R<88* *129<G<255* *0<B<178*	*0<R<55* *123<G<188* *0<B<104*	*0<R<101* *125<G<255* *0<B<132*
YCbCr	*65<Y<145* *112<Cb<135* *85<Cr<105*	*100<Y<160* *125<Cb<158* *80<Cr<110*	*50<Y<110* *120<Cb<132* *100<Cr<120*	*505<Y<141* *120<Cb<133* *95<Cr<114*
CYMK	*103<C<194* *86<Y<238* *1<M<47* *16<K<40*	*123<C<174* *45<Y<178* *0<M<29* *35<K<112*	*126<C<171* *95<Y<178* *22<M<75* *80<K<182*	*180<C<240* *0<Y<7* *95<M<194* *0<K<10*
YIQ	*0<Y<129* *0<I<110* *35<Q<82*	*0<Y<129* *0<I<110* *35<Q<82*	*0<Y<103* *55<I<65* *35<Q<82*	*0<Y<255* *0<I<110* *35<Q<82*
HSV	*0.42<H<0.51* *0.7<S<1* *0.5<V<1*	*0.42<H<0.51* *0.7<S<1* *0.5<V<1*	*0.42<H<0.51* *0.7<S<1* *0.5<V<1*	*0.42<H<0.51* *0.7<S<1* *0.5<V<1*

Table 4.5: Threshold values used to segment green colour

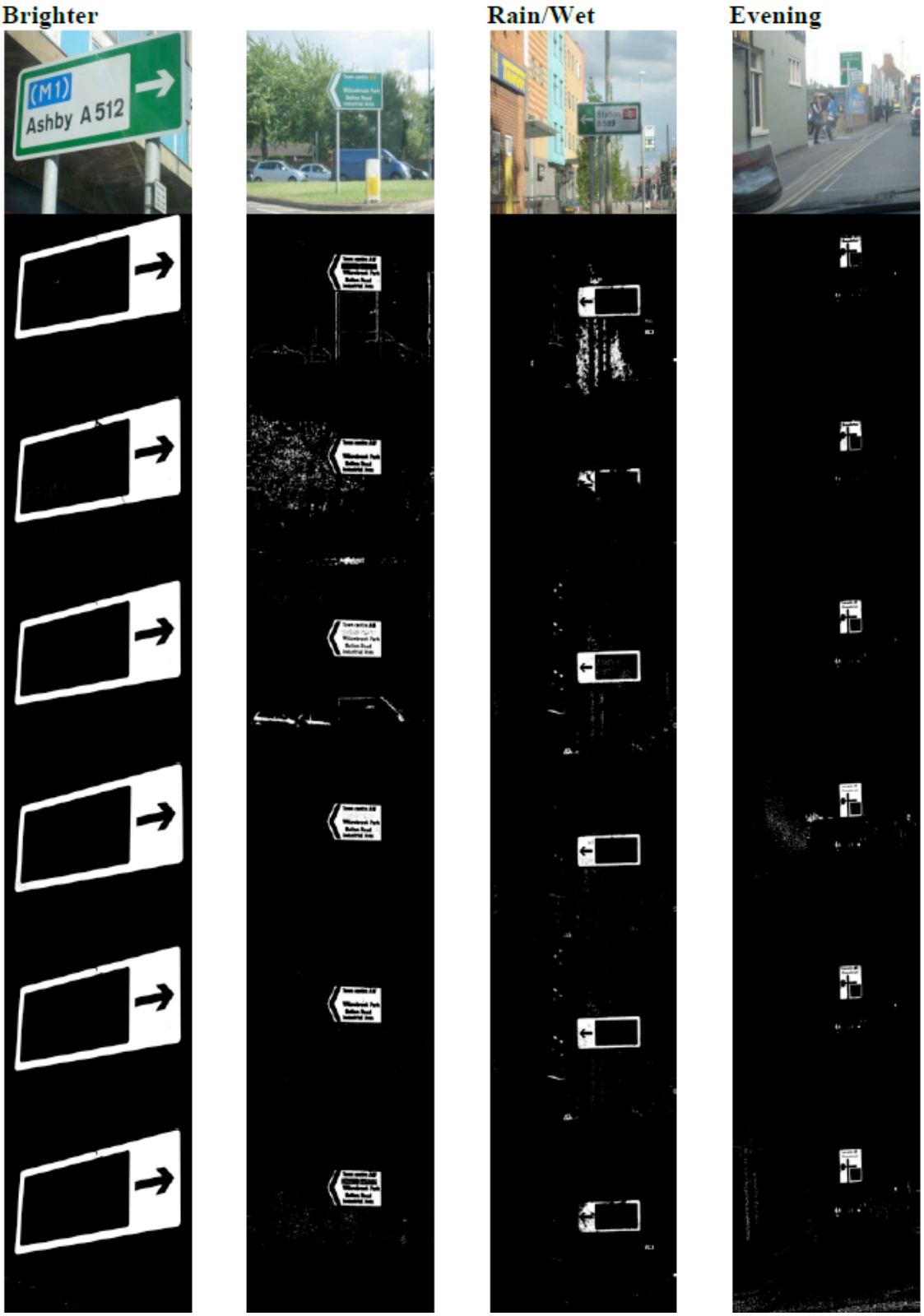

Figure 4.17: Segmentation results -top-to-bottom rows: 1: Original Image, 2: CIElab, 3: RGB, 4: YCbCr, 5: CYMK, 6: YIQ, 7: HSV

Our experiments revealed that in the $CIElab$, colour space l, and b, components remain largely constant while minor variations are noticed in a. In $RGB, YCbCr\ and\ CYMK$ colour spaces it was observed that all parameters were very sensitive to illumination changes and the presence of other green coloured area such as trees and grass. In YIQ colour space Q, component remains constant while I, and Y, components have little variation.

However the HSV, colour space demonstrated that all components remain considerably uniform under varying lighting conditions. The reason for the above behaviour was found to be that the H component will not capture any shade of green which are typically found in areas covered by grass or leaves. Under daylight conditions grass and trees present a light green shade due to reflection of the sun light, whereas typically green road sign boards are painted with a different, darker shade of green. $S\ and\ V$ components can vary when area with low intensity green colour is sought.

From the experimental results it can be concluded that HSV colour space is the most robust colour space that can be effectively utilised for colour based segmentation of road signs under varying illumination and environmental conditions. Figure 4.18 (a) illustrates examples of original road sign images. Whereas Figure 4.18(b) and (c) presents a cropped road sign from the original image and cropped segmented colour from the binary image respectively by using experimentally found threshold value of HSV colour space. It shows that road signs of different colour and shapes have been detected under varying lighting and environmental conditions. The detailed analysis revealed that an accuracy range of $90 - 95\%$ (averaged over all lighting conditions tested and three colours red, green, blue, being segmented) can be achieved when using the HSV, in conjunction with the threshold values determined by the experiments. Table 4.6 illustrates the overall average observed accuracy figures for all colour spaces for comparison purposes.

	Colour Spaces					
	CIELab	**RGB**	**YCbCr**	**CYMK**	**YIQ**	**HSV**
Accuracy %	*87.7*	*62.2*	*77.2*	*76.5*	*74.6*	*94.7*

Table 4.6: Overall average accuracy figures obtained for individual colour space

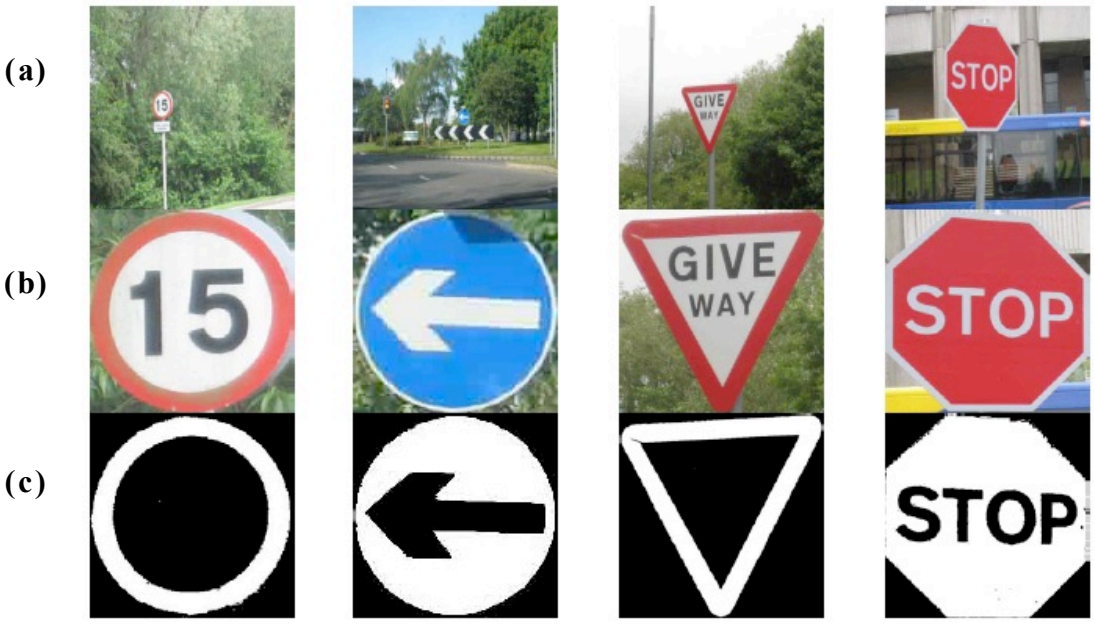

Figure 4.18: Colour segmentation using HSV colour space (a) Original Image (b) Cropped road sign from original image (c) Cropped road sign from binary image

4.4. Summary and Conclusion

This chapter carried out a detailed investigation on to the suitability of using six different colour spaces in colour based detection of road signs. The chapter presents the procedure of segmentation for three basic colours of road signs using ***HSV*** colour space. The captured images are pre processed to adjust the luminance level of the image by applying gamma correction. POI selection is carried out while analysing the histogram of each colour separately. The threshold ranges obtained through this analysis helps to generate binary image which is further analysed on the basis of aspect ratio and road sign criteria.

The experiments are carried out on over *1200* images captured during bright/day, wet/rain, evening and night time conditions. Three experiments are provided in the experimental setup and results section where obtained threshold ranges for red, blue and green colour are tabulated. It has been concluded experimentally that HSV colour space provides better segmentation results with overall accuracy of *94.7%* as compared to $CIElab, RGB, YCbCr, CYMK\ and\ YIQ$ with over all accuracy figures *87.7%, 62.2%, 77.2%, 76.5% and 74.6%* respectively.

The detailed experiments conducted in this chapter also revealed that the colour segmentation results achieved by a single colour space may vary due to illumination changes. Therefore an algorithm that is robust against wide variations in illumination will require the efficient combination of different colour spaces. Chapter 5 presents a novel method towards colour segmentation of road sign by using combined colour model; the chapter also explains its development and usage.

Chapter 5

A Combined Colour Space Model for Road Sign Region of Interest (ROI) Segmentation

5.0. Preface

In chapter 4 it was shown that the colour of a road sign plays a vital role in its automatic identification using computer based approaches. However the colour of a road sign changes due to various outdoor lighting conditions and may thus create difficulties in the correct identification of the road sign as the selection of the most appropriate colour model and the relevant parameter/threshold values to be used becomes tedious. This chapter proposes the use of a novel *CCM* that leads to a more accurate and robust colour based road sign segmentation. The proposed *CCM* performs robustly within a wide range of typical outdoor lighting conditions such as *Night, Day, Evening, Fogy and Rainy* achieving an accuracy rate of *97.5%.*

This chapter has been organized as follows: In addition to this section in which a preface to the chapter is presented section 5.1 introduces the reader to the research problem and the need for a solution. Section 5.2 presents the proposed solution to the research problem, i.e. the *CCM*. Section 5.3 provides the experimental design, results obtained and a detailed performance evaluation of the proposed system. Finally section 5.4 summarises and concludes the chapter.

5.1. Introduction

The literature review presented in chapter 2, reveals that colour based segmentation of road signs is popularly achieved by using a single colour space. Each colour space has its own limitations as they were originally defined and later developed to support certain

tasks specific to a given practical application. For example *CYMK* colour space was originally intended to be used in colour printing tasks and *YIQ* colour space was introduced to define colour in *TV* systems.

In chapter 4 where we have compared colour based road sign segmentation results of six colour spaces and it was concluded that the accuracy of the colour based segmentation results vary due to illumination changes. This is due to the fact that the determination of various parameters associated with the individual colour spaces, under varying lighting conditions is difficult. For example the parameter value used to determine the red colour of a road sign during daylight conditions will be significantly different to the parameter value used for the same purpose on a gloomy day. Further it was observed that different colour spaces have different levels of sensitivity to different illumination changes. For example a colour space that may show robustness to illumination changes from a bright to a gloomy day may show higher sensitivity to illumination changes that are caused by fog. Yet again another colour space will show high sensitivity to the initial illumination change described above and more robustness to the latter. Therefore combining different colour spaces may provide a solution which can demonstrates the best robustness to the illumination change that the road sign is undergoing at a given time.

The following section presents the methodology of the *CCM* that is proposed to address the above research problem.

5.2. ROI Segmentation – The Methodology

Figure 5.1 illustrates the block diagram of the segmentation algorithm that uses the proposed *CCM*. The images captured via the imaging source are firstly pre processed to remove the unwanted areas of the scene being viewed and are luminance corrected as explained in section 5.2.1. The colour pixels belonging to the potential road sign are defined using the *CCM* (section 5.2.2). This result into a binary image where the pixels belonging to road signs are represented as *white* while the pixels belonging to non-road signs are marked as *black*. Subsequently, the aspect ratios of all *ROI* (i.e. white regions)

in the scene are analysed. The regions of which the aspect ratio falls within a tolerance of a specified value are selected as candidate road sign regions. Regions that do not satisfy the above aspect ratio criterion or regions smaller than a specified size are ignored from further consideration. Finally the selected *ROI* is passed to the subsequent stage of shape based classification (see chapter 6) for further processing.

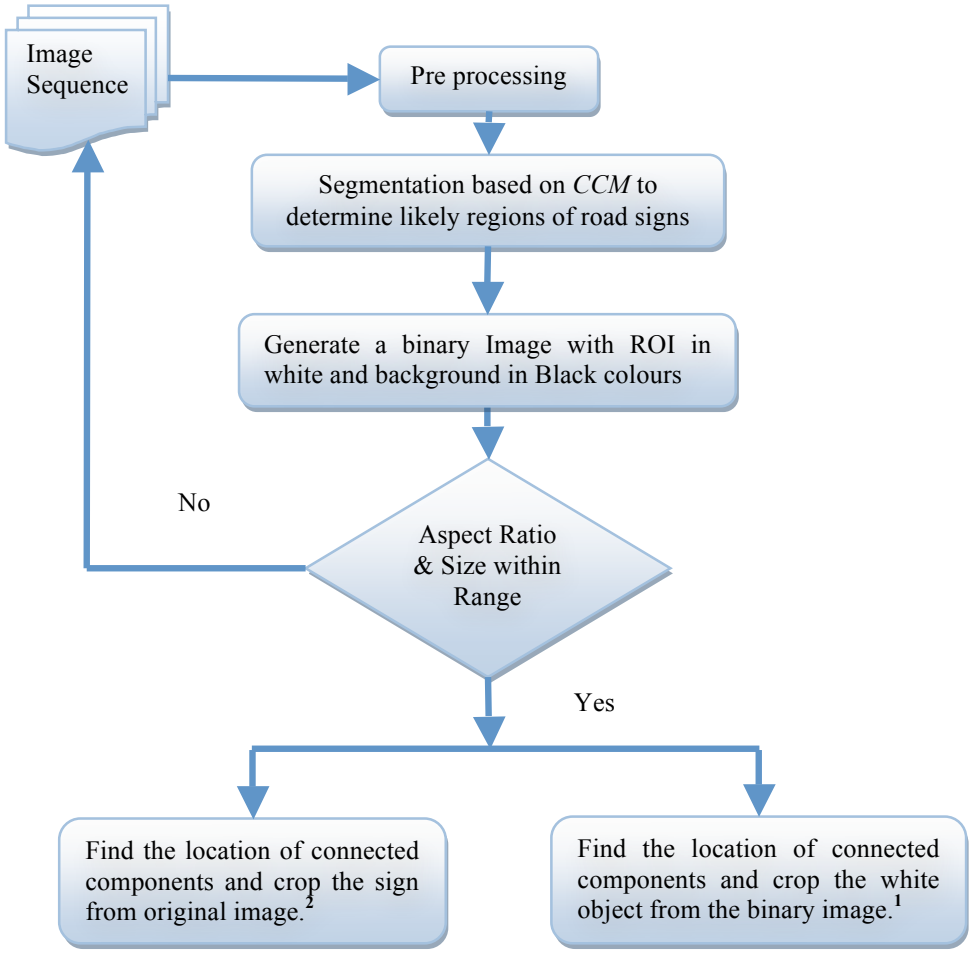

Figure 5.1: Road sign ROI segmentation using the proposed *CCM*

1. Objects used for shape classification (see chapter 6)

2. Objects used for content recognition (see chapter 7)

5.2.1. Pre processing

The input images (see figure 5.2) are initially gamma corrected in a way similar to that described in section 4.2.1 (see chapter 4). Gamma correction [109] adjusts the luminance level present in the images according to the *NTSC* [75] video system (see figure 5.3). In the subsequent pre-processing operation it is assumed that the camera is mounted on a vehicle at approximately a position closer to the view point of the driver. Based on this assumption we deduce that the bottom fifth of the image frame can be ignored from processing as it is likely that this bottom part of the scene contains an area within the vehicle or contains areas from the surface of the road (see figure 5.4). The next section explains about the algorithm followed to develop *CCM* for colour based segmentation of pre processed image/image sequence.

Figure 5.2: Original images captured at driver view position

Figure 5.3: Gamma corrected images

Figure 5.4: Image regions showing 80% cropping of the original images

5.2.2. Combined Colour Model (*CCM*)

In the previous chapter (see chapter 4) it was discussed that the appearance of road sign colour may change over time due to changes in illumination and due to being exposed to severe weather conditions, such as heavy rain or bright sunlight. The various effects on road sign colour due to reflections from sun light, car headlight lamp or street lights have already been discussed in chapter 4.

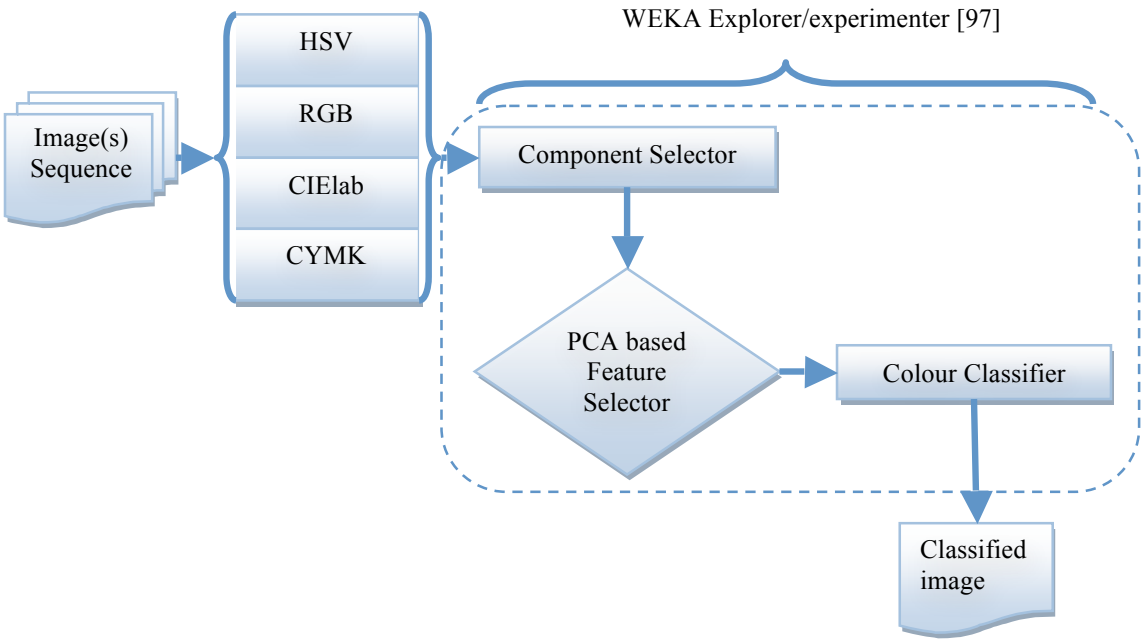

Figure 5.5: Colour segmentation approach based on the proposed *CCM*

The results of colour segmentation during these conditions may vary from one colour space to another. Since one colour space works better in one particular illumination condition and it may under or over segment the road sign colour in the other illumination condition.

The idea of *CCM* focuses on the merger of properties of four distinct colour spaces in the presence of wider range of illumination variance, which makes the segmentation task

further robust. This should enhance the colour segmentation accuracy of road signs when single colour space based segmentation fails to extract the desired information. Figure 5.5 shows the block diagram of the *CCM* approach, which is explained in this section.

This model starts with the retrieval of equivalent value of colour pixel from four distinct colour spaces i.e. $RGB, HSV, CIElab\ and\ CYMK$. The training images are the samples of road sign colours captured in varying illumination, weather and scaling conditions. In this model we have only obtained three distinct colour samples of road signs i.e. $Red, Green\ and\ Blue$. It is assumed that the training images are represented by RGB colour space. The pre processed images are transformed to three remaining colour spaces i.e. *HSV, CIElab and CYMK* (see chapter 3, section 3.1 for colour space transformation equations). Subsequently the information related to the colour of pixel is manually obtained from each training colour sample of the road sign. Table 5.1 tabulates an example of Red, Green and Blue pixel colours represented by 13 *(3 components each from HSV, RGB and CIElab and 4 components of CYMK)* components per colour. In the proposed *CCM* these components are arranged in a pre-defined order (see Table 5.2) to form a feature vector representing the colour of a pixel.

Colour	HSV	RGB	lab	CYMK
	1,1,1	255,0,0	54,81,70	0,99,100,0
	0.33,1,1	0,255,0	88,-79,81	63,0,100,0
	0.66,1,1	0,0,255	30,68,-112	88,77,0,0

Table 5.1: Colour component values from four different colour spaces of three differently coloured pixels

During the training process, each component value of a colour pixel is obtained manually from a sample pixel of a road sign captured in various illumination conditions (see table

5.3). Furthermore, it is revealed that the use of the above thirteen dimensional feature vector to represent a single colour pixel leads to an unacceptable level of computational cost in the later stages of pixel classification.

1	2	3	4	5	6	7	8	9	10	11	12	13
H	S	V	R	G	B	l	a	b	C	Y	M	K

Table 5.2: Order of 13 components formed from four different colour spaces

H	S	V	R	G	B	l	a	b	C	M	Y	K	Colour
0.94	0.7	1	255	76	136	61	71	8	0	84	17	0	
0.06	0.8	1	255	119	51	66	50	61	0	67	87	0	
0.61	1	1	0	85	255	42	34	-91	83	67	0	0	
0.71	1	0.7	45	0	179	21	54	-82	92	94	0	0	
0.30	0.7	1	106	255	76	90	-65	68	51	0	100	0	
0.36	0.8	1	51	255	85	88	-73	64	58	0	100	0	

Table 5.3: Sample pixel representations

Thus in order to reduce the size of the colour component set, the computational complexity of subsequent stages and to reduce the chances of data over-fitting; component/feature selector of *WEKA* [97] is used.

Component Selector	Selected Components	Number of Components
Best First	H,R,B,a,b,C,M	7
Exhaustive Search	H,R,B,a,b,C,M	7
Genetic Search	H,R,B,a,b,C,M	7
Greedy Stepwise	H,A,b,C,M,K	6
Random Search	H,R,G,B,a,b,C,M	8

Table 5.4: Results of Search methods with selected components and Quantity

1	2	3	4	5	6	7
H	**R**	**B**	**a**	**b**	**C**	**M**

Table 5.5: Frequently Selected Components

WEKA [97] is a data mining tool which is briefly explained in chapter 3 (see section 3.2). To obtain the optimum set of selected component combination, we have investigated the use of five different popular feature selection methods namely; Best First, Exhaustive Search, Genetic Search, Greedy Stepwise Search and Random Search of *WEKA* [97]. It was revealed that the set consisting of the 7 components, *H, R, B, a, b, C and M* (*Hue, Red, Blue, a and b chroma components, Cyan and Magenta respectively*) is the most appropriate to represent a pixel colour value (see Table 5.4). Thus the component set has been reduced from an original set of 13 components to 7 components as shown in Table 5.5. This removes any redundancy present between components by disregarding components which are non-significant in data discrimination. It was also revealed through experiments that the frequently selected components (see Table 5.5) will remain the same even by changing the order of the 13 components (see Table 5.2) of different colour spaces. The selected components are further analysed by using *Principal Component Analysis (PCA)* of *WEKA* [97]. Each colour class i.e. *Red, Green and Blue* is converted into an Eigen feature space in this analysis. This further helps in reducing the data dimensionality and redundancy. Table 5.6, 5.7 and 5.8 show the Eigen Vectors obtained against 7 components for each class respectively.

The Eigen Vectors for Red colour class are obtained from 110 sample training colour pixel instances. Similarly Eigen Vectors for Green and Blue Class are obtained from 99 sample colour pixel instances.

	V1	V2	V3
H	-0.0902	-0.0334	-0.7159
R	-0.4869	0.3552	0.1
B	-0.5188	-0.2422	-0.1549
a	-0.0367	0.6121	-0.3614
b	0.2534	0.483	0.4061
C	0.484	-0.3606	-0.0955
M	0.431	0.2757	-0.3856

Table 5.6: Eigen Vectors for Red Colour Class

	V1	V2	V3
H	0.0406	0.4721	0.6379
R	-0.4559	0.1798	0.3904
B	-0.3896	0.3487	-0.3967
a	0.2699	0.5755	0.0087
b	-0.1774	-0.5296	0.47
C	0.5222	-0.1066	-0.0809
M	0.5115	0.0098	0.2362

Table 5.7: Eigen Vectors for Blue Colour Class

	V1	V2	V3
H	0.0484	0.2146	0.7632
R	-0.4763	0.2148	-0.3829
B	-0.4358	0.3862	0.242
a	0.1893	0.5218	-0.3848
b	-0.0877	-0.6323	-0.1382
C	0.5748	-0.0458	0.0672
M	0.455	0.2908	-0.2015

Table 5.8: Eigen Vectors for Green Colour Class

The data transformation from component representation to feature space causes the dimensionality reduction. This means that the components representing a particular colour pixel with 7 dimensions can be represented with 1 dimension in feature space. Each feature represents a colour pixel that carries a unique instance within its designated class. These features are later trained on a *SVM multiclass polynomial kernel* [106] for the classification of colour pixels from the input test image. Finally the classified images are represented in binary format where pixels classified as *ROI* are represented with white and the non classified pixels are represented as black colour.

5.3. Experiments, Results and Analysis

A *Canon IXUS801S* digital camera is used to capture the images and videos required for experimentation. Using this camera images are captured at the resolution of 2592×1944 whereas the videos is captured with a resolution of 1024×768. The road sign colours considered during our data collection were only Red, Green and Blue. The captured images also represent varying illumination conditions such as N*ight, Wet, Fogy, Bright and Evening*. All images are initially subjected to a gamma correction based on experimentally determining camera operational parameters. The colour samples of Red, Green and Blue road signs are manually cropped from images reflecting various illumination levels. As the images captured were in the RGB colour space, we have analysed the relevant colour parameter representation in other three colour spaces i.e. $HSV, CIElab$ *and* $CYMK$. This analysis is carried out in *Adobe Photoshop 7.0* on sample colours obtained from road sign during various illumination levels. Figure 5.6 shows some colour samples cropped from the road sign images considering the various illumination conditions.

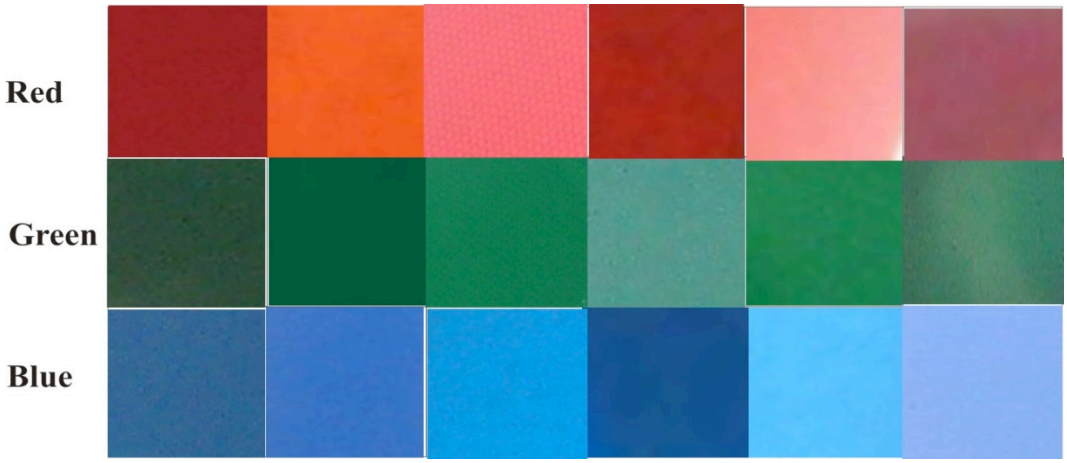

Figure 5.6: Road sign colour samples during varying illumination conditions.

Table 5.9 tabulates the maximum and minimum range for all four colour spaces investigated in the experiments. *110* pixel samples of *Red* colour and *99* pixel samples each of *Green* and *Blue* colours were used during the analysis. (i.e. a total of 308×13 pixel colour samples).

Colour Space	Minimum Value	Maximum Value
HSV	H,S,V = 0	H,S,V = 1
RGB	R,G,B=0	R,G,B=255
CYMK	C,Y,M,K = 0	C,Y,M,K = 255
CIElab	L=0,A,B =-127	L=100,A,B=127

Table 5.9: Minimum and Maximum values of components in each colour space

The component selection was carried out using the *WEKA* data mining tool [97] which contains implementations of a number of state-of-the-art search methods that can be used for attribute selection. The number of the selected components was reduced to an average of 7 components by applying popular search methods listed in table 5.4. Subsequently the 308×7 selected components listed in Table 5.5 were transformed to an Eigenspace (using *PCA*), forming a new representation of the sample pixel colour space. In the

experiments performed the *PCA* filter from the *WEKA* data mining tool [97] was utilised on the preselected 7 components representing each (i.e.$Red, Green, Blue$) pixel colour. Table 5.10 shows the properties of *PCA* Filter that was used to reduce the data dimensionality for each of three colours.

Property Name	Value
Maximum Attribute Names	7
Maximum Output Attributes	1
Normalize	True
Variance Covered	0.95

Table 5.10: PCA filter properties for dimensionality reduction

The statistical properties of *308* unique instances (*110 red, 99 each of Green and Blue pixels*) of numeric data are presented in table 5.11. Figure 5.7 represents the distribution of data within each colour class. The Output Attribute or features of three classes i.e. *Red, Green and Blue* were trained with the help of a *SVM multiclass polynomial kernel* [106]. It is noted that the classification of test image colour features with respect to the trained colour feature is entirely dependent on this module, i.e. the colour classifier.

Statistic	Value
Minimum	-0.326
Maximum	1.535
Mean	0.633
Standard Deviation	0.605

Table 5.11: Properties of PCA based selected features

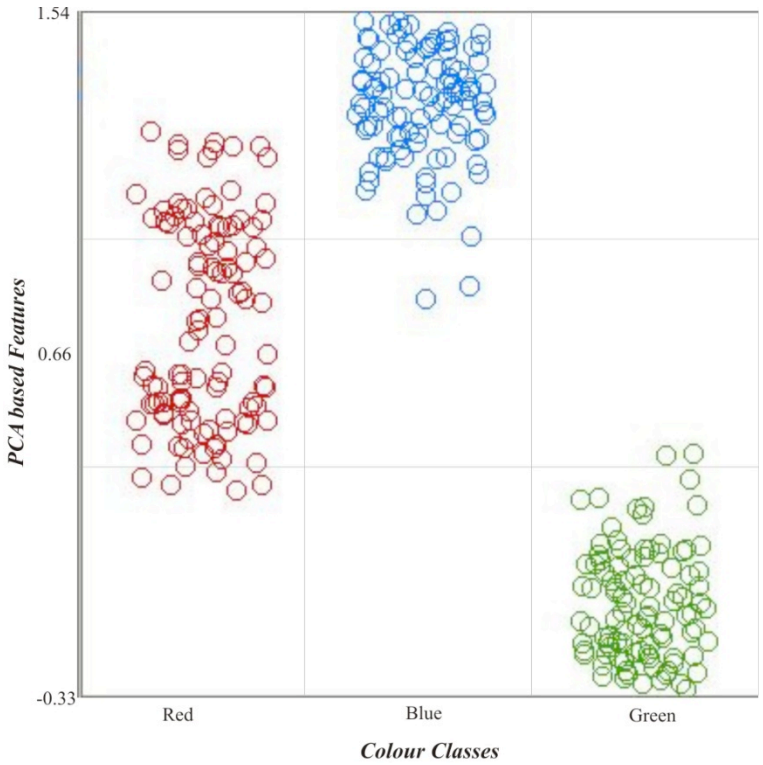

Figure 5.7: Data distribution for each colour class; along vertical axis, PCA based features presented according to their relevant colour class (horizontal axis)

The test image features can only be accurately classified when they are obtained following a procedure identical to that adopted to obtain the features of the training image set. Therefore the test image is initially pre-processed as stated in section 5.2.1 which consists of a gamma correction followed by $8:2$ image division rules. The test image is then transformed to $HSV, CIElab\ and\ CYMK$ colour spaces using equations presented in chapter 3 (see section 3.1 for colour space transformation equations). The selected components of colour spaces are then transformed into the corresponding Eigen space and are subsequently classified with the help of a colour classifier. Finally the classified image is represented as a binary image where white pixels are grouped as ROI of the image and vice versa. Figures 5.8, 5.9 and 5.10 illustrate the colour segmentation results of $Red, Green\ and\ Blue$ coloured road signs respectively. The bounding boxes of the ROI are analysed according to permitted aspect ratio and size. This helps in removing the false positives or very small objects which may or may not be a part of road sign.

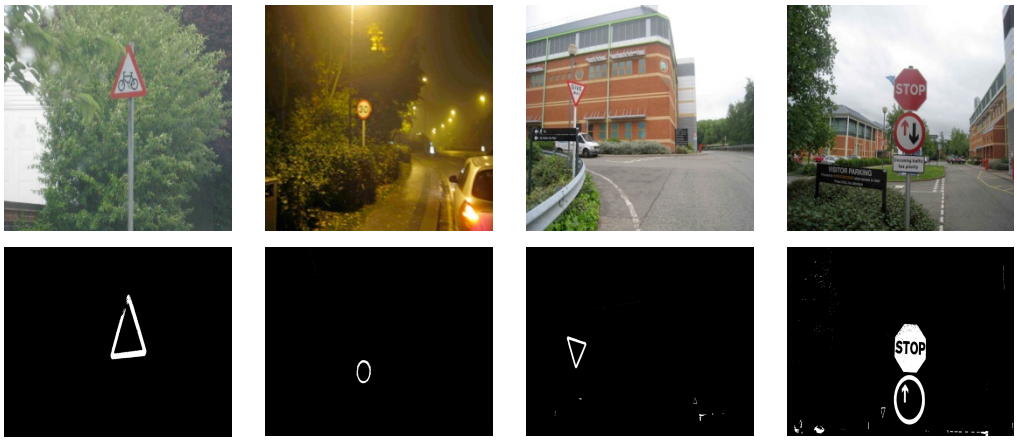

Figure 5.8: Segmentation of Red colour Road Signs

Figure 5.9: Segmentation of Green colour Road Signs

Figure 5.10: Segmentation of Blue colour Road Signs

Subsequent to the segmentation of potential $Red, Green\ and\ Blue$ road sign regions following the *CCM* based approach presented above, the qualified *ROI* in the binary image is investigated further to determine the shape type (see chapter 6). This investigation also helps the algorithm to determine the segmentation accuracy of the road sign. The experiments are carried out on over *1200* images/image sequences captured in lighting conditions such as *Night, Day, Evening, Fogy and Rainy*. The three experiments for each distinct colour i.e. red, green and blue of road signs are analysed separately. The red colour segmentation experiments provide *98.5%* (based on the *ROI* shape analysis) correctly segmented red *ROI*. Similarly blue and green colour segmentation experiments provide *98.1%* and *96.1%* correctly segmented blue and green *ROI* respectively. The low accuracy of green colour segmentation as compared to red and blue colours is majorly affected due to *ROI* shape analyser and the maximum threshold for aspect ratio and size. The green colour road signs have no specific size and shape; therefore the size appearance in the scene is slightly bigger than red and blue coloured road signs. The green colour road sign selection and rejection will be refined in the future research to improve the overall accuracy. Table 5.12 presents accuracy figures of each of the colour space along with *CCM* presented in this chapter.

	Colour Spaces						
	CIELab	**RGB**	**YCbCr**	**CYMK**	**YIQ**	**HSV**	**CCM**
Accuracy %	*87.7*	*62.2*	*77.2*	*76.5*	*74.6*	*94.7*	*97.5*

Table 5.12: overall average accuracy figures for all colour spaces with *CCM*

Our detailed analysis revealed that an accuracy range of *96-97.5%* (averaged over all lighting conditions tested and three colours red, green, blue, being segmented) have been achieved.

5.4. Summary and Conclusions

In this chapter we have presented a robust illumination invariant approach towards colour based, road sign segmentation. The algorithm utilizes a novel combined colour model for accurate segmentation of road signs from images of scenes undergoing significant variations of illumination and weather related degradation. The proposed *CCM* is a combination of selected properties of the $HSV, RGB, CIElab\ and\ CYMK$ colour spaces. The training process of this model was initiated by obtaining sample Red, Green, Blue colour pixel information from the road signs; captured under various ambient illumination levels and weather related degradations. The equivalent colour pixel values were subsequently obtained within $RGB, HSV, CIElab\ and\ CYMK$ colour spaces. The dominant components (out of total 13 components) of the above mentioned colour spaces were determined using feature selection within the *WEKA* data mining tool. Subsequently the selected components representing a particular colour pixel were transformed into the Eigen space using *PCA* for further dimensionality reduction. Finally these features are classified using a *SVM* based classifier leading to binary images indicating the segmented road signs of each colour. The training was done based on 110 samples of red colour pixels and 99 samples each of green and blue colour pixels obtained from images containing road signs taken under a wide range of illumination conditions.

Experimental results revealed that the accuracy of segmentation of road signs significantly improved when using *CCM*, compared to use of single colour model, in particular under varying levels of illumination and conditions of the road signs. *CCM* segments the colour of the road sign at overall average accuracy of *96-97.5%* as compared to $HSV, CIElab, RGB, YCbCr, CYMK\ and\ YIQ$ colour space with over all accuracy figures *94.7%*, *87.7%, 62.2%, 77.2%, 76.5% and 74.6%* respectively. It can be concluded that when using the combined colour model only 7 of the 13 possible colour space components are sufficient to perform accurate and robust segmentation. The proposed approach utilised this finding to reduce the overall computational complexity of the proposed colour based segmentation approach.

The colour based segmentation of road sings achieved using the procedure proposed has resulted in an *ROI* of a scene in which the potential road signs of colour red, green or blue may appear. The next stage of *RSDR* approach is to analyse the colour segmented ROI for their shapes. Chapter 6 presents a novel shape analysis algorithm that will lead to the identification of triangular, circular and rectangular road sign shapes.

Chapter 6

Shape Based Classification of Road Signs

6.0. Preface

Apart from colour of a road sign which was the focus of chapters 4 and 5, shape is the second most distinctive attribute, which can be used to further identify the type of a road sign. The shape of a road sign can play a vital role in distinguishing road sign from other arbitrarily shaped objects that may be detected due to being of similar colour. In addition the shape of a road sign may also be used to identify to which road sign group a given road sign belongs to; i.e. triangular, rectangular or circular.

In the work presented in this chapter the shape features are extracted by using *Contourlet Transform* and their subsequent classification is carried out by applying the popular *SVM* based approach. The robustness of the proposed shape identification and classification is particularly tested on road signs with abnormal appearances, i.e. ones that are partially occluded, may be of different size (scale) and orientation. The shape based analysis of road signs is helpful in two ways in *RSDR*. Firstly it removes the false positives extracted as candidate road signs during colour based segmentation (see chapters 4 and 5). Secondly subsequent detailed content recognition in road signs (see chapter 7) will only be performed on signs belonging to a particular group i.e., either circular, rectangular or triangular in nature in which case the identification of this basic shape is vital.

This chapter is organized as follows: Section 6.1 provides an introduction to the various shapes of the road signs and their distinctive properties. Section 6.2 provides the methodology adopted for the shape feature extraction and classification. Section 6.3 provides the experimental details, results obtained and a detailed analysis. Finally section 6.4 provides a summery and conclusion leading to the work presented in chapter 7.

6.1. Introduction

The shape information is as important as the colour of a road sign. The shape of a road sign is represented by a number of basic 2-dimensional geometric shapes having distinct but easily identifiable features. The most popular road sign shapes are illustrated in figure 6.1.

(a) **(b)** **(c)** **(d)** **(e)**

Figure 6.1: 2-dimensional geometric shape representations of road signs

The extraction of the geometric features of road sign shapes is carried out on the colour segmented candidate road sign regions (i.e. blobs) obtained by following the approaches presented in chapters 4 and 5. These segmented blobs may be of any arbitrary shape whereas a blob representing a true road sign region will be of a specific geometric shape which can be identified according to the number of sides it contains (see table 6.1).

Shape	**Number of Sides/layout**
Circular	Round/ 2π radians angle
Octagonal	8 / All Sides Equal
Triangular	3 / Equal sides at 60 degree angle
Triangular	3 / Equal sides at 60 degree angle
Rectangular	4/ Two opposite sides are equal

Table 6.1: various road sign shape properties, where Triangular and shapes are shown in figure 6.1(b) and (c) respectively

The basic shape properties listed in table 6.1 are further summarised as follow;

Circular: A circle, by definition, comprises of a set of points which are located equal in distance from its origin/centre. The circumference of a circle represents the total length

across the perimeter of the circle and it can be measured as given in equation 6.1. The area of the circle can be computed from the equation 6.2.

$$Circumference = 2\pi r, \tag{6.1}$$

$$C_{Area} = \pi r^2, \tag{6.2}$$

In the equations above r, represents the radius of the circle.

The most common circular shape road signs are illustrated in figure 6.2.

Figure 6.2: Common circular road signs [94]

Octagonal: An octagon [85] is a regular polygon consisting of 8 equal sides. The interior angle between two sides is 135^o and each side produces 45^o angle from an octagon centre. The area of an octagon can be computed according to equation 6.3 [85].

$$O_{Area} = \frac{1}{4} n s^2 \cot\left(\frac{\pi}{8}\right), \tag{6.3}$$

Where n and s are representing the number of sides and the length of one side in an octagon, respectively. An example of an octagonal road sign is illustrated in figure 6.3.

Triangular: The triangles [86] used in road signs shape are equilateral triangles in which the length of each side is equal. The angle between sides of an equilateral triangle is also uniform and is standardized as 60^0 at each corner of the triangle. Thus the area of an equilateral triangle can be computed with equation 6.4 below.

Figure 6.3: An octagonal road sign

$$T_{Area} = \frac{1}{2}ah, \tag{6.4}$$

where a represents the length of one side of an equilateral triangle whereas h represents the altitude which can be computed using the equation 6.5 below.

$$h = a \sin 60^{o}, \tag{6.5}$$

The road signs that are represented by triangular shapes are shown in figure 6.4, where the symbols *Triangle* ▼ and *Triangle* ▲ are representing the triangles pointing *downwards* and *upwards* respectively.

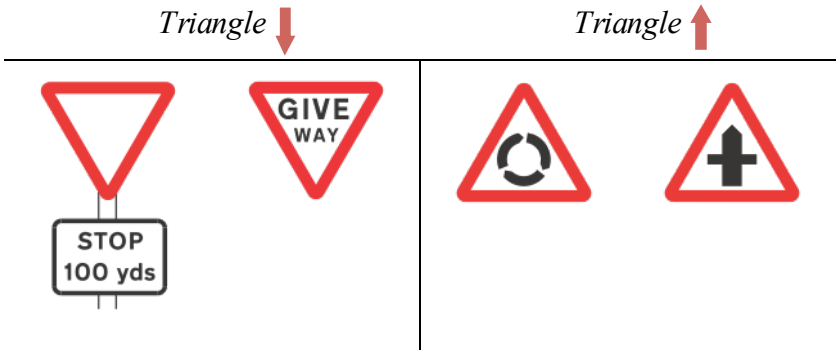

Figure 6.4: Triangular shape road signs [94] representing their distinctive orientation

Rectangular: A rectangular shape contains 4 sides in which two opposite sides are equal in length. The area of the rectangular shape can be computed as given in the equation 6.6 below.

$$R_{Area} = ab, \tag{6.6}$$

where a and b represents two equal and opposite sides of the rectangle. The road signs of rectangular shape are shown in the figure 6.5.

Figure 6.5: Rectangular shape road signs [94]

The analysis of road sign shape is helpful in removing potential false road sign objects segmented due to pure colour based ROI selection described in chapters 4 and 5. The false objects consist of those objects which can contain similar colour as of the road sign. For example the vehicles with red, green and blue colour, back lights of the vehicle, letter box and advertising billboards etc are representing potential false objects of similar colour as of the road signs. The road sign shapes carry very distinctive features from other arbitrary shape objects found in the natural environment. These distinguishing shape features are extracted with the help of the *Contourlet Transform* [53] which was briefly summarised in chapter 3. These features are subsequently used to train a *Support Vector Machine* [106] that can subsequently be used for classifying input road sign regions to different road sign shape groups. Section 6.2 presents the relevant adopted methodology used in the development of robust road sign shape classification algorithm.

6.2. Methodology

This section presents the procedure adopted for the classification of road sign shapes. It is noted here that 'shape' within the context of this chapter refers to the outside contour

shapes of the road signs. Figure 6.6 illustrates a block diagram of the proposed road sign shape classification approach. The input images to the system are the binary images resulting by applying the colour based segmentation algorithms presented in chapters 4 and 5 (*see figure 4.1 and figure 5.1*). The binary input images are pre processed in way so that only outer candidate shape is considered in later processing stages. The pre processing stage has explained in section 6.2.1. The features extraction of candidate shape is carried out by employing *Contourlet Transform* [53] with 3-level decomposition which is explained in section 6.2.2. Section 6.2.3 explains the classification of the input shape features with the trained shape features. The output of shape classification will therefore confirms that whether the candidate shape is an arbitrary shape or a road sign shape. In case of perfect match with a particular road sign shape, it will proceed for the content classification (explained in chapter 7) and vice versa.

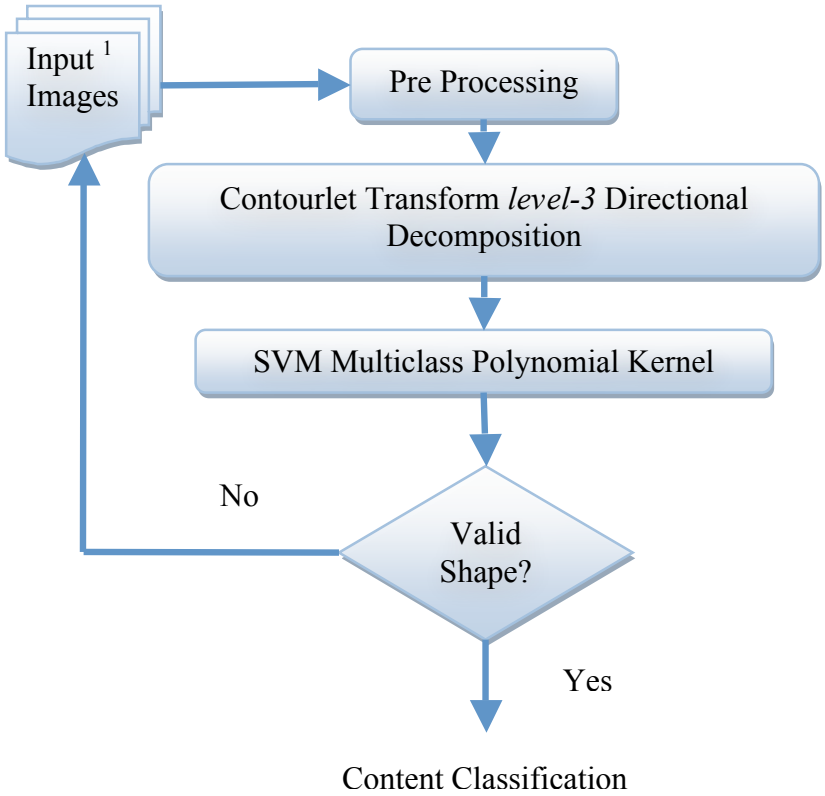

Figure 6.6: Block diagram of shape classification methodology, [1]The input images are the segmented objects from binary images.

6.2.1. Pre-processing

In this stage the road sign shape is normalized in such a way so that only those features, which represent the shape of an object, are extracted. The segmented binary candidate road sign represents *shape* and its *contents* in most cases of the colour segmentation output. The *contents* of the road signs can create difficulties in the shape classification as one *shape* can represent various *contents* of the road signs. Figure 6.7 shows some examples of binary candidate road signs reflecting different meanings according to their contents while representing similar shape. To avoid this complexity *Morphological region filling* [87] is applied on binary candidate road sings as given in the equation 6.7.

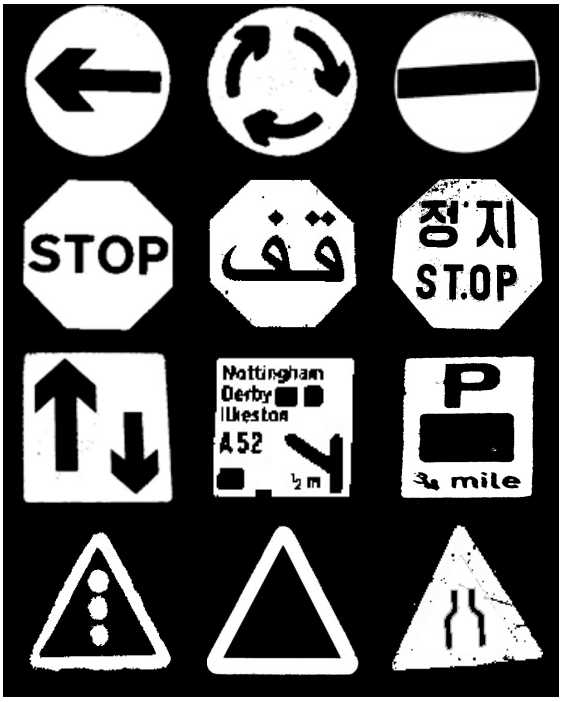

Figure 6.7: Candidate road signs of similar shape with distinct contents

$$X_k = (X_{k-1} \oplus B) \cap A^c, k = 1,2,3, \ldots \quad (6.7)$$

Let A is the input binary image then A^c is representing its complement, B is symmetric structuring element. The equation performs k, iterations until, $X_k = X_{k-1}$. Here X_k is

only representing the filled inner region of the road sign without its boundaries. The completely filled candidate road sign is obtained with the help of equation 6.8.

$$I_{filled} = \{X_k\} \cup \{A\}, \tag{6.8}$$

Where X_k, represents the set of inner region; A, is the set of boundary region and ∪ is the union operator for two sets. The region filled road signs shown in figure 6.8 are representing the outer shape of the road signs without its contents.

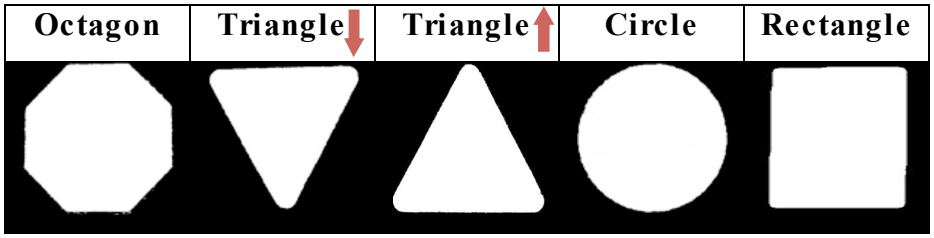

Figure 6.8: Representation of road signs after morphological region filling

6.2.2. Shape Feature Extraction

The features extraction of pre processed road sign shapes are extracted by employing *Contourlet Transform*. The Contourlet features of binary object(s), as shown in figure 6.8, are constructed by applying two successive decomposition stages. The first stage consists of transforming the binary objects in to *Laplacian Pyramid* (LP) [78, 95] which gives $1 + L$ scale levels. This result in one coarse image approximation and L band pass images. L band pass can represent 2^n number of images where n represents the number of decomposition levels. The second stage is the decomposition of each *LP [78, 95]* level into directional sub bands through a *directional filter bank* structure using *quincunx filters* [96] and critical down-sampling operators [66].

The shape features of the road sign are mainly based on contourlet features extracted across each multi resolution directional sub band. Each directional sub band is represented by a sub-image that contains its scale levels, frequency directions and total number of its coefficients. Let d be the frequency direction of the Contourlet

decomposition; the calculation of directional map Map_d, as shown in equation 6.9 acts as a key in extracting the contourlet features [53].

$$Map_d(i,j) = \frac{1}{2}B(i,j)T(i,j)^{0.2}E(d,i,j)^{0.2}, \tag{6.9}$$

Where

$$B(i,j) = 1 + \frac{1}{256}C_{L+1}(2i-1,2j-1) \tag{6.10}$$

$$T(i,j) = var\{C_{L+1}(2i-1+y, 2j-1+x)\}_{x=0,2;y=0,2} \tag{6.11}$$

$$E(d,i,j) = \frac{1}{4}\sum_{l=1}^{L}\sum_{x=0,1}\sum_{y=0,1}\left[C_{l,d}(i+y, j+x)\right]^2 \tag{6.12}$$

$C_{l,d}$, represents the Contourlet sub band image at l scale level and d frequency directions. C_{L+1}, is the coarse image and B represents its brightness. T, is representing the local texture in the low pass sub band image and E represents the oriented image edges across scales of directional resolution [66]. Figure 6.9 shows the Contourlet representation of Hexagon and Triangle shape.

6.2.3. Shape Feature Classification

This section explains the classification of shape features which is achieved by employing SVM. Let x_i are the shape features y_i are the class labels of the specific shape, then the SVM data set can be written as presented in equation 6.13 [106].

$$dataset_i = (x_i, y_i)_{1 \le i \ge n}, \tag{6.13}$$

Where,

$$x_i \in S_i \cup S_n, \tag{6.14}$$

$$y_i = \begin{cases} i, if\ x_i \in S_i \\ n, if\ x_n \in S_n \end{cases}, \quad (6.15)$$

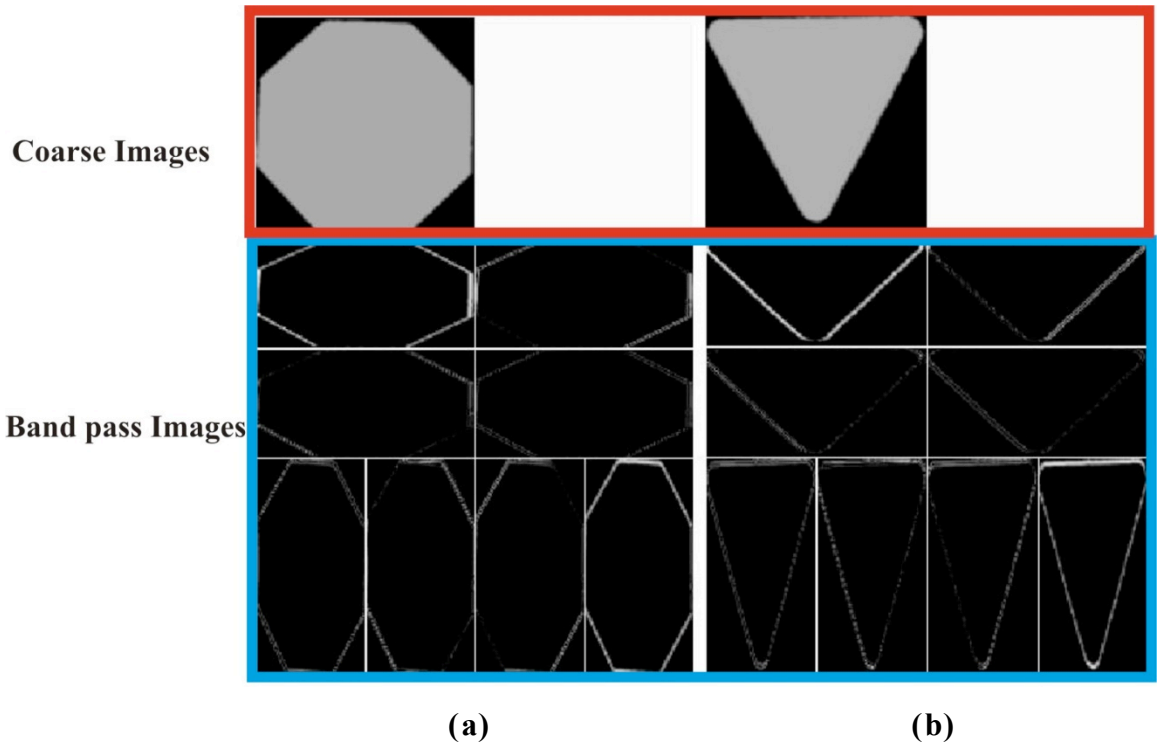

Figure 6.9: Contourlet representation (a) Hexagon Shape (b) Triangle Shape

Equation 6.16 shows the representation of shape features that are mapped in a higher dimensional space by using polynomial kernel function.

$$w = f(dataset_i, k), \quad (6.16)$$

k, is the kernel function used to train the SVM [106] data set in a higher dimensional space. The testing road sign data sets are compared with the mapped shape features as given in the equation 6.17.

$$I_{label} = f(test * w), \quad (6.17)$$

I_{label}, returns the label of classified shape class when $test$, representing datasets of input shape (test shape features) are compared with the mapping w (trained shape features).

The classified road sign shape is further processed for its content recognition which is explained in chapter 7. The shape classification significantly reduces the complexity in the recognition stage as only the contents of classified shape class will be considered for recognition.

6.3. Experimental Setup and Results

The experiments were carried out on five different shape classes i.e. Octagon, Triangle (pointing downwards), Triangle (Pointing upwards), Circle and Rectangle as shown in figure 6.8. The input images to the shape classification algorithm are *ROI* selected as candidate road signs with the help of colour based segmentation (see chapter 4 and chapter 5). The selected *ROI* always contains the contents or holes which need to be pre processed and normalised before shape features extraction. The shape of an object is represented with its outer contours edges. For this purpose the content regions of every road sign representing different shapes are filled and then normalized to the square size of 250×250 .

The shape features are obtained by employing *Controurlet Transform* from the pre-processed images. For our experiments we have used a 3- level decomposition of band pass images which produces 8 images of frequency distribution at the angle 2π. The purpose of using 3-level decomposition of *LP [78, 95]* and *DFB (Directional Filter Bank) [79]* is to obtain not only horizontal and vertical contours edges of the shape but also the diagonal contour edges which can help in distinguishing the circular and hexagonal shapes. Figure 6.10 shows 3-level ($2^3 = 8\, images$) frequency distribution at two image scale levels. Figure 6.10 is distributed into two halves; red border area represents column frequency distribution and blue border area presents row level frequency distribution.

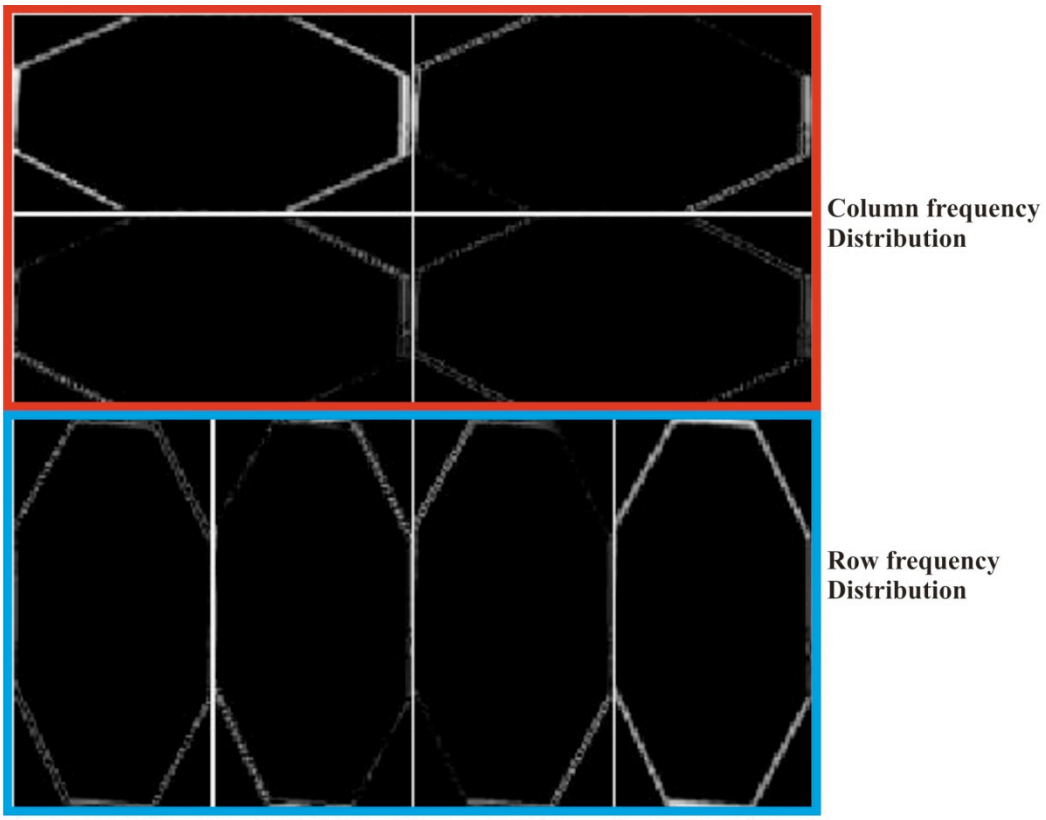

Figure 6.10: Contourlet Transform[53] frequency distribution at two scales

Further to that the distribution also utilises the most widely used filters such as *Haar*, *5-3* (MacClellan transformed), *cd* and *9-7* (Cohen and Daubechies), *pkva* and *Burt* filters with in LP [78, 95] and DFB [79].

The experiments are carried out by selecting '*Haar filter'* for both pyramidal and directional distribution. Table 6.2 shows the properties of *Contourlet Transform* selected to obtain the shape features of each road sign shape class.

These selected shape features for each road sign shape are assigned distinct labels to distinguish one class from another. The shape features and the class labels are bound together as data sets by using *SVM polynomial kernel*. The training of the shape features is carried out on 50 samples per class while considering various scales and orientation levels. The *SVM* helps in classifying the tested shape features as either one of the shape

class or non-shape class; when trained classes include five shape classes and one non-shape class.

Index	Shape	Level	Pyramidal Filter	Directional Filter	Trained Instances
1	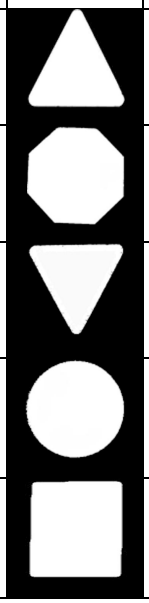	3	Haar	Haar	50
2		3	Haar	Haar	50
3		3	Haar	Haar	50
4		3	Haar	Haar	50
5		3	Haar	Haar	50

Table 6.2: Contourlet Transform [53] properties selected for each shape class

Table 6.3 shows the success percentage while using different decomposition levels on each shape class. *Level-2* decomposition produces four images ($2^2 = 4$) to represent the edge distribution of a shape. As a result it represents less (or none) diagonal edge information which are more important to distinguish one shape from another. The triangular shapes tested with this decomposition are wrongly interpreted as square or as non classified shape; where the test triangular shape is slightly tilted and angular in orientation. Similarly hexagonal shapes trained on this level are wrongly interpreted as circular shapes. Hexagon shape contains eight sides to represent the shape and *level-2* frequency decomposition does not cover all angular orientation of each side of hexagon shape. We have obtained maximum success rate when level-3 frequency distribution of band pass image is tested. *Level-3* gives directional edge information at angle 2π and considers all sides of hexagon shape. Over *1200* road sign shapes at various scales, orientations and partial occlusions are tested to obtain these accuracy figures. The testing

data set includes 600 circular, 400 triangular, 97 Octagonal and 103 samples of squared shapes of the road signs. Figure 6.11 shows the classification success percentage obtained for each shape index while considering the level of frequency decomposition. It should be noted that success percentages provided in Table 6.3 can only achieved when 50 features per shape class are trained with SVM. The shape classification is considered as a key input for the content recognition of the road sign. The next section provides the summery and the conclusion of this chapter.

Shape Index	**Classified Shapes with decomposition level**			
	Level	*Success*	*Level*	*Success*
1	2	75%	3	100%
2	2	0%	3	100%
3	2	75%	3	100%
4	2	100%	3	100%
5	2	100%	3	100%

Table 6.3: Success percentage at different decomposition Levels

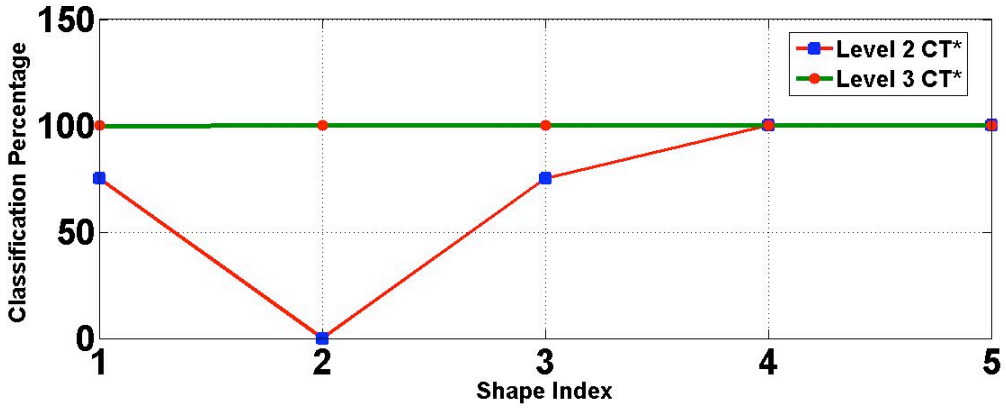

Figure 6.11: *SVM* classification results, *CT* = Contourlet Transform

6.4. Summary and Conclusion

In this chapter a robust algorithm towards road sign shapes detection and classification is presented. The algorithm introduces *Contourlet Transform* to extract the shape features and *SVM* for shape classification at various levels of orientations, scales and occlusions.

The candidate road signs (binary objects) obtained as a result of colour segmentation, are pre-processed in a way so that they reflect only the outer contour shape of the road sign. The contents of the road signs or the holes are filled using *morphological region filling* [87] and the shapes are normalized to square dimensions during the pre processing stage. The shape features are obtained by using *Contourlet Transform* at Level-3 frequency decompositions and *haar* property is utilized for each *LP* [78, 95] and *DFB* [79]. The shape features of five different shape classes are trained on *SVM* [106] and the test shape is classified as road sign shape or non road sign shape when mapped with the trained shape features. The classification results of *SVM* based shape features along two frequency decompositions i.e. *level-3* and *level-2*, are compared.

The shape classification is utilized in measuring the accuracy of colour based segmentation, while comparing selected *ROI* with the trained road sign shapes. The shape classification acts as vital information for the content recognition of the road signs which is presented in chapter 7. The complexity of the content recognition is minimized by considering those contents for recognition which are classified as a road sign shape.

Chapter 7

Road Sign Recognition using LESH Features

7.0. Preface

The ultimate recognition of a road sign depends on its contents enclosed within a basic geometric shape (e.g. circular, triangular and square shapes etc.). Although the basic geometric shapes can be detected and recognised as described in the previous chapter (see chapter 6), a new approach is required to recognise the internal contents of the road sign. The contents of the road sign vary according to the message it is intended to deliver to the road users. Let's take the example of the scenario at the crossroad of a single-carriageway emerging on to a dual-carriageway; a 'GIVE WAY' sign is placed to warn driver about the potential hazards that may be incurred when joining the dual-carriageway.

In this chapter the internal contents of a road sign are treated as to be distinguished and identified from other classes of the road signs. A method previously used in face recognition, *LESH* [107] is utilised to extract the prominent road sign features. *SVM* [106] is employed in the classification of these features. In particular the work presents the efficiency of the proposed approach on abnormal appearances of road sign contents, specifically at various scales (sizes), partial occlusion and angular rotation.

This chapter is organized as follows: Section 7.1 gives an insight into the details of contents of various road signs defined in the UK Highway Code and their intended use within a road network. Section 7.2 introduces the methodology adopted for feature extraction and classification. The detailed explanation of each operational stage is

provided in this section. Section 7.3 provides the experimental design, results obtained and an analysis, leading to summarisation and conclusion in section 7.4.

7.1. Introduction

The internal contents of a road sign contain the distinctive meanings among road signs that have the same colour and external shape, e.g. signs defining speed limits of 30 and 50 mph (miles per hour). The contents are normally located at the centre of a road sign that is bordered by a particular colour and shape as illustrated by few examples of road signs in the Table 7.1.

(a) **(b)** **(c)** **(d)** **(e)**

Table 7.1: Traffic signs [94] representing different internal content; (a) round about (b) stop (c) give way (d) no right turn (e) motorway sign

In the road signs defined by the UK Highway Code there are significant variations in the internal contents. Such contents can be broadly divided into content groups, namely, alphabetic characters, number digits, abstract symbols or their combinations. For example some road signs may present different speed limits which require use of number digits and some may contains symbols giving an abstract idea of a warning, such as the sign of flooding. The following paragraphs provide additional details about these road sign contents groups.

Alphabetic Characters: This group includes 26 characters of the English language alphabet and their additional subdivision into two classes, representing the lower case and upper case letters. Generally the font style of alphabetical characters used within road signs are unique [93] and are distinguishable from other examples of use of characters in

the outdoor environments such as advertising bill boards and vehicle number plates. More frequently in road signs the alphabetical characters are used as contents to indicate city/town names or as combinations with other groups of symbols as illustrated by Table 7.1 (e).

Numbers/Digits: The numbers or digits from 0-9 are a further common group of road sign contents (e.g. speed limit signs). More commonly in the UK road signs for road names have seen frequently adopting alphanumeric character sets (Table 7.1 (e)). For example motorways names such as M1, M4, M6, M42 and names of countryside roads such as A6, A505, A52, A74 etc. Numeric digits are also used to describe the distance of journey left to a particular named destination or it indicates about upcoming exit number on a motorway, as shown in the Table 7.1 (e). Generally and legally the font style adopted should be distinguishable from other commonly used font styles in [93] such as those used in vehicle license plates.

Symbols: Contents that do not belong to the above two groups, i.e. alphabetic and numeric characters, are classified as symbols. Symbols are used to present obligations, rules, advices and places etc to the road users. Appendix A to D of the thesis presents road sign symbols that are specifically used in training of classifiers used within the context of research presented in this thesis. It is noted that further new road sign symbols can be added as required.

The details provided above conclude that the analysis of road sign contents can help in recognising and distinguishing the road signs. In this chapter an approach based on LESH features for the shape based analysis of road sign content that may include symbols, digits and alphabetic characters is adopted. Section 7.2 presents the details of the methodology adopted including pre processing (see section 7.2.1) feature extraction for road sign contents using LESH (see section 7.2.2) and LESH feature classification using SVM polynomial kernel (see section 7.2.3).

7.2. Methodology

This section provides the methodology of the proposed contents based road sign classification approach which is illustrated as block diagram in figure 7.1. The input images / image sequences to the system are the segmented road signs extracted from the original image by following the procedures presented in chapters 4 and 5. These images not only contain the internal contents of the road sign but also the outside shape, colour sections and some of the background environment. The pre-processing (see section 7.2.1) stage helps in the normalisation of the input images by limiting the segmentation to the internal sections of the road sign that includes the possible contents. Subsequently a feature extraction approach is adopted which is based on LESH and is detailed in section 7.2.2. Finally the extracted features are classified using SVM polynomial kernel (see section 7.2.3) leading to the ultimate recognition of the road sign.

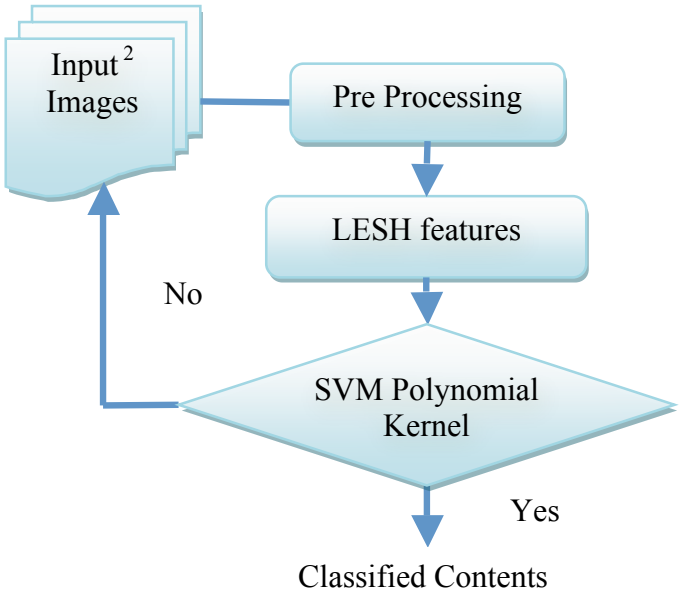

Figure 7.1: Methodology block diagram shows content based classification and recognition of the road signs, [2] Extracted candidate road sign from the original RGB image (see figure 4.1 and 5.1).

7.2.1. Pre-processing

The input images are the complete candidate road signs extracted from the original RGB image. These extracted candidate road sign images represent the contents of the road signs along with their external boundary represented by the basic shapes as extracted in chapter 6 and colour information. The internal content of the road signs are ideally represented with black, white or combination of both colours. The first *stage* of the pre-processing consists of extracting the desired internal contents of the road sign and listing them as candidate road sign content. Let I be the original RGB image, the internal contents of the road sign are finally to be represented as binary images as given in equation 7.1.

$$I_{binary} = f(I), \tag{7.1}$$

Where $f(I)$ represents the binary image conversion function applied on the original RGB image I. The image I_{binary} is obtained using adaptive threshold values of pixels.

The *second stage* of the pre-processing represents the acquisition of the connected components from I_{binary} image by using equation 7.2.

$$X_k = (X_{k-1} \oplus B) \cap I_{binary}, \quad k = 1,2,3, \ldots \tag{7.2}$$

Where X_k, represents the set of connected components; B, is the suitable structuring element and $I_{binary,}$ is the binary image. The *final stage* of the pre-processing prepares the extracted internal contents of the road sign according to the suitable inputs required by the subsequent feature extraction stage. This involves the resizing of the image into 128×128 pixels and converting the image in to a gray scale image. The following section explains the feature extraction procedure applied on pre-processed road sign contents resulting from this section.

7.2.2. Feature Extraction

The road sign contents features extraction is carried out on pre processed images by using Local Energy based Shape Histogram. LESH introduces a local energy model [89] which enables features to be extracted at those points of an image where local frequency components represent maximum uniformity. The extended framework of this energy model [89] is given by equation 7.3 which is normalised by the summation of noise cancellation factor T, *Sine* of phase deviation, and $W(x)$, the weighting of the frequency spread. $A_n(x)\ and\ \phi_n(x)$, represent amplitude and phase angle respectively of local complex value, Fourier components at location x, in the signal. Constant value ε, is incorporated to avoid division by zero. Further details about this extended framework can be found in [90].

$$E = \frac{\sum_n W(x)\left\lfloor A_n(x)\left(\cos\left(\emptyset_n(x) - \overline{\emptyset}(x)\right) - \left|\sin\left(\emptyset_n(x) - \overline{\emptyset}(x)\right)\right|\right) - T\right\rfloor}{\sum_n A_n(x) + \varepsilon} \tag{7.3}$$

The Local Energy gives reliable information to extract the interest points in an image in an invariant manner to illumination and noise. This raw energy indicates the corners, contours or edges of underlying shape of an image. LESH for road sign contents region is generated by using this local energy information along eight different orientations obtained using Gabor wavelet kernels, [91, 92], on each of sixteen sub regions of contents image as shown in the figure 7.2(b).

$$G_{u,v}(z) = I(z) * \Psi_{u,v}(z) \tag{7.4}$$

Where $z = (x, y)$ represents the image position, the symbol "$*$" is convolution operator and $G_{u,v}(z)$ is the convolution result to the Gabor kernel at orientation , u, and scale, v. Gabor Wavelet kernel $\Psi_{u,v}(z)$ can be calculated as given in the equation 7.5.

$$\Psi_{u,v}(z) = \frac{\left\|k_{u,v}\right\|^2}{\sigma^2} e^{\left(\|k_{u,v}\|^2 \|z\|^2 / 2\sigma^2\right)}\left[e^{ik_{u,v}z} - e^{-\sigma^2/2}\right] \tag{7.5}$$

Where $\Psi_{u,v}(z)$ represent Gabor Wavelet (kernel, filter) , e, represents Gaussian envelope, also $k_{u,v} = \begin{pmatrix} k_{jx} \\ k_{jy} \end{pmatrix} = \begin{pmatrix} k_v cos\phi_u \\ k_v sin\phi_u \end{pmatrix}, k_v = f_{max}/2^{v/2}$, where v represents the frequency and u, is the orientation. Further to that value of σ is defined as $\sigma = 2\pi$.

The orientation label map is produced representing labels of orientation of pixels containing largest energy across all scales in an image. The local histogram h can be calculated as presented in the equation 7.6.

$$h_{r,b} = \sum w_r \times E \times \delta_{L-b} \tag{7.6}$$

Where w_r , is the Gaussian weighting function of region r, E, represents the local energy computed as equation 7.3 and δ_{Lb}, represents Kronecker's delta of orientation label map L , and current bin b. From the above description it can be seen that the LESH descriptor of an input image is a $8\times16 = 128$ dimensional feature vector as illustrated in figure 7.2(c). The input image(s) for LESH feature extraction are the pre processed road sign contents.

7.2.3. LESH Feature Classification

This section explains the classification of extracted LESH features which is achieved by employing a *SVM polynomial kernel*. Suppose that x_i are the LESH features and y_i are representing their respective class labels, then the SVM data set can be written as presented in equation 7.7.

$$dataset_i = (x_i, y_i)_{1\leq i\geq n}, \tag{7.7}$$

Where

$$x_i \in S_i \cup S_n, \tag{7.8}$$

$$y_i = \begin{cases} i\ ,if\ x_i \in S_i \\ n, if\ x_n \in S_n \end{cases}\ , \tag{7.9}$$

$dataset_i$ in equation 7.10 is the representation of LESH features that are mapped in a higher dimensional space by using a linear kernel function of SVM.

$$w = f(dataset_i, k), \tag{7.10}$$

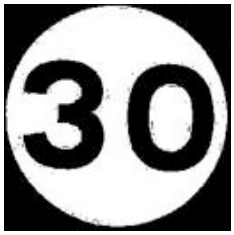

(a)

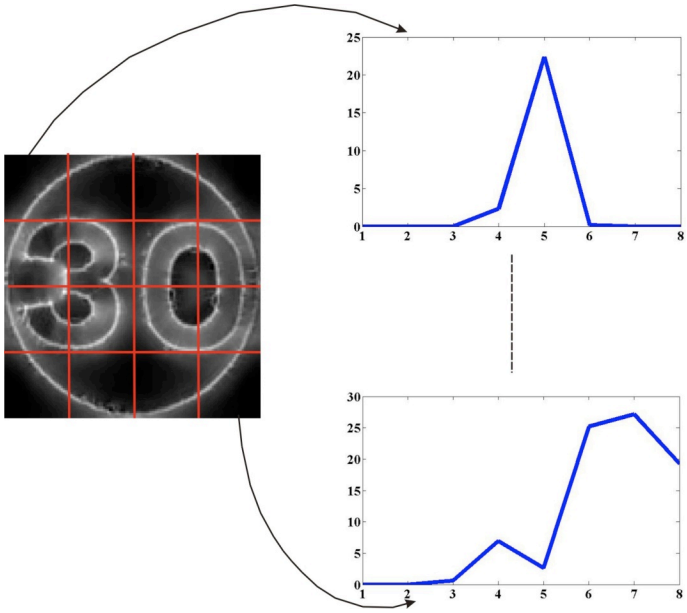

(b)

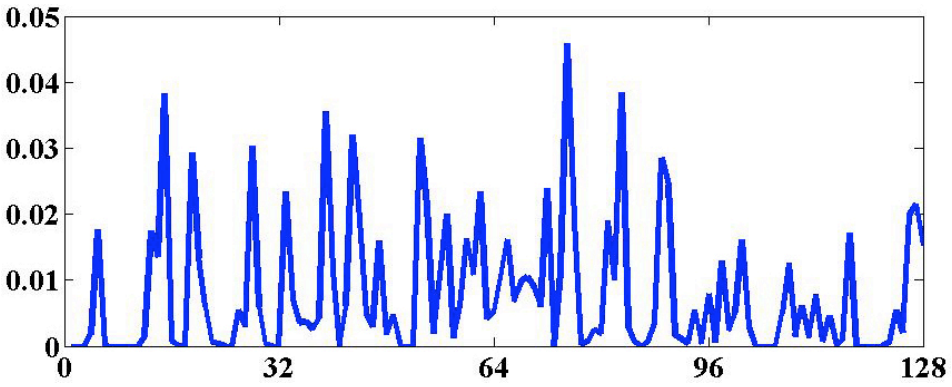

(c)

Figure 7.2: LESH feature extraction (a) The input image (b) 4×4 location grid imposed on the corresponding local energy map of input image with 8-bin local histogram extracted from each partition of the image (c) Concatenation of all histograms of the image-(b) to generate a 128 dimensional feature vector.

where k, is the kernel function used to train the SVM data set in a higher dimensional space. The *test* road sign image sequence is compared with the mapped LESH features w, as given in the equation 7.11.

$$C_{label} = f(test * w), \tag{7.11}$$

C_{label}, returns the label of classified road sign content class when $test$, representing dataset of test input road sign contents and are compared with the mapping w (trained LESH features). Section 7.3 provides details of experimental setup, results obtained and an analysis.

7.3. Experiments, Results and Analysis

The experiments to recognise road sign contents are carried out on segmented regions of the road signs excluding their basic shape and colour, as described above. These image regions are pre processed to remove noise and to normalise according to subsequent feature extraction requirements. The following three paragraphs briefly present the pre-processing stage and the results.

The internal contents of road signs are normally represented as black and white colours illustrated in figure 7.3(a). The white and black areas can be extracted by simple black and white region extraction [110] using adaptive threshold. Figure 7.3(b) shows the extracted white and black regions of the road sign.

Figure 7.3: White and Black area extraction (a) Original road Sign image (b) Binary image representation

After obtaining the binary images as illustrated in figure 7.3 (b), the connected components from the binary image are extracted which removes the noisy objects (non sign objects) at the same time. The image(s) are normalised to a square dimensional image of size 128×128 and at the same time converted to gray level image.

Figure 7.4 illustrates examples of the extracted binary objects using the above pre processing algorithm which are later used for LESH feature extraction. It should be reminded that the image normalisation to a fixed dimensional size and its gray level conversion are the valid input requirements for LESH feature extraction.

The next stage is to extract the LESH features of the normalized images obtained through the pre processing stage. LESH features are obtained by computing the local energy along each filter orientation of image sub-region. The overall histogram represents the concatenated histograms computed along each sub-region of the image as explained in figure 7.2(c).

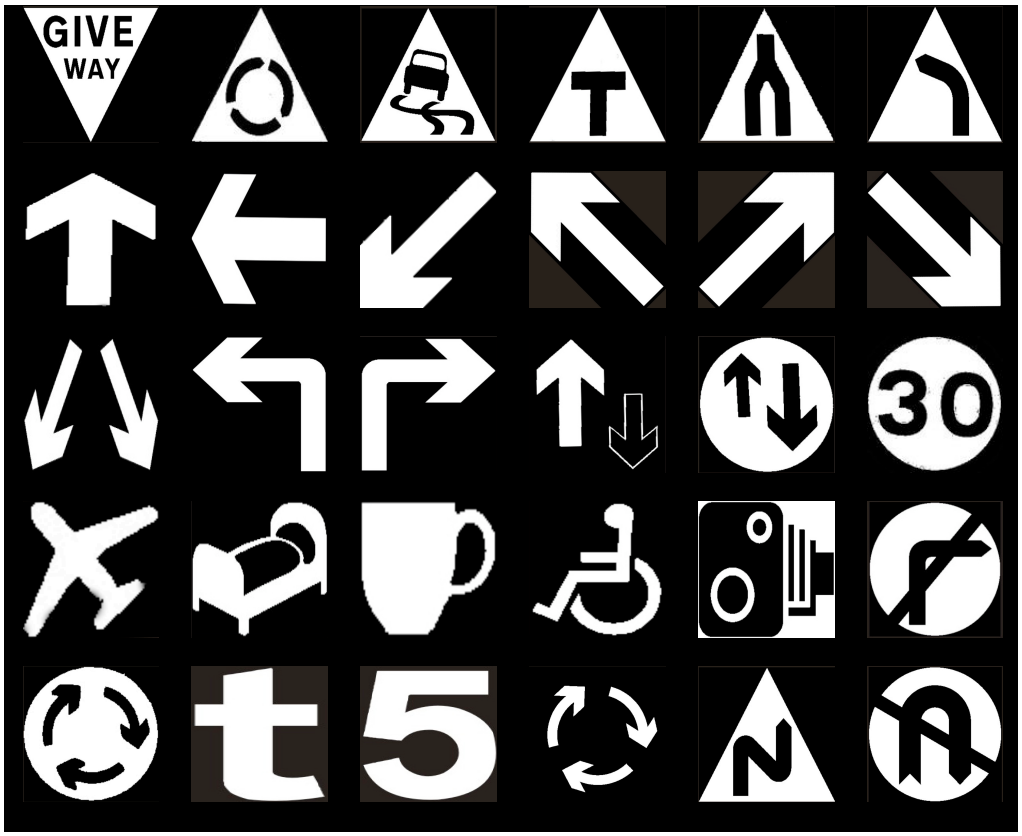

Figure 7.4: Examples of extracted binary objects representing the internal contents of road signs normalised to 128×128 pixels.

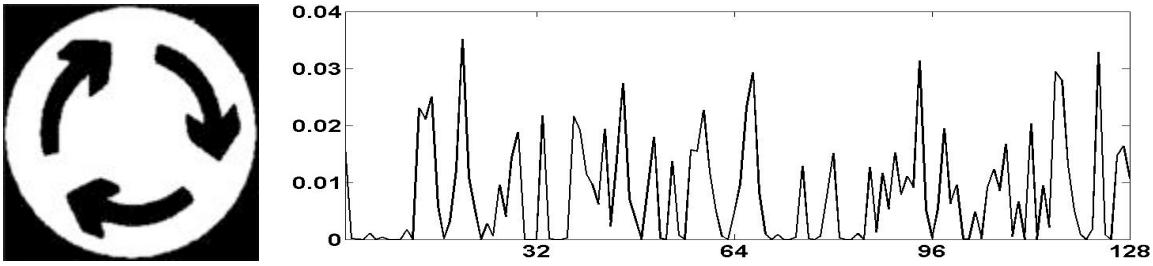

Figure 7.5: LESH representation of blue *round-about* road sign

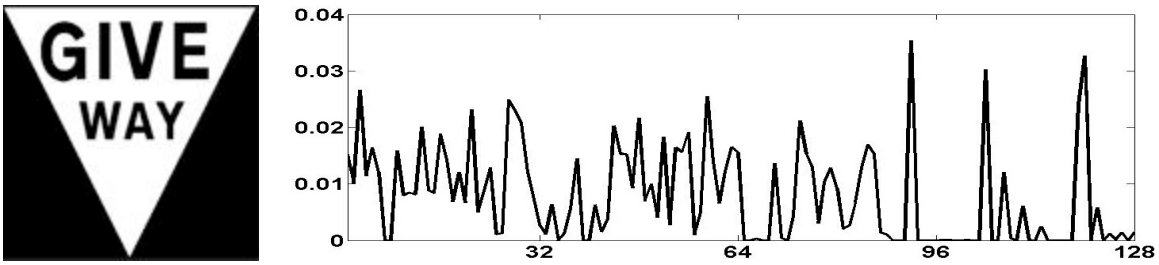

Figure 7.6: LESH representation of *GIVEWAY* road sign

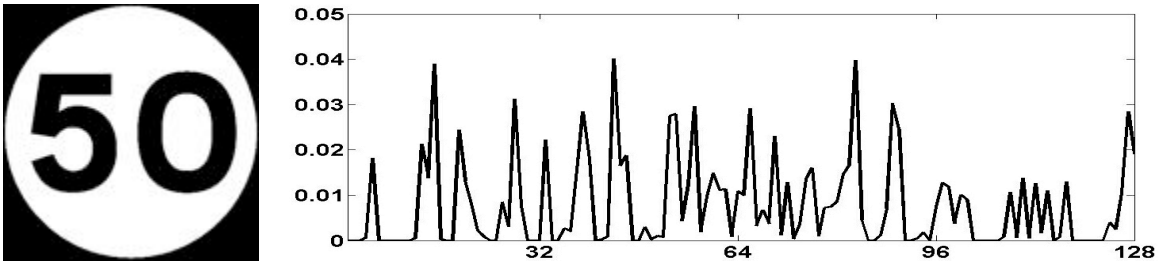

Figure 7.7: LESH representation of *'50' Speed limit* road sign

Figure 7.5, 7.6 and 7.7 show the distinctive Local Energy based Shape Histograms of 'Round About', 'GIVEWAY' and '50' speed limit road signs respectively.The feature classification of road signs is finally carried out by training the LESH features using a SVM polynomial kernel. The road signs used in training the SVM are manually extracted from still images and from a wide range of real-life video samples representing various scale levels and other distortions.

In the following sub sections the performance of the above mentioned road sign recognition approach is analysed through provided experiments on a number of different road signs presented in Table 7.2.

1	2	3	4	5	6	7	8	9	10	11	12	13	14	15
														

Table 7.2: Road signs presented with class labels on top of each other which are specifically considered in the experiments

True Labels	Estimated Labels															Totals
	1	2	3	4	5	6	7	8	9	10	11	12	13	14	15	
1	**40**	0	0	0	0	0	0	0	0	0	0	0	0	0	0	**40**
2	0	**40**	0	0	0	0	0	0	0	0	0	0	0	0	0	**40**
3	0	0	**40**	0	0	0	0	0	0	0	0	0	0	0	0	**40**
4	0	0	0	**40**	0	0	0	0	0	0	0	0	0	0	0	**40**
5	0	0	0	0	**40**	0	0	0	0	0	0	0	0	0	0	**40**
6	0	0	0	0	0	**40**	0	0	0	0	0	0	0	0	0	**40**
7	0	0	0	0	0	0	**40**	0	0	0	0	0	0	0	0	**40**
8	0	0	0	0	0	0	0	**40**	0	0	0	0	0	0	0	**40**
9	0	0	0	0	0	0	0	0	**40**	0	0	0	0	0	0	**40**
10	0	0	0	0	0	0	0	0	0	**40**	0	0	0	0	0	**40**
11	0	0	0	0	0	0	0	0	0	0	**40**	0	0	0	0	**40**
12	0	0	0	0	0	0	0	0	0	0	0	**40**	0	0	0	**40**
13	0	0	0	0	0	0	0	0	0	0	0	0	**40**	0	0	**40**
14	0	0	0	0	0	0	0	0	0	0	0	0	0	**40**	0	**40**
15	0	0	0	0	0	0	0	0	0	0	0	0	0	0	**40**	**40**
Totals	**40**	**40**	**40**	**40**	**40**	**40**	**40**	**40**	**40**	**40**	**40**	**40**	**40**	**40**	**40**	**600**

Table 7.3: Confusion Matrix of training samples of road signs given in Table 7.2

Table 7.3 presents the confusion matrix of the training samples for each of the road sign presented in Table 7.2. The classifier is trained on 40 normalised training samples for each class of the image presented in Table 7.2.

7.3.1. Experiment-1

The experiment provided in this section is carried out on speed limit (*Set-1*) signs i.e. '15','30','40','50' and ,'70' which are given class labels as T1,T2,T3,T4 and T5 respectively as presented in table 7.4. The *Set-1* road signs were already trained using 40 image samples per class as presented in Table 7.3. The testing is performed on video samples containing only speed limit signs; captured during various lighting conditions, were influenced by scale changes and partial occlusions. The confusion matrix of tested

road signs is tabulated in table 7.5. The ROC curve for tested *Set-1* signs is presented in Figure 7.8 in red colour where true positives are plotted against false positives.

T1	T2	T3	T4	T5
				

Table 7.4: Speed limit (Set-1) road signs

True Labels	Estimated Labels					Totals
	1	2	3	4	5	
T1	28	0	0	0	0	**28**
T2	0	64	0	0	1	**65**
T3	0	0	40	1	1	**42**
T4	0	0	0	18	4	**22**
T5	0	2	1	2	24	**29**
Totals	**28**	**66**	**41**	**21**	**30**	**186**

Table 7.5: Confusion Matrix of tested speed limit road signs

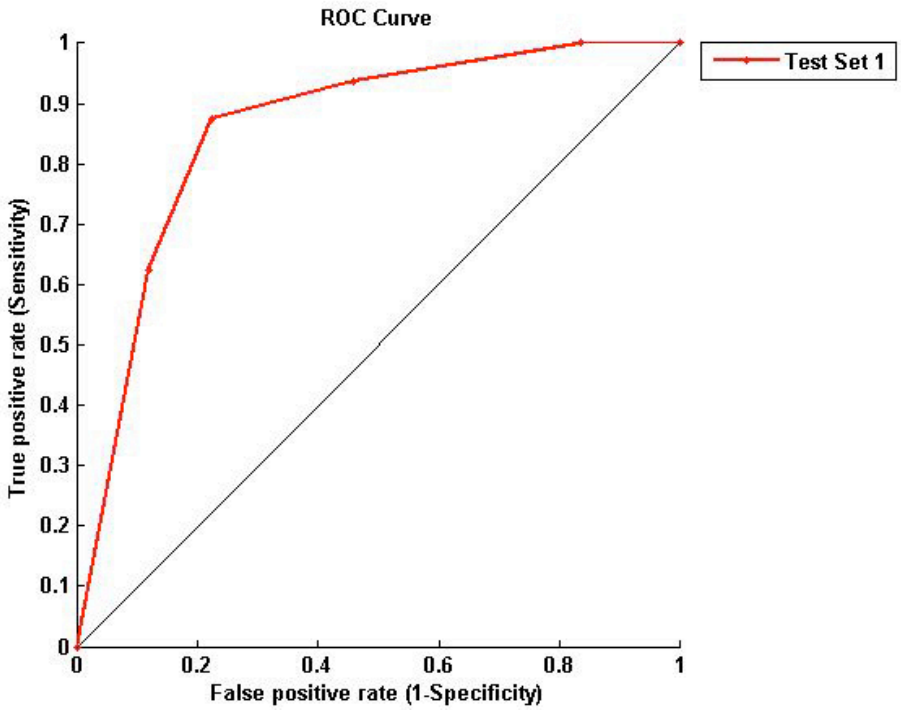

Figure 7.8: ROC curve of Set-1

7.3.2. Experiment-2

This experiment is carried out on 5 different triangular (*Set-2*) signs, i.e., 'GIVEWAY', 'Round about', 'Bend to Left Ahead', 'T-Junction' and 'Slippery Road' which are given class labels as T6,T7,T8,T9 and T10 respectively (see table 7.6). The training of *Set-2* road signs was performed on 40 image samples per class as given in Table 7.3. The testing is performed on the video samples which represents only *Set-2* road signs, captured during varying lighting and environmental conditions, with changes in scale and includes partial occlusion. The confusion matrix of tested road signs for this experiment is presented in table 7.7. Finally the ROC curve for the tested *Set-2* road signs is presented in figure 7.9 in blue colour where true positives are plotted against false positives.

T6	T7	T8	T9	T10
				

Table 7.6: Set-2 road signs

True Labels	Estimated Labels					Totals
	6	7	8	9	10	
T6	56	0	0	0	0	56
T7	0	64	0	1	0	65
T8	0	0	49	0	1	50
T9	0	1	1	35	7	44
T10	0	0	0	9	52	61
Totals	56	65	50	45	60	276

Table 7.7: Confusion Matrix of tested Set-2 road signs

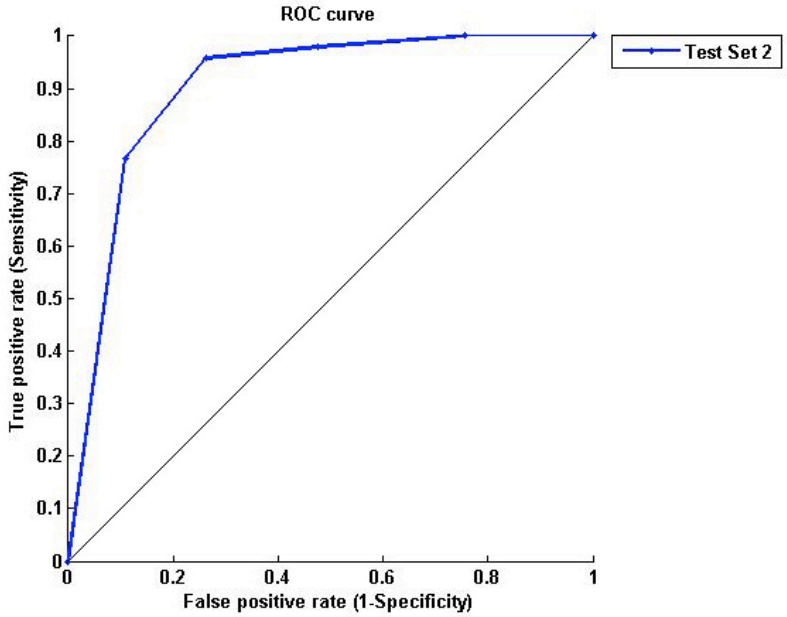

Figure 7.9: ROC curve of Set-2

7.3.3. Experiment-3

Set-3 is a further group of miscellaneous road signs (e.g. Advisory and Obligatory etc.) i.e. '*Priority*', '*Stop*', '*Turn Left*', '*No Entry*' and '*Round About*', and they are given class labels for this experiment as *T11, T12, T13, T14 and T15* presented in table 7.8. The training of *Set-3* road signs is performed on 40 image samples per class as given in table 3. The testing is performed on the video samples of Set-3 road signs captured during poor weather conditions, partial occlusion and abnormal orientation. The confusion matrix of tested road signs belongs to *Set-3* is presented in table 7.9. The ROC curve for tested *Set-3* road signs is presented in figure 7.10 in colour green where true positives are plotted against false positives.

T11	T12	T13	T14	T15
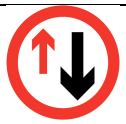				

Table 7.8: Set-3 road signs

True Labels	Estimated Labels					Totals
	11	12	13	14	15	
T11	12	0	0	0	1	**13**
T12	1	28	0	0	2	**31**
T13	0	0	8	0	6	**14**
T14	1	3	3	12	0	**19**
T15	0	0	3	5	18	**26**
Totals	**14**	**31**	**14**	**17**	**27**	**103**

Table 7.9: Confusion Matrix of tested Set-3 road signs

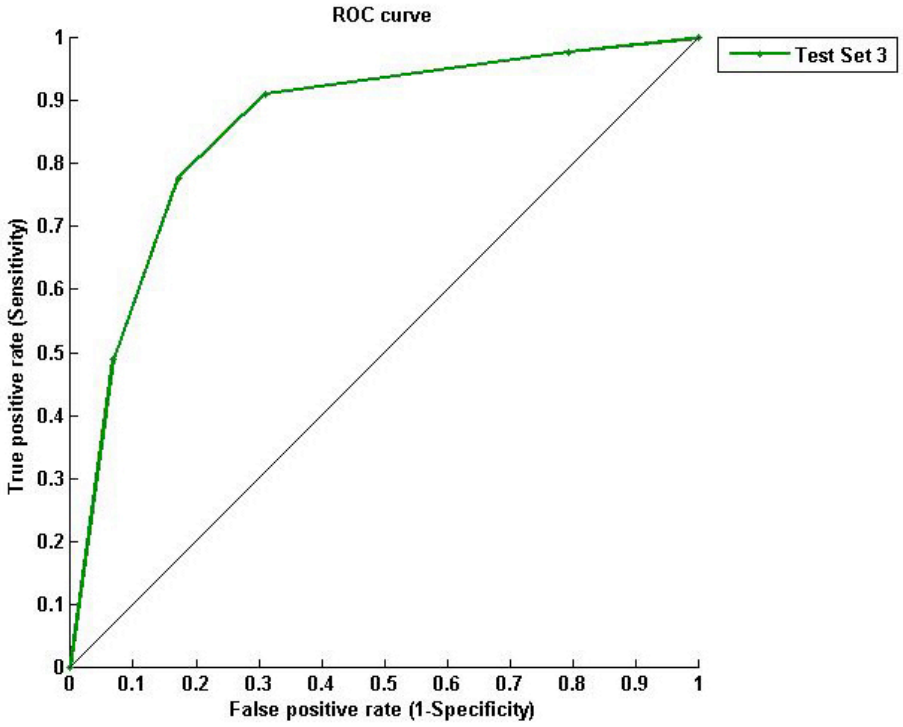

Figure 7.10: ROC curve of Set-3

It is noted that the experiments above were carried out on videos and image samples captured using *Canon IXUS80IS* digital camera. The images are captured at the resolution of 2592×1944 pixels where as video samples are captured at the resolution of 640×480 pixels. The accuracy [111] of the provided algorithm in this chapter according to above mentioned experiments can be measured by using the equation 7.12.

$$Accuracy = \frac{Number\ of\ TP + Number\ of\ TN}{Numbers\ of\ TP + FP + FN + TN} \tag{7.12}$$

Where from the above equation $TP, TN, FP\ and\ FN$ are acronyms of True Positives, True Negatives, False Positives and False Negatives respectively. Using the above equation accuracies of tested image samples of *Set-1*, *Set-2* and *Set-3* are recorded as 94.0%, 93.1% and 76.02% respectively. Table 7.10 presents the entire system evaluation while considering varying day light conditions.

Weather Conditions	Experiment Set	No. Of Video Frames	No. of Detected Road Signs	FP	FN	Accuracy
Cloudy/Sunny	Set-1	1670	186	7	3	94.0%
Rainy/Cloudy	Set-2	1535	276	9	11	93.1%
Evening/Night	Set-3	830	103	9	16	76.02%

Table 7.10: The entire system evaluation considering variable weather conditions, FP = False Positives, FN = False Negatives

Table 7.11 presents experimental results reported in a number of key existing RSDR algorithms and conceptually compared with the algorithms presented in this thesis. It is noted that some algorithms (e.g. [56]) perform real time whereas some others perform at a significantly lower speeds (e.g. [4]). Further the accuracy level varies with the change in the lighting conditions. The implementation of the *RSDR* systems is carried out in [4] by utilizing *2.2 Ghz Pentium 4-M*, *C language*, *Canon MVX30i* and images are captured at the resolution of 720×576 pixels. Whereas in [56] images are captured at the resolution 640×480 pixels by using *JVC GR-X5EK DV* camcorder.

Reference No.	No. Of Signs	Experimental Conditions	Processing Speed	Accuracy
[56]	164	Day light	20-25 frames per second	93.5%
[4]	62	Day light	1.77 seconds per frame	93.24%
	25	Rainy day		
	17	Night		
[5]	100	Day light	Images	86.0%
Proposed Algorithm	186	Day light	20-25 frames per second	94.0%
	276	Rainy day		93.1%
	103	Night		76.02%

Table 7.11: Comparison of recognition accuracies obtained by using varying datasets and lighting conditions

Unfortunately a comparison between results presented in Table 7.11 is not fair due to the use of different data sets for experiments. For those readers who are interested in a comparison of the performance of state-of-the art systems with that of presented in this thesis, the test database will be made available publically.

Figure 7.11 illustrates examples of false detection and classification of the road signs. A closer investigation of these results identified significant scaling, occlusions and possible shaking of the camera as reasons for the false detections and classifications.

Figure 7.11: Examples of false detections and classifications

7.4. Summary and Conclusions

This chapter has introduced a novel approach to the recognition of internal contents of the road signs. The algorithm has utilized the *Local Energy based Shape Histogram* for feature extraction of normalized road sign contents and *Support Vector Machine* is introduced for extracted contents features classification.

The work presented in this chapter initiates with the pre-processing of coloured candidate road signs extracted by using colour based segmentation (see chapter 4 and 5) and also satisfying the condition of valid road sign shape (see chapter 6). The prominent regions are extracted by converting the original RGB image into binary image format using adaptive thresholding and the connected binary components are extracted. The extracted connected objects are normalised to validate with the requirement of feature extractor where *LESH* is utilized to extract the content features. Training and testing of *LESH* features are performed by utilizing *SVM Polynomial Kernel*. In this chapter efficiency of the algorithm is tested on a large set of test image samples (video frames) captured under real-life conditions; where classification is tabulated as confusion matrix for each experiment and final results are presented as *ROC curves*.

The detailed analysis of the experimental results revealed that in combination with the approaches presented for the initial, colour based road sign region segmentation and external shape based pre-classification approaches presented in chapters 4, 5 and 6 respectively, the internal road sign content classification approach presented in this chapter results in an overall, robust road sign recognition system. The analysis further revealed that the proposed system is robust to illumination variations, degradation of colour due to weathering, partial occlusions and scale variations. However under severe partial occlusions and degradation of image quality the proposed system can be challenged.

Chapter 8

Conclusions

8.0. Introduction

This chapter provides a summary to the key ideas presented in chapters 4, 5, 6 and 7 by drawing conclusions and emphasizing on the important research contributions presented in this thesis. Further to that it also provides an insight into possible future directions of research, in particular with the intentions of improving/enhancing the functionality and efficiency of the proposed algorithms.

The motivation towards the research presented in this thesis comes from the fact that *RSDR* is relatively new research area in *Advanced Driver Assistance Systems* [105] and significant amount of research is yet to be performed. This thesis presents solutions to the important research challenges in *RSDR* while considering the presence of variable illumination, partial occlusion, scale variance, angular rotation and also computational complexity and robustness achieved by proposed algorithms. Four novel techniques that will benefit RSDR have been proposed in which two techniques focus on local/global colour feature extraction/classification, where as one technique each focuses on local/global, shape and content features extraction/classification, respectively. The proposed techniques have been compared conceptually or experimentally with state of the art *RSDR* techniques where significant amount of improved accuracy is achieved in detection and recognition stages of *RSDR*. The presentation of this chapter is organised in such a way that in section 8.1, each of the contributory chapters 4 to 7, are briefly revisited. Section 8.2 provides highlights of each contribution, research motivation applications and limitations. Further the chapter presents future work in section 8.3 where

insights to improve and enhance the functionality and the efficiency of each proposed algorithm, are presented.

8.1 Contributions of Research

The original contributions made by this thesis are briefly presented in this section and were further detailed in *chapters 4 to 7*. The full details of associated conference and journal proceedings published can be found in *Appendix E*.

8.1.1 Road Sign Segmentation Based on Colour Spaces: A Comparative Study [68]

In chapter 4, a detailed analysis related to the performance of various colour spaces in colour based detection of road signs was presented. The chapter proposed an algorithm for road sign colour segmentation based on the *HSV* colour space, whereas threshold values for 'Red', 'Green' and 'Blue' colours were tabulated by using each of six colour spaces (*YCbCr, YIQ, RGB, CIElab, CYMK* and *HSV)* while considering various day light conditions.

8.1.2 A Combined Colour Space Model for Road Sign Region of Interest (ROI) Segmentation [99]

In chapter 5, a robust approach towards real-time road sign colour segmentation was presented. *CCM* is the combination of properties of *HSV, RGB, CIElab and CYMK* colour spaces constructed with the help of WEKA data mining tool. The dominant attributes of the above mentioned colour spaces were selected using average results of popular search methods i.e. *Exhaustive Search*, *Basic Search*, *Genetic Search*, *Greedy Stepwise* and *Random Search*. The selected components were transformed to feature space by using the *PCA* filter of the WEKA package and were later trained and classified by utilizing *SVM Polynomial Kernel*.

8.1.3 Shape Based Classification of Road Signs [107]

In chapter 6, an approach towards the road sign shape detection and its classification was presented. The algorithm used *Contourlet Transform* to extract the shape features and *SVM Polynomial Kernel* for the classification of shape features at various levels of orientation, scale and occlusions. The candidate shapes obtained as a result of the colour segmentation were pre-processed in a way so that they should reflect only the outer geometric properties of the road sign shapes.

8.1.4 Road Sign Recognition using LESH Features [99] and [107]

In chapter 7, a content recognition system that can be used to recognise and classify detailed contents of a road sign was proposed. The algorithm utilized LESH for feature extraction of the road sign contents. These extracted features were trained and tested by employing SVM with Polynomial Kernel. Three experiments were presented with five different content classes in each experiment. The number of training and testing samples of each class contents were presented with the help of confusion matrices. The specificity and sensitivity of road sign contents were presented by plotting the *ROC* curve for each experiment.

8.2. Summary and Conclusions

The thesis presented four contributions to the state of the art in *RSDR*. The first contribution was presented in chapter 4, which has represented an approach to road sign colour segmentation using *HSV* colour space. The chapter provided a detailed performance analysis of various colour spaces in colour based detection of the road signs. The experiments were performed according to the colour behaviour in conjunction to the change in illumination and the environmental conditions. The experimental section provided segmentation results of red, green and blue colours of the road signs by using

YCbCr, YIQ, RGB, CIElab, CYMK and *HSV* colour spaces while considering the images captured during brighter/day, rain/wet, evening and night times of the day. The algorithm provided in this chapter was divided into three stages. The first stage was pre-processing, which has utilised *gamma correction* to adjust the luminance level of the images according the *NTSC* video capturing system. The second stage consisted of pixels of interest selection using *HSV* colour space, due to its higher detection accuracy as compared to other computer based colour spaces mentioned above. The chapter provided the details of *HSV* gamut partitioning and histogram analysis to extract the pixels of interest. The third stage of this algorithm represented the bounding box analysis of binary image objects according to their aspect ratio and road sign criteria. The experiments were carried out on 1200 road sign images captured during the above mentioned day light conditions on the UK roads. The colour segmentation accuracy while considering different illumination conditions using *HSV, CIElab, RGB, YCbCr, CYMK* and *YIQ* colour spaces was reported as *94.7%, 87.7%, 62.2%, 77.2%, 76.5%* and *74.6%* respectively. The algorithm is highly dependent on the complete information about image/video capturing source.

Chapter 5 proposed the creation and utilisation of an illumination invariant colour based segmentation approach towards road sign detection. A C*ombined Colour Model (CCM)* named after its inclusion of combined properties of *HSV, RGB, CIElab* and *CYMK* colour spaces was constructed with the help *WEKA,* a data mining tool providing efficient implementations of data classification algorithms. The motivations to introduce *CCM* was to combine the best performance features of different colour spaces at given illumination conditions and to generate an extended colour gamut that can cover all possible shades of red, green, blue colours. The colour features represented in the above mentioned colour spaces were extracted while considering Night, Day, Evening, Fogy and Rainy day light conditions and the dominant components were selected using the average of results of popular search methods i.e. Exhaustive Search, Basic Search, Genetic Search, Greedy Stepwise and Random Search. The selected components were further analysed with the help of Principal Component Analysis filter. To reduce its data dimensionality and redundancy, the most dominant Eigen Vectors were selected for the colour representation. Finally these Eigen Vectors were trained and tested by utilising a

SVM. *CCM* colour detection accuracy for 1200 UK road sign images was recorded as *97.5%* which outperformed the single colour space based colour segmentation solutions experimented in chapter 4. Though *CCM* provides better colour based segmentation but it is also three times more computationally expensive than a single colour space based colour segmentation solution.

Chapter 6 presented a novel approach towards geometric shape detection and classification. Road signs were represented with distinctive shapes such as circles, Triangles (pointing upwards), Triangles (pointing downwards), Octagons and Squares, which distinguished them from other arbitrary outdoor shapes. The motivations to introduce this novel algorithm was making the road sign detection more robust by detecting the shapes; a road sign can represent and at the same time making it less error prone, which helps removing noise prior to its recognition. The candidate shapes obtained as a result of colour segmentation, were pre-processed in a way so that they reflect only the outer geometric shape properties of the road sign. The algorithm introduced *Contourlet Transform* to extract the shape features of normalised candidate shapes at various levels of angular orientation, variable scale and partial occlusion. The shape features were obtained by using a 3-level frequency decomposition of the pyramidal filter and the *'Haar'* transform was utilized for each *pyramidal filter* and *directional filter bank*. These features were trained with the help of *SVM polynomial kernel* and tested on over *1500* sample road sign shapes. The experiments revealed *99.9 %* accuracy of shape classification while using level-3 *Contourlet Transform* directional decomposition. The algorithm permits only 5 to 7 degree angular rotation of an object.

Finally chapter 7 presented the fourth novel algorithm of this thesis which aimed to recognise and classify the road sign contents. The motivations to introduce such an algorithm was to utilize a computationally inexpensive and robust feature selector while targeting the possible challenging conditions of road sign appearance such as illumination variance, partial occlusion, variable scale and angular rotation. The road sign contents considered in this thesis are composed of alphabets, digits/numbers and symbols (see appendix A-D). The candidate road signs captured from the original image were pre-

processed for the normalisation of illumination, scale and extraction of inner contents for feature selection. The feature selection introduced the use of *LESH* that extracted the features of the internal contents by dividing the content area into sixteen equal sub regions and calculating the eight bin histogram of each sub region. The division of content area and the calculation of a separate histogram extraction make it more robust feature selector towards partial Occlusion and angular Orientation problems. These extracted features were trained by employing *SVM Polynomial Kernel* and tested on over *1500* sample road sign contents. Three experiments with five different content classes per experiment and number of training and testing samples were presented with the help of confusion matrices. The specificity and sensitivity figures of road sign content recognition was measured and presented by plotting *ROC* curves for each experiment. The image quality performs as an important aspect of content recognition. Images captured at low scale, abnormal rotation of the contents and camera shake can possibly limit the effectiveness of the algorithm.

8.3. Future Work

In this thesis a number of contributions to the state of the art in *RSDR* were proposed. However there exist possibilities to further enhance the research work which can lead to further improvement of functionality and robustness of the algorithms proposed. This section suggests a number of possible enhancements by introducing new software toolboxes, image capturing devices, colour correction algorithms, object tracking algorithms, advance feature selectors and classifiers.

- The implementations of proposed algorithms have been carried out by using different programming platforms such as *MATLAB, C/C++, C#* and *Java.* The implementations of colour space transformation of an image is carried out in *C#* which has significantly reduced the processing time as compared to algorithms previously implemented in *MATLAB*. One of the future tasks is to transform all algorithms into one software development environment such as *C#* that has the capability to increase the speed of execution and processing of the *RSDR* system

as desired by real time applications. It is believed that the conversion of the *MATLAB* implementation to *C#* has the ability to increase the speed of algorithms by up to eight times.

- The performance of the proposed colour segmentation techniques still need to be compared with other classical segmentation techniques such as clustering, edge detection, region based methods, vector based methods and fuzzy techniques as well as physics based methods.

- The possible improvement to the current colour segmentation stage described in chapter 4 is the colour pixel enhancement in the presence of varying lighting conditions by using *Edge-Based Colour Constancy [101]* and *Retinex processing for automatic image enhancement [102]*, where images are captured by using standard digital cameras. This idea can significantly improve the colour segmentation process by enhancing the visibility of the adaptively selected colours such as red, green and blue.

- The computational efficiency of CCM can be improved by reducing the search region of the image sequence, by introducing object tracking. For this purpose in future work prediction based method for object tracking such as *Kalman filter [103]* and *Particle filtering [104]* can be analysed to improve the efficiency of the *CCM*.

- The efficiency of the algorithm presented in chapter 6 can be improved by including the angular information of the shape. For this purpose addition of more training samples of a particular shape along its possible angular orientation will make the proposed shape descriptor more robust even on abnormal rotation of a shape.

- *Phase Congruency [90]* which is proven to be better edge filter as compared to *Canny*, *Haar, Sobel* and *pkva*, can be used to extract the shape features as future enhanced algorithms.

- The proposed algorithms in this thesis were tested on UK road signs which can easily be extended to detect and classify the road signs used by former British colonies.

- The position and installation of image acquisition device in the car is also very important to improve the accuracy of detection and recognition of the road signs. Recently car manufactures have included the speed limit sign detection systems in the cars and the camera installation point is selected as the back side of the windscreen mirror, to avoid the possible shake during image acquisition.

- In future work the study of dual camera based image acquisition systems can be investigated with careful design of their position and installation within the car, to obtain meaningful information (including depth) as well as helping to avoid possible shake and vibration during image acquisition.

- The present state of the art and the fundamental theories of computer vision provide a large number of feature detectors which can be combined with large number of advance classifiers to obtain the best recognition accuracy.

It is highly recommended that research shall be carried out to determine the use of appropriate feature descriptors and classifiers which are not listed and investigated within this thesis. It is an open research problem to find the best possible feature descriptor and classifier pair that gives optimum accuracy.

References

[1] Y. Nguwi and A. Z. Kouzani, Automatic Road Sign Recognition Using Neural Networks, *International Joint Conference on Neural Networks Sheraton Vancouver Wall Centre Hotel*, Vancouver, BC, Canada Jul. 16-21, 2006.

[2] L. D. Lopez and O. Fuentes, Color-Based Road Sign Detection and Tracking, Springer, *Lecture Notes in Computer Science*, 2007.

[3] M. Benallal and J. Meunier, Real-time color segmentation of road signs, *IEEE CCECE 2003 Canadian Conference on Electrical and Computer Engineering*, 2003.

[4] S. Maldonado-Bascon, S. Lafuente-Arroyo, P. Gil-Jimenez, H. Gomez-Moreno, F. Lopez-Ferreras, Road-Sign Detection and Recognition Based on Support Vector Machines, *IEEE Transactions on Intelligent Transportation Systems,* 8(2), Jun. 2007.

[5] R. Malik ,J. Khurshid, S.N. Ahmad, Road Sign Detection and Recognition, Using Colour Segmentation, Shape Analysis and Template Matching, *Proceedings of the Sixth International Conference on Machine Learning and Cybernetics*, Hong Kong, Aug. 2007.

[6] A. Broggi, P. Cerri, P. Medici, P.P. Porta, G. Ghisio, Real Time Road Signs Recognition, *Proceedings of the 2007 IEEE Intelligent Vehicles Symposium*, Turkey, Jun. 2007.

[7] H. Ohara, I. Nishikawa, S. Miki, N. Yabuki, Detection and Recognition of Road Signs using Simple Layered Neural Networks, *Proceedings of the 9th International Conference on Neural Information Processing*, Nov. 2002.

[8] X. Gao, K. Hong, P. Passmore, L. Podladchikova and D. Shaposhnikov, Colour Vision Model-Based Approach for Segmentation of Traffic Signs, *Journal on Image and Video Processing*, Volume 2008, Jan. 2008.

[9] M. Shneier, Road Sign Detection and Recognition, *IEEE Computer Society International Conference on Computer Vision and Pattern Recognition*, Jun. 2005.

[10] A. Ruta, Y. Li, X. Liu, Towards Real-Time Traffic Sign Recognition by Class-Specific Discriminative Features, *In Proceedings of the British Machine Vision Conference*, UK, Sep. 2007.

[11] K. G. Siogkas, S. E. Dermatas, Detection, Tracking and Classification of Road Signs in Adverse Conditions, *IEEE Mediterranean Electrotechnical Conference*, May 2006.

[12] S.Lafuente-Arroyo, S. Maldonado-Bascon, P. Gil-Jimenez, H. Gomez-Moreno and F.Lopez-Ferreras, Road Sign Tracking with a Predictive Filter Solution, *IEEE 32nd Annual Conference on Industrial Electronics*, Nov. 2006.

[13] A. A. Farag, A. E. Abdel-Hakim, Detection, Categorization and Recognition of Road Signs for Autonomous Navigation, *Proceedings of Advanced Concepts for Intelligent Vision Systems* Belgium, Sep. 2004.

[14] H. Liu, D. Liu, J. Xin, Real- Time Recognition of Road Traffic Sign in Motion Image Based on Genetic Algorithm, *Proceedings of First International Conference on Machine Learning and Cybernetics*, Beijing Nov. 2002.

[15] L. Sekanina, J. Torresen, Detection of Norwegian Speed Limit Signs, *In Proceedings of the 16th European Simulation Multi conference* 2002.

[16] A. de la Escalera, J. M. Armingol, J. M. Pastor, F. J. Rodriguez, Visual Sign Information Extraction and Identification by Deformable Models for Intelligent Vehicles, *IEEE Transactions on Intelligent Transportation Systems*,5(2) Jun. 2004.

[17] W.J. Kuo, C.C. Lin, Two-Stage Road Sign Detection and Recognition, *IEEE International Conference on Multimedia and Expo*, Jul. 2007.

[18] C. F. Paulo, P. L. Correia, Automatic Detection and Classification of Traffic Signs, *Proceedings of the Eight International Workshop on Image Analysis for Multimedia Interactive Services*, 2007.

[19] V. Andrey, K. H. Jo, Automatic Detection and Recognition of Traffic Signs using Geometric Structure Analysis, *International Joint Conference SICE-ICASE*, Korea, Oct., 2006.

[20] N. Bose, M. Shirvaikar, R. Pieper, A Real Time Automatic Sign Interpretation System for Operator Assistance, *Proceedings of the 38th Southeastern Symposium on System Theory Tennessee Technological University Cookeville*, USA, Mar., 2006.

[21] W. K. I. L. Wanniarachchi, D. U. J. Sonnadara, M. K. Jayananda, Detection and Extraction of Road Traffic Signs, *Proceedings of the Technical Sessions, Institute of Physics*, Sri Lanka, 2008.

[22] A.V. Reina, R. L. Sastre, S. L. Arroyo, P. G. Jimenez, Adaptive traffic road sign panels text extraction, *Proceedings of the 5th WSEAS International Conference on Signal Processing, Robotics and Automation*, Spain, Feb., 2006.

[23] Y. Y. Nguwi, S. Y. Cho, Two-tier Self-Organizing Visual Model for Road Sign Recognition, *IEEE International Joint Conference on Neural Networks*, Jun., 2008.

[24] H. Huang, C. Chen, Y. Jia, S. Tang, Automatic Detection and Recognition of Circular Road Sign, *IEEE/ASME International Conference on Mechatronic and Embedded Systems and Applications*, Oct., 2008.

[25] J. Wu,Y.Tsai, Enhanced Roadway Inventory Using a 2-D Sign Video Image Recognition Algorithm, *Computer-Aided Civil and Infrastructure Engineering* 21(5), Jul. 2006.

[26] S. Arroyo, S. M. Bascon, P. G. Jimenez, J. A. Rodrıguez, R. J. L. Sastre, A Tracking System for Automated Inventory of Road Signs, *Proceedings of the IEEE Intelligent Vehicles Symposium* Turkey, Jun., 2007.

[27] L. W. Tsai, J. W. Hsieh, C. H. Chuang, Y. J. Tseng, K. C. Fan, C. C. Lee, Road sign detection using eigen colour, *Computer Vision, IET* 2(3) Sep. 2008.

[28] P. Medici, C. Caraffi, E. Cardarelli, P. P. Porta, G. Ghisio, Real Time Road Signs Classification, *Proceedings of the IEEE International Conference on Vehicular Electronics and Safety Columbus*, USA, Sep., 2008.

[29] G. H. Kim, H. G. Sohn, Y. S. Song, Road Infrastructure Data Acquisition Using a Vehicle-Based Mobile Mapping System, *Computer-Aided Civil and Infrastructure Engineering*, 21(5), Apr. 2006.

[30] S. M. Bascon, S. L. Arroyo, P. Siegmann, H. G. Moreno, F. J. A. Rodriguez, Traffic Sign Recognition System for Inventory Purposes, *IEEE Intelligent Vehicles Symposium Eindhoven University of Technology Eindhoven*, Netherlands, Jun., 2008.

[31] A. Z. Kouzani, Road-Sign Identification Using Ensemble Learning, *Proceedings of the IEEE Intelligent Vehicles Symposium* Turkey, Jun., 2007.

[32] M. L. Eichner, T. P. Breckon, Integrated Speed Limit Detection and Recognition from Real-Time Video, *In Proceedings of the IEEE Intelligent Vehicles Symposium*, 2008.

[33] D. Matsuura, H. Yamauchi, H. Takahashi, Extracting Circular Road Signs Using Specific Color Distinction and Region Limitation, *Systems and Computers in Japan*, 38(11), 2007.

[34] Y.Y. Nguwi and A.Z. Kouzani, Detection and classification of road signs in natural environments, *Neural Computing & Applications*, 265–289, 2008

[35] P. Silapachote, A. Hanson, R. Weiss, A Hierarchical Approach to Sign Recognition, *Seventh IEEE Workshops on Application of Computer Vision*, Jan. 2005.

[36] J. Torresen, J. W. Bakke, Y. Yang, A Camera Based Speed Limit Sign Recognition System, *In Proceedings of 13th ITS World Congress and Exhibition*, 2006.

[37] Q. Zhang, S. Kamata, Automatic Road Sign Detection Method Based on Color Barycenters Hexagon Model, *19th International Conference on Pattern Recognition*, Dec., 2008.

[38] U. L. Jau, C. S. Teh, G. W. Ng, A comparison of RGB and HSI color segmentation in real time video images: A preliminary study on road sign detection, *International Symposium on Information Technology*, Malaysia, Aug., 2008.

[39] Y. Y. Nguwi, A. Z. Kouzani, A Study on Automatic Recognition of Road Signs, *IEEE Conference on Cybernetics and Intelligent Systems*, Bangkok, Jun., 2006.

[40] S. L. Arroyo, P. G. JimCnez, R. M. Bascon, F. L. Ferreras, S. M. Bascon, Traffic sign shape classification evaluation I: SVM using Distance to Borders, *In Proceedings of IEEE Intelligent Vehicles Symposium*, Jun. ,2005.

[41] H. Fleyeh, Traffic Sign Recognition by Fuzzy Sets, *IEEE Intelligent Vehicles Symposium Eindhoven University of Technology,* Netherlands, Jun., 2008.

[42] H. Fleyeh, M. Dougherty, Road and Traffic Sign Detection and Recognition, *Proceedings of the 16th Mini Euro Conference and 10th Meeting of EWGT*, Poland, Sep. 2005.

[43] H. Fleyeh, Color Detection and Segmentation for Road and Traffic Signs, In *Proceedings of IEEE Conference on Cybernetics and Intelligent Systems*, Singapore, Dec., 2004.

[44] A. D. L. Escalera, J. M. Armingol, M. Mata, Traffic sign recognition and analysis for intelligent vehicles, *Image and Vision Computing*, 21(3), Mar., 2003.

[45] H. M. Yang, C. Lin. Liu, K. H. Liu, S. M. Huang, Traffic Sign Recognition in Disturbing Environments, Foundations of Intelligent Systems, *Lecture Notes in Computer Science*, Volume 2871/2003, 2003.

[46] N. Kehtarnavaz, A. Ahmad, Traffic Sign Recognition in Noisy Outdoor Scenes, *Proceedings of the Intelligent Vehicles Symposium*, USA, Sep. 1995.

[47] W. G. Shadeed, D. I. A. Nadi, M. J. Mismar, Road Traffic Sign Detection In Color Images, *Proceedings of the 10th IEEE International Conference on Electronics, Circuits and Systems*, Dec., 2003.

[48] W. Y. Wu, T. C. Hsieh, ,C. S. Lai, Extracting Road Signs using the Color Information, *World Academy of Science, Engineering and Technology*, 2007.

[49] G. C. Kiran, V. L. Prabhu, V. R. Abdu, K. Rajeev, Traffic Sign Detection and Pattern Recognition using Support Vector Machine, *Seventh International Conference on Advances in Pattern Recognition*, Kolkata, Feb., 2009.

[50] J. Miura, T. Kanda, Y. Shirai, An Active Vision System for Real-Time Traffic Sign Recognition, *Proceedings of IEEE Intelligent Transportation Systems*, USA, Oct., 2000.

[51] A. A. Moustafa, Z. A. Alqadi, Color Image Reconstruction Using A New R'G'I Model, *Journal of Computer Science* 5 (4) 2009.

[52] P. G. Jimenez, S. L. Arroyo, H. G. Moreno, F. L. Ferreras, S. M. Bascon, Traffic sign shape classification evaluation II: FFT applied to the signature of Blobs, *Proceedings of IEEE Intelligent Vehicles Symposium*, Jun. 2005.

[53] M. N. Do, M. Vetterli, The Contourlet Transform: An Efficient Directional Multi resolution Image Representation, *IEEE Transactions on Image Processing* 14(12), Dec. 2005.

[54] C. Bahlmann, Y. Zhu, V. Ramesh, M. Pellkofert, T. Koehled, A System for Traffic Sign Detection, Tracking, and Recognition Using Color, Shape, and Motion Information, *Proceedings of IEEE Intelligent Vehicles Symposium*, Jun., 2005.

[55] Y. Ohta, T. Kanade, T. Sakai, Color Information for Region Segmentation, *Computer Graphics and Image Processing* 13(3), Jul. 1980.

[56] A. Ruta, Y. Li, X. Liu, Detection, Tracking and Recognition of Traffic Signs from Video Input, *Proceedings of the 11th International IEEE Conference on Intelligent Transportation Systems,* Beijing, China, Oct., 2008.

[57] A. Ruta, Y. Li and X. Liu, Real-Time Traffic Sign Recognition from Video by Class-Specific Discriminative Features, *Pattern Recognition*, Vol. 43(1), pp. 416-430, 2010.

[58] A. Ruta, F. Porikli, S. Watanabe, Y. Li, In-vehicle camera traffic sign detection and recognition, *Machine Vision and Applications*, 22(2), 359-375, 2009.

[59] A. Ruta, F. Porikli, Y. Li, S. Watanabe, H. Kage, K. Sumi, , A New Approach for In-Vehicle Camea Traffic Sign Detection and Recognition, *IAPR Conference on Machine vision Applications (MVA)*, Session 15: Machine Vision for Transportation, May 2009.

[60] A. Arlicot, B. Soheilian, N. Paparoditis, Circular road sign extraction from street level images using colour, shape and texture database maps, *International Archives of Photogrammetry Remote Sensing and Spatial Information Sciences* Vol. XXXVIII Part 3W4, XXXVIII(c), 3-4, 2009.

[61] Y. Wang, L. Liu, Y. Zhao, Traffic Sign Detection Based on Fixed Color Combination and Intensity Restraint, *International Symposium on Computer Network and Multimedia Technology*, pp.1-5, 18-20, Jan. 2009.

[62] R. Belaroussi, P. Foucher, J. P. Tarel, B. Soheilian, P. Charbonnier, N. Paparoditis, Road Sign Detection in Images: A Case Study, *20th International Conference on Pattern Recognition (ICPR)* , pp.484-488, 23-26 Aug. 2010.

[63] Y. R. Fatmehsan, A. Ghahari, R. A. Zoroofi, Gabor wavelet for road sign detection and recognition using a hybrid classifier, *International Conference on Multimedia Computing and Information Technology*, pp.25-28, 2-4 Mar. 2010.

[64] X. Liu, S. Zhu, K. Chen, Method of Traffic Signs Segmentation Based on Color-Standardization, *International Conference on Intelligent Human-Machine Systems and Cybernetics*, vol.2, pp.193-197, 26-27 Aug. 2009.

[65] M. Tkalcic, J. Tasic, Colour spaces - perceptual, historical and applicational background, *In The IEEE Region 8 EUROCON 2003 proceedings* (2003), pp. 304-308.

[66] A. Bouzidi, N. Baaziz, Contourlet Domain Feature Extraction for Image Content Authentication, *IEEE 8th Workshop on Multimedia Signal Processing*, pp.202-206, 3-6 Oct. 2006.

[67] L. Zhang, F. Lin, B. Zhang, Support vector machine learning for image retrieval, *International Conference on Image Processing*, pp.721-724 vol.2, 7-10 Oct. 2001.

[68] U. Zakir, A. N. J. Leonce and E. A. Edirisinghe, Road sign segmentation based on colour spaces: A Comparative Study, *In Proceedings of the 11th Iasted International Conference on Computer Graphics and Imgaing*, Innsbruck, Austria, 2010.

[69] H. Fleyeh, Traffic and Road Sign Recognition, PhD Thesis submitted at Napier University, July 2008, [Internet], Available from <*http://dalea.du.se/research/?itemId=3396*> [Accessed: Jul. 07, 2011].

[70] RGB Colour Space, [Internet] Available from <*http://www.machinevision.ca/machinevissupport*> [Accessed: Jul. 07 2011].

[71] A. Koschan, M. A. Abidi, *Digital Color Image Processing*, ISBN 978-0-470-14708-5.

[72] YIQ, [Internet] Available from <*http://en.wikipedia.org/wiki/YIQ*> [Accessed, Jul. 08, 2011].

[73] YCbCr, [Internet] Available from <*http://en.wikipedia.org/wiki/YCbCr*> [Accessed: Jul. 12, 2011].

[74] RGB/XYZ Matrices, [Internet] Available from <*http://www.brucelindbloom.com/index.html?Equations.html*> [Accessed: Jul. 12, 2011].

[75] NTSC, [Internet] Available from <*http://en.wikipedia.org/wiki/NTSC*> [Accessed: Jul. 12, 2011].

[76] PAL, [Internet] Available from <*http://en.wikipedia.org/wiki/PAL*> [Accessed: Jul. 12, 2011].

[77] SECAM, [Internet] Available from <*http://en.wikipedia.org/wiki/SECAM*> [Accessed: Jul. 13, 2011].

[78] P. J. Burt, E. H. Adelson, The Laplacian pyramid as a compact image code, *IEEE Trans on Communications*, vol. 31, no. 4, pp. 532–540, Apr. 1983.

[79] R. H. Bamberger, M. J. T. Smith, A filter bank for the directional decomposition of images: Theory and design, *IEEE Transactions on Signal Processing*, vol. 40, no. 4, pp. 882–893, Apr. 1992.

[80] HSI / HSV Colour gamut, [Internet] Available from <*http://www.mathworks.com/access/helpdesk/help/toolbox/images/hsvcone.gif*> [Accessed: Jul. 23, 2010].

[81] Gamma Correction, [Internet] Available from <*http://en.wikipedia.org/wiki/Gamma_correction*> [Accessed: Nov. 3, 2010].

[82] A. Ford and A. Roberts, Colour space conversions, [Internet] Available from <*http://www.poynton.com/PDFs/coloureq.pdf*> [Accessed: Nov. 3, 2010].

[83] D. Travis, *Effective Color Displays Theory and Practice. Academic Press*, 1991, ISBN 0-12-697690-2.

[84] I. H. Witten and E. Frank, *Data Mining Practical Machine Learning Tools and Techniques. United States of America: Morgan Kaufmann, Elsevier*, 2005, ISBN: 0-12-088407-0.

[85] Weisstein, Eric W. "Octagon." From MathWorld--A Wolfram, [Internet] Available from <*http://mathworld.wolfram.com/Octagon.html*> [Accessed: Nov. 29, 2010].

[86] Weisstein, Eric W. "Equilateral Triangle." From MathWorld--A Wolfram, [Internet] Available from <*http://mathworld.wolfram.com/EquilateralTriangle.html*> [Accessed: Nov. 30, 2010].

[87] R. C. Gonzalez, R. E Woods, *Digital image processing, Second Edition*, 2002, ISBN 0-201-18075-8.

[88] C. M. Morrone , A. R. Owens, Feature Detection from Local Energy, *PR Letters* 6, 303–313, 1987.

[89] D. P. Kovesi, Phase Congruency: A Low-Level Image Invariant, *Psychological Research* 64, 136–148, 2000.

[90] S. Shiguang, C. Xilin, and G. Wen, Histogram of Gabor Phase Patterns (HGPP): A Novel Object Representation Approach for Face Recognition, *IEEE Trans. on Image Processing* 16 (1), 57–68, 2007.

[91] M. Bingpeng, Z. Wenchao, S. Shiguang, C. Xilin, C. Wen, Robust Head Pose Estimation Using LGBP, *ICPR* 2, 512–515, 2006.

[92] Road Sign Fonts, [Internet] Available from <*http://www.roadsuk.com/downloads/fonts.html*> [Accessed: Apr. 08, 2011].

[93] Select traffic signs by categories, [Internet] Available from <*http://www.dft.gov.uk/trafficsignsimages/SelectCategory.php*> [Accessed: Apr. 08, 2011].

[94] M. N. Do, M. Vetterli, Framing pyramids, *IEEE Transactions on Signal Processing*, pp. 2329–2342, Sep. 2003.

[95] M. Vetterli, Multidimensional subband coding: Some theory and algorithms, *Signal Processing*, vol. 6, no. 2, pp. 97–112, Feb. 1984.

[96] M. Hall, E. Frank, G. Holmes, B. Pfahringer, P. Reutemann, I. H. Witten; The WEKA Data Mining Software: An Update; *SIGKDD Explorations*, Volume 11, Issue 1, 2009.

[97] G. K. Siogkas, E.S. Dermatas, Detection Tracking and Classification of Road Signs in Adverse Conditions. *IEEE Mediterranean Electrotechnical Conference, MELECON*, 2006.

[98] U. Zakir, I. Zafar, E. A. Edirisinghe. A Novel Approach to In-Car Road Sign Recognition. *The 14th International Conference on Machine Design and Production, Cyprus* 2010, pp.317-331, ISBN:978-975-429-282-4

[99] L. Simon, P. J. Tarel, R. Bremond, Alerting the Drivers about Road Signs with Poor Visual Saliency, *Proceedings of the IEEE Intelligent Vehicle Symposium*, China, 2009.

[100] J. Weijer, T. Gevers, A. Gijsenij, Edge-Based Color Constancy, *IEEE Transactions on Image Processing*, Vol. 16, No. 9, Sep. 2007.

[101] Z. Rahman, D. J. Jobson, G. A. Woodell, Retinex processing for automatic image enhancement, *Journal of Electronic Imaging,* 13, 100, 2004; doi:10.1117/1.1636183

[102] Kalman Filter, [Internet] Available from <*http://en.wikipedia.org/wiki/Kalman_filter*> [Accessed: Jul. 15, 2011].

[103] M. Z. Islam, C. M. Oh, C. W. Lee, Video Based Moving Object Tracking by Particle Filter, *International Journal of Signal Processing, Image Processing and Pattern* Vol. 2, No.1, Mar., 2009.

[104] Traffic sign recognition, [Internet] Available from <*http://en.wikipedia.org/wiki/Traffic_sign_recognition*> [Accessed: Jul. 15, 2011].

[105] R. P. W. Duin, P. Juszczak, P. Paclik, E. Pekalska, D. de Ridder, D. M. J. Tax, S. Verzakov, PRTools4.1, A Matlab Toolbox for Pattern Recognition, *Delft University of Technology*, 2007.

[106] M. S. Sarfraz and O. Hellwich, An Efficient Front-end Facial Pose Estimation System for Face Recognition, *In International Journal of Pattern Recognition and Image Analysis, distributed by Springer*, 18(3):434–441, 2008.

[107] U. Zakir, I. Zafar, E. A. Edirisinghe, Road Sign Detection and Recognition by using Local Energy Based Shape Histogram (LESH), *International Journal of Image Processing* Volume 4 Issue 6 , ISSN: 1985-2304, pp: 566-582, 2011.

[108] Gamma Correction, [Internet] Available from <*http://en.wikipedia.org/wiki/Gamma_correction*> [Accessed: Nov. 10, 2010].

[109] Gamma Correction, [Internet] Available from <*http://graphics.stanford.edu/courses/cs178/applets/gamma.html*> [Accessed: Nov.-10, 2010].

[110] im2bw, [Internet] Available from <*http://www.mathworks.com/help/toolbox/images/ref/im2bw.html*> [Accessed: Aug. 07, 2011].

[111] Accuracy and Precision, [Internet] Available from <*http://en.wikipedia.org/wiki/Accuracy_and_precision*> [Accessed: Aug. 09, 2011].

Appendix A

Warning Signs [94]

Junction ahead controlled by a STOP or GIVE WAY sign

Crossroads ahead

Crossroads ahead

Crossroads ahead

T-junction ahead (left)

T-junction ahead (right)

Side road ahead (right)

Side road ahead (left)

Side road ahead (left)

Staggered junction ahead (left/right)

Staggered junction ahead (right/left)

Staggered junction ahead (right/left)

Side road ahead (right)

Staggered junction ahead (left/right)

Traffic merges ahead from the left

Traffic queues likely on road ahead

Traffic merges ahead onto main carriageway.

Roundabout

Reduction in speed necessary for a change in road layout

Bend ahead to the right

Junction on right bend ahead

Junction on left bend ahead

Junction on right bend ahead

Junction on left bend ahead

Bend ahead to the left

Double bend or series of bends ahead, first to the left

Double bend or series of bends ahead, first to the right

Road narrows on both sides ahead

Road narrows on right ahead

Road narrows on left ahead

Dual carriageway ends ahead

Two-way traffic

Two-way traffic on route crossing ahead

Steep hill downwards ahead (10%)

Steep hill upwards ahead (20%)

Hump bridge ahead

Opening or swing bridge ahead

Tunnel ahead

Traffic signals ahead

Zebra crossing ahead

Pedestrians in road ahead

Frail or disabled pedestrians likely to cross road ahead

Children going to or from school or playground ahead

Cattle likely to be in road ahead

Sheep likely to be in road ahead

Wild horses or ponies likely to be in road ahead

Accompanied horses or ponies likely to be in or crossing road ahead

Horse drawn vehicles likely to be in road ahead

Wild animals likely to be in road ahead

Migratory toad crossing ahead

Wild fowl likely to be in road ahead

Cattle grid ahead

Agricultural vehicles likely to be in road ahead

Risk of ice or packed snow ahead

Quayside or river bank ahead

Water course alongside road ahead

Uneven road ahead

Soft verges ahead

Slippery road ahead

Low flying aircraft or sudden aircraft noise likely ahead

Slow moving vehicles likely on incline ahead

Risk of falling or fallen rocks ahead

Other danger ahead. Plate beneath indicates the nature of the hazard

Side winds likely ahead

Slow moving military vehicles likely to be crossing or in the road

Appendix B

Regulatory signs [94]

Stop before crossing the traverse line on the road and ensure the way is clear before entering a major road

Give way to traffic on the major road

Vehicular traffic must proceed in the direction indicated by the arrow

Vehicular traffic must proceed in the direction indicated by the arrow

Vehicular traffic must turn ahead in the direction indicated by the arrow

Vehicular traffic must turn ahead in the direction indicated by the arrow

Vehicular traffic passing the sign must keep to the left of the sign

Vehicular traffic may reach the same destination by passing either side of the sign

Vehicles entering the junction must give way to traffic to vehicles coming from the right

No right turn for vehicular traffic

No left turn for vehicular traffic

No U-turns for vehicular traffic

Priority must be given to vehicles from the opposite direction

No entry for vehicular traffic

All vehicles prohibited except pedal cycles being pushed by pedestrians

Motor vehicles prohibited

Motor vehicles prohibited

Solo motor cycles prohibited

Goods vehicles prohibited

End of prohibition of goods vehicles

Articulated vehicles prohibited

Horse drawn vehicles prohibited

Ridden or accompanied horses prohibited

Towed caravans prohibited

One-way traffic

Pedestrians prohibited

Vehicles exceeding 6'-6" in width indicated prohibited

Vehicles exceeding 32'-6" in width indicated prohibited

No overtaking

Vehicular traffic must not go beyond the sign

Appendix C

Speed limit signs [94]

Maximum speed limit of 10 miles per hour

Maximum speed limit of 15 miles per hour

Maximum speed limit of 20 miles per hour

Maximum speed limit of 30 miles per hour

Maximum speed limit of 40 miles per hour

Maximum speed limit of 50 miles per hour

Maximum speed limit of 60 miles per hour

Maximum speed limit of 70 miles per hour

National speed limits apply

Minimum speed limit of 30 miles per hour

Minimum speed limit of 40 miles per hour

End of 30 miles per hour minimum speed limit

End of 40 miles per hour minimum speed limit

End of 20 miles per hour zone and start of 30 miles per hour zone

Speed camera ahead and reminder of 30 miles per hour speed limit

Appendix D

Motorway signs [94]

300 yards to a roundabout or the next point at which traffic may leave a route

200 yards to a roundabout or the next point at which traffic may leave a route

100 yards to a roundabout or the next point at which traffic may leave a route

Additional traffic lane joining from the left ahead

In 200 yards the number of lanes of traffic lanes reduces from three lanes to two.

Additional traffic lane joining from the left ahead in 200 yards. Traffic on the main carriageway has priority over joining traffic

Start of motorway regulations, including the national speed limit

Direction to a motorway at the junction shown, indicating route number and destination reached along the motorway

Direction to a motorway at the junction shown, indicating route number

Motorway junction ahead, displaying the route number and destination reached by taking this route

Motorway junction, displaying route number and destination reached

Number of route reached from a motorway exit road

Route number of the motorway with destinations and distances to places along or reached from that route

Junction ahead with another motorway

Availability of motorway service areas ahead with distances

Entrance to a motorway service area at a junction ahead on a motorway slip road

Motorway junction ahead leading to a town or geographical area containing several tourist attractions and a Tourist Information Point or Centre

End of motorway regulations, including the national speed limit

Drivers should keep a distance of two chevron markings from the vehicle in front

Appendix E

Scholarly Contributions

The work presented in this thesis has resulted in a number of conference and journal proceedings. The work is also utilized in other image processing domains. The list of accepted Conference and Journal proceedings with future work is listed as under;

E.0. Refereed Conference / Journal Publications

- Zakir, U., Edirisinghe, E.A. and Zafar, I., "Road Sign Detection and Recognition by using Local Energy based Shape Histogram (LESH)", International Journal of Image Processing, 4(6), 2011, pp.566-582, ISSN:1985-2304

- Zakir, U., Zafar, I. and Edirisinghe, E.A., "A Novel Approach to In-Car Road Sign Recognition", Proceedings of the 14th International Conference on Machine Design and Production, Cyprus, July 2010, pp.317-331, ISBN:978-975-429-282-4

- Zakir, U., Leonce, A.N.J. and Edirisinghe, E.A., "Road Sign Segmentation Based on Colour Spaces: A Comparative Study", Proceedings of 11th IASTED International Conference on Computer Graphics & Imaging, Innsbruck, Austria, February 2010, pp.72-79, ISBN:978-0-88986-824-3

E.1. Journal Publication(s) to submit

- U. Zakir, A.Hussain, E.A.Edirisinghe, “Road Sign Detection and Recognition from Video Stream using HSV, Contourlet Transform and Local Energy Shape Histogram”, 2012 Brain Inspired Cognitive Systems (BICS 2012).